Title

Studies of Brønsted/Lewis Acid-Catalyzed Dehydration of Xylose to Furfural and Simultaneous Separation of Furfural by Pervaporation

Author

Wang, Alex

Publication Date

2017

Peer reviewed|Thesis/dissertation

Studies of Brønsted/Lewis Acid-Catalyzed Dehydration of Xylose to Furfural and Simultaneous Separation of Furfural by Pervaporation

By

Alex Wang

A dissertation submitted in partial satisfaction of the

requirements for the degree of

Doctor of Philosophy

in

Chemical Engineering

in the

Graduate Division

of the

University of California, Berkeley

Committee in charge:

Professor Nitash P. Balsara, Co-Chair
Professor Alexis T. Bell, Co-Chair
Professor Clayton J. Radke
Professor F. Dean Toste

Summer 2017

Studies of Brønsted/Lewis Acid-Catalyzed Dehydration of Xylose to Furfural and Simultaneous Separation of Furfural by Pervaporation

Abstract

Studies of Brønsted/Lewis Acid-Catalyzed Dehydration of Xylose to Furfural and Simultaneous Separation of Furfural by Pervaporation

by

Alex Wang

Doctor of Philosophy in Chemical Engineering

University of California, Berkeley

Professor Nitash P. Balsara, Co-Chair

Professor Alexis T. Bell, Co-Chair

A major component of lignocellulosic biomass is hemicellulose, a polysaccharide composed of monomeric sugars, principally xylose. Xylose can be dehydrated, most often in aqueous solution, using Brønsted acid catalysts to form furfural, which can be further reacted to produce fuels, lubricants, polymers, solvents, and pharmaceutical precursors. Furfural production can also be enhanced by using Lewis acid catalysts, which promote the formation of xylulose, an isomer of xylose which more readily dehydrates to form furfural. With either type of catalyst, side reactions consume furfural to produce a group of soluble and insoluble products known as humins. Humins formation has been stymied by extracting furfural as it is produced. This is done on the industrial scale with steam stripping, but researchers have also explored the use of liquid-liquid extraction (LLE) by an organic solvent (typically 2:1 organic:aqueous volume ratio) for the same purpose. Both extraction methods increase furfural yield, but dilute the product phase, which raises the cost of furfural production. A new method, *e.g.* pervaporation, must be developed to increase furfural yield and concentrate furfural in the product simultaneously.

Pervaporation is a membrane-based process in which a liquid mixture is placed in contact with the feed side of the membrane while a vapor is located on the permeate side. A vacuum is used to reduce the partial pressure, and therefore the fugacity, of components in the permeate, which provides the driving force for mass transfer. Pervaporation is most often used to separate water from concentrated ethanol solutions, but may also be used to remove organics selectively, *e.g.* furfural, from aqueous solutions. Membranes used for such applications are typically made of polydimethylsiloxane (PDMS), but researchers have also used the PDMS-containing triblock copolymer poly(styrene-*block*-dimethylsiloxane-*block*-styrene) (SDS). Pervaporation with a furfural-selective membrane may be used to extract furfural as it is produced and concentrate it, rather than dilute it as steam stripping and LLE do.

The objective of this investigation was to assess pervaporation as a method to extract furfural during its production. This was done by designing and constructing membrane reactors, comparing them to LLE-assisted reactors through experiments and simulations, and studying how Lewis acid

catalysts can improve reaction and pervaporation compatibility and lead to the formation of novel products.

The feasibility of pervaporation as a means for *in situ* furfural extraction was studied in comparison to LLE and a reaction without extraction during batch-mode furfural production. Both LLE and pervaporation with a commercial PDMS membrane were found to improve furfural yield over the reaction without extraction, but pervaporation with PDMS yielded a product phase that was 6.6x as concentrated as that obtained with LLE. Additionally, switching the PDMS membrane with an SDS membrane resulted in similar furfural yields, but the product with SDS was 10x as concentrated as the LLE product. Furthermore, the amount of furfural extracted was qualitatively different for LLE- and pervaporation-assisted reactions: LLE was limited to 85%, the equilibrium distribution of furfural among the organic and aqueous, whereas the amount of furfural extracted by pervaporation increased monotonically over time, reaching as high as 67% during experiments. The reaction/pervaporation system was simulated in order to identify the full extent of the benefits of reaction with pervaporation. In the simulations, water lost from the reactor due to removal by pervaporation was replenished at the equivalent rate. The simulations revealed that as the reaction approached complete xylose conversion, both the PDMS and SDS membranes led to product concentrations greater than was possible with LLE, while extracting nearly all (>98%) of the furfural formed. Ultimately, pervaporation with the SDS membrane could produce a product phase with 33% greater furfural yield than that achievable by LLE.

The membrane-reactor design was revised to permit continuous, pervaporation-assisted reaction in both batch- and continuous-mode operation, with both reaction and pervaporation occurring at the same temperature. Batch-mode reactions were fed water, while continuous-mode reactions were fed an aqueous xylose solution. The reactions took place at a relatively low temperature of 90 °C, catalyzed by chromium (III) chloride ($CrCl_3$), which contributed both Brønsted and Lewis acidity. Batch-mode reactions with varying rates of pervaporation revealed that furfural extraction had no effect on furfural yield under these conditions, but a moderate pervaporation rate did lead to an order-of-magnitude increase in furfural concentration relative to that obtained without pervaporation. Pervaporation was also found to retain all of the $CrCl_3$ inside the reactor, demonstrating a simple way to separate product from homogeneous catalyst. This enabled continuous furfural production with only an initial charge of catalyst, in which an aqueous xylose solution was fed to the reactor while a furfural/water vapor was permeated from the reactor. The furfural permeability of the SDS membrane decreased over time during the course of reactions carried out at 90 °C due likely to interactions of soluble humins with the membrane. Experiments with the cross-linked PDMS membrane demonstrated that cross-linking of the membrane can inhibit this behavior and result in a much more stable furfural permeability. Additionally, cross-linking could lead to greater membrane thermal stability, permitting the pervaporation-assisted reaction at higher temperatures, which would benefit the chemistry by allowing extraction to have an impact on furfural yield.

Pervaporation-assisted furfural production with $CrCl_3$ and sulfuric acid at 130 °C was then simulated. Reaction rate constants were measured at this temperature but in the absence of pervaporation. Pervaporation data collected at lower temperatures were extrapolated to represent a hypothetical membrane that could operate at 130 °C. Simulations of batch-mode reactions demonstrated that increasing the membrane-area-to-reactor-volume ratio, *a*, would lead to higher

furfural yield and more furfural extracted, but also reduce the permeate furfural concentration, demonstrating a tradeoff between furfural production and concentration. Simulations of continuous-mode reactions showed that furfural concentration and selectivity were maximized at an intermediate value of a = 0.17 cm^{-1}. Conversely, furfural production rate increased nearly linearly with a, indicating that the optimal value of a depends on process economics and not just technical considerations.

The Lewis acidity of $CrCl_3$ was beneficial for reducing reaction temperature within the membrane stability limits, but Lewis acids, such as the Sn-containing zeolite Sn-BEA, have been shown to convert sugars (*i.e.*, xylose and glucose) at a rate greater than the rate of formation of identified products, suggesting that additional, unidentified products are formed. Through extensive analytical chemistry, these products were determined to be hydroxyl-rich carboxylic acids and furanone esters that form by structural isomerization of the sugars, followed by dehydration, and constitute as much as 45% of the yield. These side-produced acids and esters may find use as monomers for the synthesis of biodegradable polyesters, which are often used for sutures, bone prostheses, and controlled drug delivery. This work demonstrates that Lewis acid catalysts are not only useful for bridging the gap between pervaporation-membrane limits and furfural production temperatures, but also for the formation of additional value-added chemicals.

To my wife Sarah

Table of Contents

List of Schemes

List of Figures

List of Tables

Acknowledgments

My five years in graduate school have encompassed a significant and challenging time in my life. I lived for the first time outside of Michigan 2,400 miles from my family, many of my friends, and the places I was so familiar with. I moved in with my girlfriend, our relationship evolved enormously since then, and we got married. I learned to cook, took up new hobbies, and explored so much more than the bubble I lived in back in Michigan. And I gained the skills to be confident that, with enough effort, I could handle any problem I encounter. This journey has been the most difficult one in my life and I could not have done it without the help of many people, both in and out of lab.

I would first like to thank my wife Sarah for all her love and support over our 10 years together, and particularly in these last five here in Berkeley. We have been through so much together: our last year in high school, four years of college, and this latest adventure in the Bay Area. We have learned so many things together, like what it means to have a loving partner, how to take care of ourselves, and how to balance the many aspects of our individual lives and our life as a couple. We have leaned on each other for support during trying times when we grappled with family crises, work issues, and personal demons, always there for each other to listen or wipe away tears. And we have had countless fun times together, from our many lazy nights on the futon, to our week-long Habitat for Humanity trips, to our recent addiction to bubble tea. She has also been a consistent source of inspiration for me, both intentionally and unintentionally. An example of the former is my recent decision to re-learn how to play the piano, while an example of the latter, and one of my proudest accomplishments, is when I learned Polish in secret for a year. Then, during our wedding, I surprised her and her (Polish) family by delivering my wedding vows in Polish. I did these things for her. She is an incredibly kind, empathetic, thoughtful, intelligent, fun, and warm person and I could not ask for a better partner in life.

I must also thank my family for their role in making me who I am today. My parents imparted on me excellent core values, namely a strong work ethic and an unwavering desire to learn more. They also supported me through college, allowing me to pursue study in whichever field(s) I desired, resulting in me completing my PhD without any financial burdens—a freedom I will always be grateful for. It has also been wonderful to return to Michigan at least once a year to see them and stay in my childhood home, play countless hours of card games, and eat roast duck and homemade dumplings. My older brother Arthur has also had a significant influence on my life. Much of my humility and, consequently, drive to push myself to improve comes from our relationship. I always have and always will look up to him. Our shared memories over the past five years are some of my favorites: watching him crash as he inappropriately vaulted over a rock climbing wall, talking about and playing video games, getting to know his fiancée Nia, having Thanksgiving dinners together, spending lots of time together every year around Christmas, and my bachelor party. I would also like to recognize Sarah's family for so happily welcoming me as part of the group. Sarah's mother has been unconditionally supportive and excited for us, despite the tumultuous times in her own life. And seeing Marilyn, Ania, Jurek, Rena, and Rahim has become a staple of every visit to Michigan, cementing themselves as the local extended family that I did not have when growing up.

Day-to-day life in Berkeley was far better than I expected it to be, often despite my student/work life, and I owe a lot of that to my friends here. I spent most of my Thursday nights playing trivia at Red Tomato Pizza House with a combination of friends from my class and other local friends: Mike, Margaret, Nico, Alex, Ellyn, Lisa, and Emily (and Sarah). Even outside of winning countless free pizzas and drinking beer all those Thursday nights, we spent plenty of time together, sharing the highs and lows of grad school and life as twenty-somethings. Mike is a thoughtful and silly guy who talked me through some of the toughest times in my life, and I will cherish our memories of sushi feasts, Mario Kart, and running. Margaret is an enthusiastic friend, always excited to see everyone and never one to shy away from making plans. Nico is a talented researcher with a great sense of humor and confidence. Alex is incredibly witty and funny, whose seal of approval I hold in very high regard. Ellyn is courageous and humble, always ready to invite us over for board games and puppy time. Lisa is a fierce, independent, and incredibly fit woman with a knack for cooking. Emily is a devoted researcher whose enormous and infectious love of the outdoors motivated me to explore the gorgeous Bay Area. These friends are some of the best friends I have ever had, and I am grateful for all that we have shared together.

In addition to my trivia team, I shared much of my free time with various other graduate students and friends from other parts of my life. Kari, Brian, and Adri, a.k.a. the Wolf Pack, were there with me during that difficult first semester, and always around later on to share meals, drinks, and Halloween celebrations. Jacob, Lin, and Clay pushed me to start and improve at rock climbing, a sport that blends problem solving, physical exertion, and (in my case) conquering a fear of heights. Neelay has a jovial and uplifting spirit, consistently there when I needed him. Marie is always so sunny and optimistic and was never content with having fewer than half a dozen plans together on the horizon. She was also a stalwart and dependable runner who was indispensable in helping me achieve my goal of running a marathon. Katie, Michael H., Adam, and of course Marie were always up for a strenuous hike up Mount Tamalpais or around Point Reyes. I should also thank Tom, Jackson, Ryan, Matt, Rachael, and Max for their friendship before these Berkeley years, for always making time to catch up during my occasional trips back to Michigan, and for being there at mine and Sarah's wedding. I have been incredibly fortunate to have such a vast network of friends.

As I mentioned previously, I learned Polish while at Cal, which made for an unforgettable wedding ceremony. I am very grateful to my teacher Kasia for being so receptive and accommodating while I struggled with this complicated language. Her patience and positive feedback were invaluable during some of my hardest semesters here, as I struggled to balance post-qualifying-exam motivation issues, research difficulties, wedding planning, teaching undergraduates, half-marathon training, and mentoring a visiting student. Of course, learning Polish would not have been as smooth or as fun without my classmates throughout the three years of classes: Jill, Sandy, Justin, Zach, Kevin, Ellie, and Jackie.

Not all my time was spent outside the lab—I somehow managed to put together this dissertation. Chaeyoung, Nikos, Kris, Eric, Lin, Stefan, and Mara were all great guides at various points in my PhD, but especially in the beginning when I had no idea what I was doing. Later on, Adam and Julie joined the Energy Biosciences Institute and made our relatively lonely lab much friendlier with our many lunches together (also with Lin) in the Energy Biosciences Building and in Downtown Berkeley. I always knew I could count on Adam when I needed help setting something

up in lab and Julie was there for me when I was struggling with a transition between projects. I also had the opportunity to mentor two students: Hsiang-Sheng and Montana. Hsiang-Sheng is an enthusiastic and hard-working researcher and I consider myself very fortunate to have had the opportunity to work with him and get to know him. I have no doubt that he will continue to do great research in the future. Montana worked with me for a summer and, while I was unable to include his work in this dissertation, I appreciate his dedication and patience and the lessons he taught me about mentoring.

Finally, I would like to thank my two advisors Alex and Nitash. They showed me how to take a problem and ask the right questions to break it down into manageable pieces. They always challenged me to dig a little deeper and realize the underlying reasons behind my findings. Communication is paramount to both of them, so they helped me improve my technical communication skills in conversations, written manuscripts, and formal oral presentations. They also fostered two excellent research groups, full of talented people studying a wide variety of subjects who were always willing to support their colleagues. The relationships formed in these groups were more akin to family than coworkers. Under their guidance, I have matured immensely as a researcher.

Chapter 1: Introduction

1.1 Uses and Source of Furfural

Furfural, or 2-furaldehyde, is a biomass-derived platform molecule that can be used for the production of chemicals. Fuels can be produced, *e.g.* by conversion of furfural to 2-methylfuran and subsequent trimerization and hydrodeoxygenation.[1-11] Polymers can also be made from furfural-derived 2-methylfuran, or by transforming furfural into γ-valerolactone, followed by coupling with formaldehyde to create α-methylene-γ-valerolactone, a monomer similar to methyl methacrylate.[12-16] Solvents, such as γ-valerolactone and tetrahydrofuran can also be derived from furfural.[5,15-17] Furthermore, furfural can be used to synthesize high-value chemicals, such as lubricants[9,16,18] and the pharmaceutical precursors cyclopentanol and cyclopentanone.[16,18,19]

The hemicellulose fraction of lignocellulosic biomass is the source of furfural. A particularly desirable form of biomass is *Miscanthus* × *giganteus* because it requires no irrigation, gives a high biomass yield per hectare, and protects the soil on which it is grown against soil erosion.[20,21] A significant fraction (20-40% by mass) of *Miscanthus* is hemicellulose, an amorphous polysaccharide comprised of a backbone of five-carbon, xylose monomers and side chains of four other sugars – arabinose, glucose, mannose, and galactose. Xylose can be obtained from hemicellulose by hydrolysis catalyzed by, for example, dilute sulfuric acid.[10-12,22,23]

Xylose can be dehydrated to furfural. This reaction typically takes place in water at temperatures of 130-240 °C and is catalyzed by Brønsted acids (most commonly mineral acids such as sulfuric acid and hydrochloric acid).[6,23,24] Alternatively, Lewis acids can be used to promote the isomerization of xylose to form lyxose and xylulose, the latter of which undergoes dehydration to furfural more readily, enabling reduction of the reaction temperature to as low as 100 °C.[25-29] Regardless of the catalyst used, xylose dehydration is accompanied by side reactions involving the condensation of furfural with reaction intermediates as well as with furfural itself to form a collection of aqueous-soluble and insoluble products known as humins.[23,30,31] Humins are a complex set of compounds varying broadly in molecular weight and having many oxygen-containing functional groups (*e.g.*, carbonyls and alcohols), as well as a conjugated molecular structure stemming from numerous linked furan rings.[32,33]

1.2 Production of Furfural

The Quaker Oats Company has manufactured furfural for nearly a century (since 1921). Their batch process utilizes steam to heat oat hulls (containing hemicellulose) and aqueous sulfuric acid to 153 °C for 5 h.[30] Sulfuric acid catalyzes the depolymerization of polysaccharides and their subsequent dehydration to form furfural in a single reactor. The steam not only heats the reactors, but also strips furfural from the liquid as it is produced, thereby mitigating the formation of humins. The steam/furfural mixture is then separated in an azeotropic distillation column, decanted, and the furfural-rich phase is further purified by passage through a dehydration column, resulting in the retention of 40-52% of the theoretical yield furfural with a final moisture content of 29-54%.[30]

The commercial production of furfural today has not changed dramatically from the original Quaker Oats process; steam stripping is still the dominant method of furfural extraction. Reactions are carried out in both batch and continuous reactors aided with 30 tons of steam per ton

of furfural produced (prior to purification downstream of the reactor). The reactor is typically loaded with about 25-33 wt% lignocellulosic biomass (*e.g.* corn cobs and bagasse, not just oat hulls) and 3 wt% sulfuric acid, yielding 40-70% of the theoretical furfural yield.[6,12,18,24] Residence times have decreased to between 3 h (operating at 170-185 °C) and 5-60 s (operating at 230-250 °C).[12]

On the laboratory scale, researchers have explored the use of liquid-liquid extraction (LLE) with organic solvents to minimize production of humins. Solvents include toluene,[34-39] methyl isobutyl ketone,[39-43] various alcohols,[42,43] dichloromethane,[42] tetrahydrofurans,[43-45] and cyclopentyl methyl ether.[46-48] The solvents are used in large quantities (typical organic:aqueous volume ratio is 2, but can be as high as 5.5)[39] in order to increase furfural partitioning into the organic phase, and thereby decrease its concentration in the reactive, aqueous phase. As with steam stripping, LLE increases the furfural yield beyond what is achievable without extraction, in rare cases approaching 100%.[46] However, both these processes result in the dilution of furfural in the product phase. With steam stripping, the product stream obtained is commonly about 3 wt% furfural.[12] With LLE, furfural is often diluted because of an organic:aqueous volume ratio greater than 1 and constitutes approximately only 1.5 wt% of the organic phase. Dilution can be avoided, however, by using an extraction method that concentrates furfural in the product phase, such as pervaporation.

1.3 Pervaporation

Pervaporation, a combination of "permeation" and "evaporation," is a membrane process that uses a non-porous, semi-permeable membrane separating a feed-side liquid from a permeate-side vapor. This phase change (evaporation) is caused by a reduction in the fugacity, or chemical potential, of permeants. A vacuum pump is often used for this purpose, although a sweep gas may be used instead. Both approaches reduce the partial pressure, and thus the fugacity, of permeants, providing the thermodynamic driving force for permeation. Permeants cross the membrane *via* the solution-diffusion mechanism: they absorb into the membrane from the feed liquid, diffuse across the membrane, and desorb from the membrane into the permeate vapor. [49,50]

Pervaporation has been used for separation of an organic from an aqueous solution and *vice versa*; examples being the selective removal of water from equilibrium-limited transesterification reactors[51-54] or biofuels from product-inhibited fermenters.[55-59] Commercially, pervaporation is most often used to dehydrate concentrated ethanol solutions in order to circumvent the water-ethanol azeotrope.[50] Despite the five-fold difference in molecular weight between water and furfural (18 g/mol and 96 g/mol, respectively), researchers have successfully permeated the latter selectively,[60-66] resulting in as high as a 47-fold increase in furfural concentration in the permeate relative to the feed.[61] Membranes used to separate organics from aqueous solutions are predominantly made of polydimethylsiloxane (PDMS),[50,67] although other materials such as polyurethaneurea,[61,62] ZIF-8-PMPS nanocomposite,[63] and a PDMS-based block copolymer[65,66] have been similarly successful. Pervaporation may be used to extract furfural as it is produced and concentrate it in the permeate, in contrast to steam stripping and LLE which both dilute furfural in the product.

1.4 Outline of Dissertation

The overall goal of this work was to demonstrate the feasibility of pervaporation as a means for extracting furfural during its production. This was accomplished by designing and building membrane reactors, utilizing them to understand simultaneous furfural production and pervaporation, assessing membrane-reactor design, and understanding how unconventional, Lewis acid catalysts may improve compatibility between reaction conditions and pervaporation-membrane limitations, as well as lead to novel products.

Chapter 2 begins this investigation with an experimental demonstration of the pervaporation-assisted reactor concept for furfural production. The performance of this reaction, catalyzed by a Brønsted acid, is compared to that of an LLE-assisted reaction using three metrics: furfural yield, concentration of extracted furfural, and amount of furfural extracted. The reaction is then simulated to predict performance for experimentally inaccessible durations.

Chapter 3 builds upon the insights gained from Chapter 2 to improve the membrane reactor design and enable a continuous reaction under milder conditions, catalyzed by a salt that upon dissolution produces both Lewis and Brønsted acidity. This reactor uses very little catalyst, takes in a stream of aqueous xylose solution, and puts out a stream of aqueous furfural vapor. Reaction in batch and continuous pervaporation-assisted modes are then simulated to study the effects of pervaporation rate on furfural yield, permeate concentration, reaction selectivity, and production rate.

Chapter 4 discussed the use of a Lewis acid catalyst to create novel chemicals from xylose and glucose. These chemicals are identified through extensive analytical chemistry and are quantified, and the reaction pathways that lead to their formation are proposed based on insights from analogous work published in the literature. These new products are hydroxyl-rich carboxylic acids and furanone esters that form by structural isomerization of xylose and glucose and subsequent dehydration. These acids and esters may further increase the versatility of biomass as a feedstock for value-added chemicals, *e.g.* as monomers for the synthesis of hyperbranched polymers. Typical biodegradable polyesters, which are often used for sutures and controlled drug delivery, are improved by copolymerization with acids (*e.g.*, gluconic acid) to increase biocompatibility.[68-71] The acids identified in this chapter may also be useful in this way, since they contain similar functional groups as gluconic acid.

1.5 References

1. G. W. Huber, J. N. Chheda, C. J. Barrett and J. A. Dumesic, *Science*, 2005, **308**, 1446-1450.
2. D. M. Alonso, J. Q. Bond and J. A. Dumesic, *Green Chem.*, 2010, **12**, 1493.
3. A. Corma, O. de la Torre, M. Renz and N. Villandier, *Angew. Chem.*, 2011, **50**, 2375-2378.
4. M. Balakrishnan, E. R. Sacia and A. T. Bell, *ChemSusChem*, 2014, **7**, 1078-1085.
5. J. J. Bozell and G. R. Petersen, *Green Chem.*, 2010, **12**, 539.
6. J. P. Lange, E. van der Heide, J. van Buijtenen and R. Price, *ChemSusChem*, 2012, **5**, 150-166.
7. G. A. Tompsett, N. Li and G. W. Huber, in *Thermochemical Processing of Biomass: Conversion into Fuels, Chemicals and Power*, ed. R. C. Brown, John Wiley & Sons, Ltd, Chichester, UK, First edn., 2011, ch. 8, pp. 232-279.
8. F. K. Kazi, A. D. Patel, J. C. Serrano-Ruiz, J. A. Dumesic and R. P. Anex, *Chem. Eng. J.*, 2011, **169**, 329-338.
9. M. Balakrishnan, E. R. Sacia, S. Sreekumar, G. Gunbas, A. A. Gokhale, C. D. Scown, F. D. Toste and A. T. Bell, *Proc. Natl. Acad. Sci. U. S. A.*, 2015, **112**, 7645-7649.
10. G. Dautzenberg, M. Gerhardt and B. Kamm, *Holzforschung*, 2011, **65**.
11. G. W. Huber, S. Iborra and A. Corma, *Chem. Rev.*, 2006, **106**, 4044-4098.
12. A. S. Mamman, J.-M. Lee, Y.-C. Kim, I. T. Hwang, N.-J. Park, Y. K. Hwang, J.-S. Chang and J.-S. Hwang, *Biofuels, Bioprod. Bioref.*, 2008, **2**, 438-454.
13. F. B. Oliveira, C. Gardrat, C. Enjalbal, E. Frollini and A. Castellan, *J. Appl. Polym. Sci.*, 2008, **109**, 2291-2303.
14. A. Gandini and M. N. Belgacem, *Prog. Polym. Sci.*, 1997, **22**, 1203-1379.
15. D. M. Alonso, S. G. Wettstein and J. A. Dumesic, *Green Chem.*, 2013, **15**, 584.
16. K. Yan, G. Wu, T. Lafleur and C. Jarvis, *Renewable Sustainable Energy Rev.*, 2014, **38**, 663-676.
17. L. Bui, H. Luo, W. R. Gunther and Y. Roman-Leshkov, *Angew. Chem. Int. Ed.*, 2013, **52**, 8022-8025.
18. R. Mariscal, P. Maireles-Torres, M. Ojeda, I. Sádaba and M. López Granados, *Energy Environ. Sci.*, 2016, **9**, 1144-1189.
19. M. Hronec, K. Fulajtarová and T. Liptaj, *Appl. Catal., A*, 2012, **437-438**, 104-111.
20. C. Somerville, H. Youngs, C. Taylor, S. C. Davis and S. P. Long, *Science*, 2010, **329**, 790-792.
21. N. Brosse, A. Dufour, X. Meng, Q. Sun and A. Ragauskas, *Biofuels, Bioprod. Bioref.*, 2012, **6**, 580-598.
22. C. E. Wyman, B. E. Dale, R. T. Elander, M. Holtzapple, M. R. Ladisch and Y. Y. Lee, *Bioresour. Technol.*, 2005, **96**, 1959-1966.
23. B. Danon, G. Marcotullio and W. de Jong, *Green Chem.*, 2014, **16**, 39-54.
24. C. M. Cai, T. Zhang, R. Kumar and C. E. Wyman, *J. Chem. Technol. Biotechnol.*, 2014, **89**, 2-10.
25. V. Choudhary, A. B. Pinar, S. I. Sandler, D. G. Vlachos and R. F. Lobo, *ACS Catal.*, 2011, **1**, 1724-1728.
26. V. Choudhary, S. I. Sandler and D. G. Vlachos, *ACS Catal.*, 2012, **2**, 2022-2028.
27. V. Choudhary, S. Caratzoulas and D. G. Vlachos, *Carbohydr. Res.*, 2013, **368**, 89-95.
28. K. R. Enslow and A. T. Bell, *Catal. Sci. Technol.*, 2015, **5**, 2839-2847.

29. J. B. Binder, J. J. Blank, A. V. Cefali and R. T. Raines, *ChemSusChem*, 2010, **3**, 1268-1272.
30. K. J. Zeitsch, *The Chemistry and Technology of Furfural and its Many By-Products*, Elsevier Science, Amsterdam, 2000.
31. J. M. J. Antal, T. Leesomboon, W. S. Mok and G. N. Richards, *Carbohydr. Res.*, 1991, **217**, 71-85.
32. I. van Zandvoort, Y. Wang, C. B. Rasrendra, E. R. van Eck, P. C. Bruijnincx, H. J. Heeres and B. M. Weckhuysen, *ChemSusChem*, 2013, **6**, 1745-1758.
33. S. Wang, H. Lin, Y. Zhao, J. Chen and J. Zhou, *J. Anal. Appl. Pyrolysis*, 2016, **118**, 259-266.
34. A. S. Dias, S. Lima, P. Brandão, M. Pillinger, J. Rocha and A. A. Valente, *Catal. Lett.*, 2006, **108**, 179-186.
35. S. Lima, A. Fernandes, M. M. Antunes, M. Pillinger, F. Ribeiro and A. A. Valente, *Catal. Lett.*, 2010, **135**, 41-47.
36. H. Gao, H. Liu, B. Pang, G. Yu, J. Du, Y. Zhang, H. Wang and X. Mu, *Bioresour. Technol.*, 2014, **172**, 453-456.
37. N. K. Gupta, A. Fukuoka and K. Nakajima, *ACS Catal.*, 2017, **7**, 2430-2436.
38. C. García-Sancho, J. M. Rubio-Caballero, J. M. Mérida-Robles, R. Moreno-Tost, J. Santamaría-González and P. Maireles-Torres, *Catal. Today*, 2014, **234**, 119-124.
39. S. Peleteiro, V. Santos and J. C. Parajo, *Carbohydr. Polym.*, 2016, **153**, 421-428.
40. R. Weingarten, J. Cho, J. W. C. Conner and G. W. Huber, *Green Chem.*, 2010, **12**, 1423.
41. H. Li, A. Deng, J. Ren, C. Liu, W. Wang, F. Peng and R. Sun, *Catal. Today*, 2014, **234**, 251-256.
42. J. N. Chheda, Y. Román-Leshkov and J. A. Dumesic, *Green Chem.*, 2007, **9**, 342.
43. H. Amiri, K. Karimi and S. Roodpeyma, *Carbohydr. Res.*, 2010, **345**, 2133-2138.
44. R. Xing, W. Qi and G. W. Huber, *Energy Environ. Sci.*, 2011, **4**, 2193.
45. W. Wang, J. Ren, H. Li, A. Deng and R. Sun, *Bioresour. Technol.*, 2015, **183**, 188-194.
46. M. J. Campos Molina, R. Mariscal, M. Ojeda and M. Lopez Granados, *Bioresour. Technol.*, 2012, **126**, 321-327.
47. S. Le Guenic, F. Delbecq, C. Ceballos and C. Len, *J. Mol. Catal. A: Chem.*, 2015, **410**, 1-7.
48. Y. Wang, F. Delbecq, W. Kwapinski and C. Len, *Mol. Catal.*, 2017, **438**, 167-172.
49. J. Wijmans and R. W. Baker, *J. Membr. Sci.*, 1995, **107**, 1-21.
50. R. W. Baker, *Membrane Technology and Applications*, John Wiley & Sons Ltd, The Atrium, Southern Gate, Chichester, West Sussex, P19 8SQ, United Kingdom, 2012.
51. M. T. Sanz and J. Gmehling, *Chem. Eng. J.*, 2006, **123**, 1-8.
52. K. L. Wasewar, S. Patidar, V. K. Agarwal, A. Rathod, S. S. Sonawane, R. V. Agarwal, H. Uslu and I. Inci, *Int. J. Chem. React. Eng.*, 2010, **8**, A57.
53. F. Zhang, M. E. Rezac, S. Majumdar, P. Kosaraju and S. Nemser, *Sep. Sci. Technol.*, 2014, **49**, 1289-1297.
54. Y. Han, E. Lv, L. Ma, J. Lu, K. Chen and J. Ding, *Energy Convers. Manage.*, 2015, **106**, 1379-1386.
55. G. Liu, W. Wei, H. Wu, X. Dong, M. Jiang and W. Jin, *J. Membr. Sci.*, 2011, **373**, 121-129.
56. W. Van Hecke, T. Hofmann and H. De Wever, *Bioresour. Technol.*, 2013, **129**, 421-429.

57. C. Chen, Z. Xiao, X. Tang, H. Cui, J. Zhang, W. Li and C. Ying, *Bioresour. Technol.*, 2013, **128**, 246-251.
58. C. Shin, Z. C. Baer, X. C. Chen, A. E. Ozcam, D. S. Clark and N. P. Balsara, *J. Membr. Sci.*, 2015, **484**, 57-63.
59. C. Fu, D. Cai, S. Hu, Q. Miao, Y. Wang, P. Qin, Z. Wang and T. Tan, *Bioresour. Technol.*, 2016, **200**, 648-657.
60. M. Sagehashi, T. Nomura, H. Shishido and A. Sakoda, *Bioresour. Technol.*, 2007, **98**, 2018-2026.
61. U. K. Ghosh, N. C. Pradhan and B. Adhikari, *Desalination*, 2007, **208**, 146-158.
62. U. K. Ghosh, N. C. Pradhan and B. Adhikari, *Desalination*, 2010, **252**, 1-7.
63. X. Liu, H. Jin, Y. Li, H. Bux, Z. Hu, Y. Ban and W. Yang, *J. Membr. Sci.*, 2013, **428**, 498-506.
64. F. Qin, S. Li, P. Qin, M. N. Karim and T. Tan, *Green Chem.*, 2014, **16**, 1262.
65. D. R. Greer, T. P. Basso, A. B. Ibanez, S. Bauer, J. M. Skerker, A. E. Ozcam, D. Leon, C. Shin, A. P. Arkin and N. P. Balsara, *Green Chem.*, 2014, **16**, 4206-4213.
66. D. R. Greer, A. E. Ozcam and N. P. Balsara, *AIChE J.*, 2015, **61**, 2789-2794.
67. L. M. Vane, *J. Chem. Technol. Biotechnol.*, 2005, **80**, 603-629.
68. M. Tang, A. F. Haider, C. Minelli, M. M. Stevens and C. K. Williams, *J. Polym. Sci., Part A: Polym. Chem.*, 2008, **46**, 4352-4362.
69. K. Marcincinova-Benabdillah, M. Boustta, J. Coudane and M. Vert, *Biomacromolecules*, 2011, **2**, 1279-1284.
70. A. F. Haider and C. K. Williams, *J. Polym. Sci., Part A: Polym. Chem.*, 2008, **46**, 2891-2896.
71. B. Witholt and B. Kessler, *Curr. Opin. Biotechnol.*, 1999, **10**, 279-285.

Chapter 2: Pervaporation-Assisted Catalytic Conversion of Xylose to Furfural

Abstract

Furfural produced from the biomass-derived xylose may serve as a platform molecule for sustainable fuel production. The Brønsted acid-catalyzed dehydration of xylose to furfural is plagued by side reactions that form a set of soluble and insoluble degradation products, collectively known as humins, which reduce the yield of furfural. The formation of humins can be minimized by removal of furfural, either by steam stripping or by liquid-liquid extraction (LLE). However, both these techniques are very costly. The goal of this study was to demonstrate the feasibility of using pervaporation, a membrane process, to remove furfural as it is produced. A laboratory-scale reactor/membrane system was designed, built, and tested for this purpose and its performance for furfural production was compared with that achieved by carrying out the reaction with and without furfural extraction by LLE. Furfural production assisted by pervaporation (with a commercially available membrane or a triblock copolymer membrane) or LLE produced comparable amounts of furfural, and more than could be achieved by reaction without extraction. A model of the reaction kinetics and the rate of furfural extraction was fit to the pervaporation- and LLE-assisted furfural production data and was used to predict the performances of these processes at near-complete xylose conversion. Pervaporation is shown to have two advantages over LLE: pervaporation extracts a greater fraction of the furfural produced and the furfural concentration in the permeate phase is significantly higher than that present in the extractant phase obtained by LLE. It is noted that further improvement in the separation of furfural from the aqueous phase where it is produced can be achieved by using a more-permeable, thinner pervaporation membrane of larger area, and by operating the membrane at the reaction temperature.

2.1 Introduction

A significant component of lignocellulosic biomass is hemicellulose (20-40% by weight), a polysaccharide consisting primarily of xylose units.[1-3] Upon physical or chemical pretreatments, most notably with dilute sulfuric acid, hemicellulose depolymerizes to produce xylose.[3,4] Further treatment with dilute Brønsted acid results in the dehydration of xylose to furfural, a platform molecule for the production of gasoline, diesel, and jet fuel.[2,5-10]

The dehydration of xylose, most often in water, proceeds as shown in Scheme 2.1.[4,10,11] During this process, side reactions that consume xylose and furfural detract significantly from the furfural yield. These side reactions produce soluble and insoluble humic substances, or humins.[4,11-13] Industrial manufacturers of furfural have improved furfural yields and minimized humins production through furfural extraction by continuous steam stripping.[1,11,12] More recently, higher furfural yields have been achieved by liquid-liquid extraction (LLE) with an organic phase, such as toluene,[14-16] methyl isobutyl ketone,[17-19] various alcohols,[18,19] dichloromethane,[18]

This chapter was reported in *Green Chemistry*, 2016, **18**, 4073-4085 and is adapted with permission from co-authors Nitash P. Balsara and Alexis T. Bell.

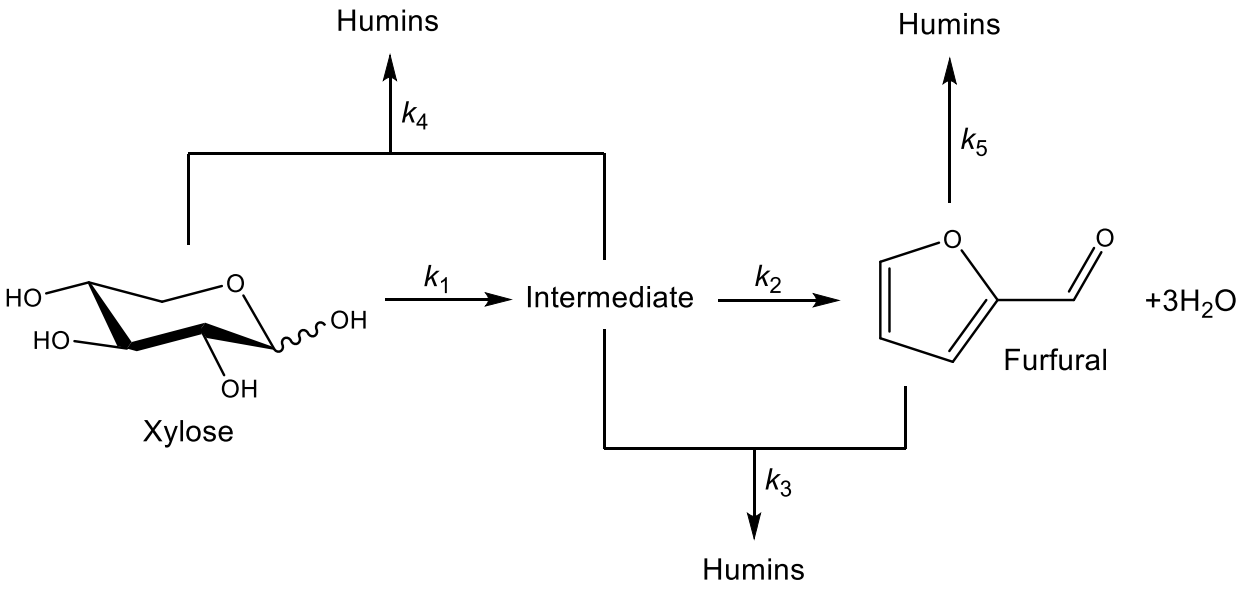

Scheme 2.1. Reaction network for furfural production from xylose

tetrahydrofurans,[19-21] or cyclopentyl methyl ether.[22,23] Both forms of furfural extraction (*i.e.*, steam stripping and LLE) improve the yield of furfural, but introduce significant processing costs. Steam stripping requires approximately 30 tons of steam per ton of furfural produced[10,12] while LLE utilizes large volumes of organic solvents, with organic:aqueous volume ratios reaching as high as 3.7.[18] Moreover, both processes significantly dilute the furfural, necessitating downstream furfural purification. These costly furfural separation processes limit its potential as a cost-competitive fuel precursor,[10,12] indicating that cheaper and more energy efficient production processes must be developed. An attractive option for meeting this challenge is pervaporation.

Pervaporation is a membrane-based process in which a liquid mixture contacts the feed side of a membrane while a vacuum is maintained on the permeate side. The vacuum reduces the chemical potential of the permeating components below their respective chemical potentials in the feed liquid, thus providing the driving force for mass transfer. Pervaporation has been used to separate organic compounds from water,[24-28] and is currently used commercially to remove water from concentrated ethanol solutions.[29] Membranes suitable for the selective pervaporation of furfural have also been reported.[30-35] Furfural separation by pervaporation has a noteworthy advantage over steam stripping and LLE: both of the latter two processes significantly dilute furfural in the product stream, whereas pervaporation concentrates furfural in the permeate, provided a furfural-selective membrane is used. This eases the downstream purification of furfural, and is expected to reduce overall production costs. In the present study, we demonstrate that pervaporation is a promising extraction process for the production of furfural and offers advantages over LLE.

2.2 Experimental Methods

2.2.1 Materials

D-(+)-xylose (≥99%), furfural (99%), toluene (≥99.5%), dodecane (99%), and cyclohexane (≥99%) were purchased from Sigma-Aldrich and used as received. Amberlyst 70, an ion-exchange resin donated by Dow Chemical Co., was washed with nanopure water until the pH of the supernatant was >5.5, then dried overnight at 80 °C in a vacuum oven. The concentration of acid sites on Amberlyst 70 was confirmed to be equal to the manufacturer's reported value of 2.55 eq H^+/kg by H^+/Na^+ exchange with NaCl solution, then titration of the resulting acidic supernatant with NaOH solution using phenolphthalein as the indicator. Cross-linked polydimethylsiloxane (PDMS) thin-film composite membranes were purchased from Pervatech and had a 130 µm-thick polyethylene terephthalate support layer, a 100 µm-thick polyisoprene intermediate ultrafiltration membrane layer, and a 3-5 µm-thick pervaporation PDMS layer (4 µm was used in all calculations requiring membrane thickness). These membranes were received as sheets and were cut to fit the membrane cell. The block copolymer polystyrene-*block*-polydimethylsiloxane-*block*-polystyrene (SDS), which was previously shown to be permeable to furfural,[36] was purchased from Polymer Source and was used as received. The number-averaged molecular weight of the polydimethylsiloxane block is 104 kg/mol, and that of the polystyrene blocks is 22 kg/mol. The dispersity of the polymer sample is 1.3, and 86 wt% of the sample is the triblock copolymer with the balance being mostly diblock copolymer.

2.2.2 SDS Membrane Preparation

A solution consisting of 1 g of SDS dissolved in 20 mL of cyclohexane was used to prepare each solvent-cast SDS membrane. The solution was poured onto a 100 mm polytetrafluoroethylene (PTFE) evaporation dish (Fisher, 02-617-148), which was covered and allowed to dry in a fume hood for three days. The resulting membrane was then peeled off the dish, sandwiched between two filter papers, and cut to fit the pervaporation cell. The thickness of each solvent cast membrane was measured at 15 points by a micrometer and the mean thickness was found to be 120 µm.

A solution consisting of 0.8 g of SDS dissolved in 8 mL of cyclohexane was used to prepare each spin-coated SDS membrane. The solution was deposited onto a 10 cm × 10 cm square of Biomax 50 PBQK polyethersulfone nanofiltration support membrane taped to a 3 in diameter silicon wafer and then spun at 300 rpm for one minute. The membrane was then covered, allowed to dry in a fume hood for one day, then cut to fit the membrane cell. The thicknesses of the SDS layers of the spin-coated membranes were determined by pervaporation of DI water at 75 °C. The thickness of these membranes was determined by equating the products of membrane thickness times DI water flux for the spin-cast membranes of unknown thickness to that of a 120 µm-thick solvent-cast membrane. By this means the average thickness of the spin-cast membranes was found to be 4.8 µm.

2.2.3 Xylose Dehydration

Batch reactions without simultaneous product separation by pervaporation were carried out in 10 mL thick-walled glass vials (Sigma-Aldrich, 27198) sealed with PTFE/silicone crimp top septa (Agilent, 8010-0420) and immersed in a silicone oil bath. Separate reactors were used for each reaction time. The temperature of the oil bath was maintained with a magnetic-stirring

hotplate (Sigma-Aldrich, Z645060). Reactor contents were stirred using PTFE-coated stir bars rotating at a rate of 600 rpm. When LLE was not conducted, each reactor received 4 mL of the reactant solution comprising 375 μmol/mL xylose in water and 52.3 mg/mL Amberlyst 70 (equivalent to 133 mM H^+ based on the liquid volume). When *in situ* LLE was conducted, each reactor received 2 mL of the reactant solution and 4 mL of toluene. Upon completion of the reaction, the reactors were removed from the oil bath and quenched in an ice bath. An aliquot of each phase (water and toluene, if applicable) was removed from the reactor for analysis by high-performance liquid chromatography (HPLC) or gas chromatography-mass spectroscopy (GC-MS). An internal standard (5 mg/mL dodecane in toluene) was added to toluene-phase samples prior to analysis by GC-MS.

Reactions with simultaneous product separation by pervaporation were carried out in a custom-built apparatus, shown schematically in Figure 2.1. This reactor was a stirred stainless steel autoclave equipped with 40-μm-fritted dip tubes (Parr, 4564). The reactor was heated with a heating mantle controlled by a temperature controller (Parr, 4848). To carry out product pervaporation, the contents of the reactor were withdrawn through an inline filter with 2-μm pores and a shell-and-tube heat exchanger cooled with circulating water (Cole-Parmer, EW-12122-02) using a gear pump (Cole-Parmer, EW-74013-70) and passed through a custom-built membrane pervaporation cell, after which the retentate flowed past a sampling port, and was then directed back to the reactor. A thermocouple (Omega, TC-K-NPT-U-72) and temperature sensor (Omega, DP7002) were used to measure the temperature of the membrane. All components of the membrane reactor were connected by ¼-in stainless steel tubing and fittings to give a total available volume of 210 mL (150 mL in the autoclave and 60 mL in the rest of the unit). The tubing between the heat exchanger and the membrane thermocouple was wrapped in silicone heating tape (BriskHeat, HSTAT101010), which was not turned on. With the exception of the autoclave, the circulation pump, and the membrane cell, all components were wrapped in thermally insulating silicone tape (Sigma Aldrich, Z175633). Unless otherwise stated, all components of the membrane reactor were purchased from Swagelok. The interstage cooling provided by the shell-and-tube heat exchanger was used to keep the membrane at temperatures below the glass transition temperature (~100 °C) of the structural units of SDS (polystyrene), so as to maintain the mechanical stability of the membrane. The membrane module was a flat, circular cell made of polyether ether ketone (PEEK) in which the membrane was supported by a porous stainless steel frit and was restrained by an o-ring to obtain a permeation area of 37 cm^2. The feed entered the cell normal to the membrane at the center of the circular housing while the retentate exited the cell at a point on the circumference. The feed-side fluid within the cell was mixed by a custom-built PTFE-coated magnetic stirring bar suspended above the membrane surface. A vacuum of ≤3 mbar was maintained on the permeate side of the membrane using a vacuum pump (Welch, 2014). The permeate vapor was condensed in a cold trap (ChemGlass, CG-4516-02) cooled with liquid nitrogen.

At the start of each experiment, the membrane module was loaded with a new membrane (either PDMS or 4.8 μm-thick spin-coated SDS) and the reactor was filled with 180 mL of 375 μmol/mL xylose in water. At any given moment, 60 mL of solution were located outside the heated autoclave, *i.e.* in the rest of the unit, while the heated tank contained the remainder of the solution. The autoclave was also charged with 9.41 g Amberlyst 70 (equivalent to 133 mM H^+ based on the initial 180 mL in the reactor), all of which was kept in the autoclave by the fritted dip tubes. The circulation rate through the gear pump was set to 40 mL/min, the stirring rate in the tank was set to its maximum value of 690 rpm, and the stirring rate in the membrane cell was fixed at 120 rpm.

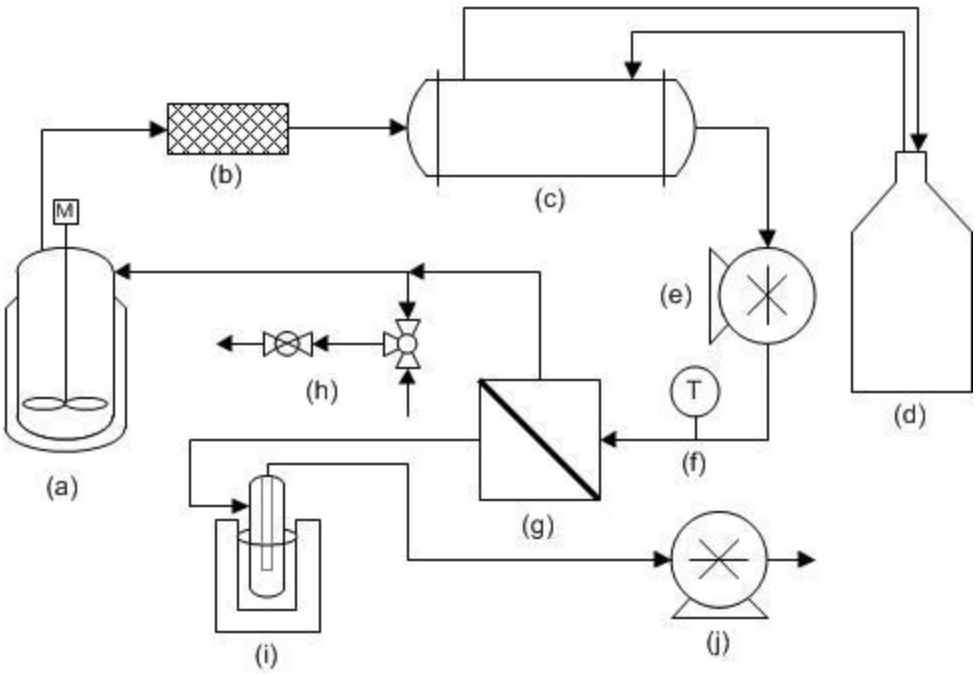

Figure 2.1. Pervaporation-assisted dehydration reactor featuring (a) a heated and stirred stainless steel tank reactor, (b) an inline filter, (c) a shell-and-tube heat exchanger, (d) a circulating cooling water bath, (e) a gear pump, (f) a thermocouple, (g) a flat membrane cell, (h) a sampling port, (i) a cold trap for permeate collection cooled by liquid nitrogen, and (j) a vacuum pump.

The steady-state temperature of the autoclave was 140 °C and the steady-state temperature of the membrane was 75 °C. The autoclave (which contained the catalyst) reached 132 °C by 20 min from the start of heating and circulation and it reached the reaction temperature of 140 °C by 40 min. The membrane reached 71 °C in 20 min, and 75 °C in 40 min.

The reactor was sampled using the sampling port, first taking a sample to flush the sampling port, then taking another sample for analysis. The total volume removed per sample was 1 mL, a small fraction of the total reactor volume (180 mL). The permeate was collected at the same time as the reactor was sampled by switching the accumulating cold trap with a fresh one. The thawed permeate was a single-phase mixture under the conditions used in this study. The accumulated cold trap was weighed and an aliquot was removed for analysis. The total flow rate through the membrane was about 18 g/h when using PDMS membranes and about 12 g/h when using SDS membranes.

2.2.4 Equilibrium Distribution of Furfural

The equilibrium distribution of furfural between water and toluene was measured by filling 10 mL thick-walled glass vials (Sigma-Aldrich, 27198) with 4 mL of toluene, 2 mL of aqueous furfural solution, and a PTFE-coated stir bar. Each vial was matched to a time point from the LLE-assisted reactions with the total furfural in each vial corresponding to the total furfural produced in its matched time point. The vials were then sealed with PTFE/silicone crimp top septa (Agilent, 8010-0420), shaken vigorously by hand for 10 s, then placed on a stir plate for one hour, with the stir bar rotating at 600 rpm. The vials were then opened and an aliquot of each phase was removed

for analysis by HPLC or GC-MS, with an internal standard (5 mg/mL dodecane in toluene) added to toluene-phase samples prior to analysis by GC-MS.

2.2.5 Product Analysis

Samples of the aqueous phase were analyzed by HPLC using an Ultra High Performance Liquid Chromatograph system (Shimadzu, Kyoto, Japan). 10 µL aliquots of the samples were injected onto a Phenomenex Rezex RFQ-Fast Acid H+ column (100 x 7.8 mm; 0.01 N H_2SO_4; 1.0 ml/min; 55 °C) equipped with a refractive index detector (RID). Product quantities were determined by converting integrated peak areas into concentrations using a 9-point calibration curve generated from standards created with analytical grade chemicals.

Samples of the organic phase from the LLE-assisted reactors were analyzed by GC-MS using a Varian CP-3800 Gas Chromatograph equipped with a FactorFour Capillary Column (UF-5ms 30 m, 0.25 mm, 0.25 µm, P/N CP8944) connected to a Varian quadrupole-mass spectrometer (MS) and flame ionization detector (FID). After product identification by mass spectrometry, product concentrations were determined from integrated FID peak areas using a 7-point calibration curve generated from standards created with analytical grade chemicals.

2.2.6 Calculations

Xylose conversions and furfural yields are reported as molar percentages relative to the initial moles of xylose and furfural, *i.e.*

$$\text{Conversion} = \frac{(\text{Initial moles of xylose}) - (\text{Remaining moles of xylose})}{(\text{Initial moles of xylose})} \times 100\% \quad (2.1)$$

$$\text{Yield} = \frac{(\text{Moles of furfural}) - (\text{Initial moles of furfural})}{(\text{Initial moles of xylose})} \times 100\% \quad (2.2)$$

The moles of xylose and furfural were calculated by multiplying the molar concentration of each species in a given phase by that phase's volume. In the case of reactions without simultaneous product separation by pervaporation, the phase volumes were assumed to be equal to their initial values. In the case of reactions with simultaneous product separation by pervaporation, the total initial liquid volume was assumed to be constant throughout the experiment. Any permeated mass collected in cold traps was converted to volume by assuming a density of 1 g/mL. That volume, in addition to that which was removed by the reactor sampler, was subtracted from the initial liquid volume to calculate the volume in the reactor at each time point.

For reactions conducted without a membrane, initial moles were determined by preparing and analyzing extra reactors (time = 0 min) as stated previously, but without heating in an oil bath. For reactions with a membrane, initial moles were taken to be those in the reactor and in the permeate 20 min after heating and circulation began when the autoclave reached at least 132 °C and the membrane reached at least 71 °C. Conversion of xylose and production of furfural were minimal in those first 20 min.

The equilibrium distribution of furfural is reported as the proportion of the total furfural loaded that was present in the toluene phase, *i.e.*

$$\text{Equilibrium distribution} = \frac{\text{Moles of furfural in toluene phase}}{\text{Total moles of furfural loaded in vial}} \times 100\% \quad (2.3)$$

The equilibrium distribution is related to the equilibrium constant *K*, defined as the ratio of furfural concentration in the toluene phase to the aqueous phase, and the toluene:water volume ratio *v*, as follows:

$$\text{Equilibrium distribution} = \frac{Kv}{Kv+1} \times 100\% \quad (2.4)$$

The molar permeation rate of component *i*, $\dot{n}_i$, in pervaporation is described as follows:[29,37]

$$\dot{n}_i = \frac{\Delta m_i}{M_i \Delta t} = A \cdot J_i = A \cdot \frac{P_i}{l}\left(x_i \gamma_i p_i^{\text{sat}} - y_i p_{\text{permeate}}\right) \quad (2.5)$$

where Δm_i is the change in mass of the permeate during the length of time Δt, M_i is the molecular weight, A is the area of the membrane, J_i is the molar flux, P_i is the permeability, l is the thickness of the membrane, x_i is the mole fraction in the liquid feed, γ_i is the activity coefficient in the liquid feed, p_i^{sat} is the saturation vapor pressure at the feed conditions, y_i is the mole fraction in the vapor permeate, and p_{permeate} is the total permeate pressure. Activity coefficients were assumed to be constant at 75 °C of water (1) and furfural (85), and were estimated from binary water-furfural vapor-liquid equilibrium data.[38] Saturation vapor pressures were determined by the Antoine equation, using constants calculated from binary water-furfural vapor-liquid equilibrium data.[38] Equation (2.5) was then used to calculate the membrane permeabilities of water and furfural.

All experiments in this study, with the exception of the equilibrium distribution of furfural measurement and the pervaporation experiments at approximately 115 °C, were duplicated. Each plot showing experimental data was constructed using the mean values for each time point, with the error bars representing the range of the two trials. Some error bars are not visible because the ranges for those time points are smaller than the symbols used in the plots. The data point at 120 min time for the LLE-assisted reaction has large error bars caused by significantly different results obtained during the two trials; however, the mean values shown coincide with the values one would expect, given the data points that precede them.

2.3 Results and Discussion

2.3.1 Comparisons of Furfural Production Methods

Xylose was dehydrated to form furfural in three reactor configurations: without extraction, with LLE, and with pervaporation using commercially available PDMS membranes. Xylose conversions and furfural yields from these experiments are shown in Figure 2.2a. All three sets of xylose conversion data followed the same trend, reaching approximately 31% conversion after 120 min when pervaporation was not used and 37% conversion after 120 min when pervaporation was used. The parity in conversion in reactors without extraction and with LLE indicates that LLE of furfural had no significant impact on the rate of xylose conversion. We attribute the increase in conversion when comparing reactions without pervaporation to reactions with pervaporation to the removal of water by the membrane; the liquid volume in the reactor decreased over time, leading

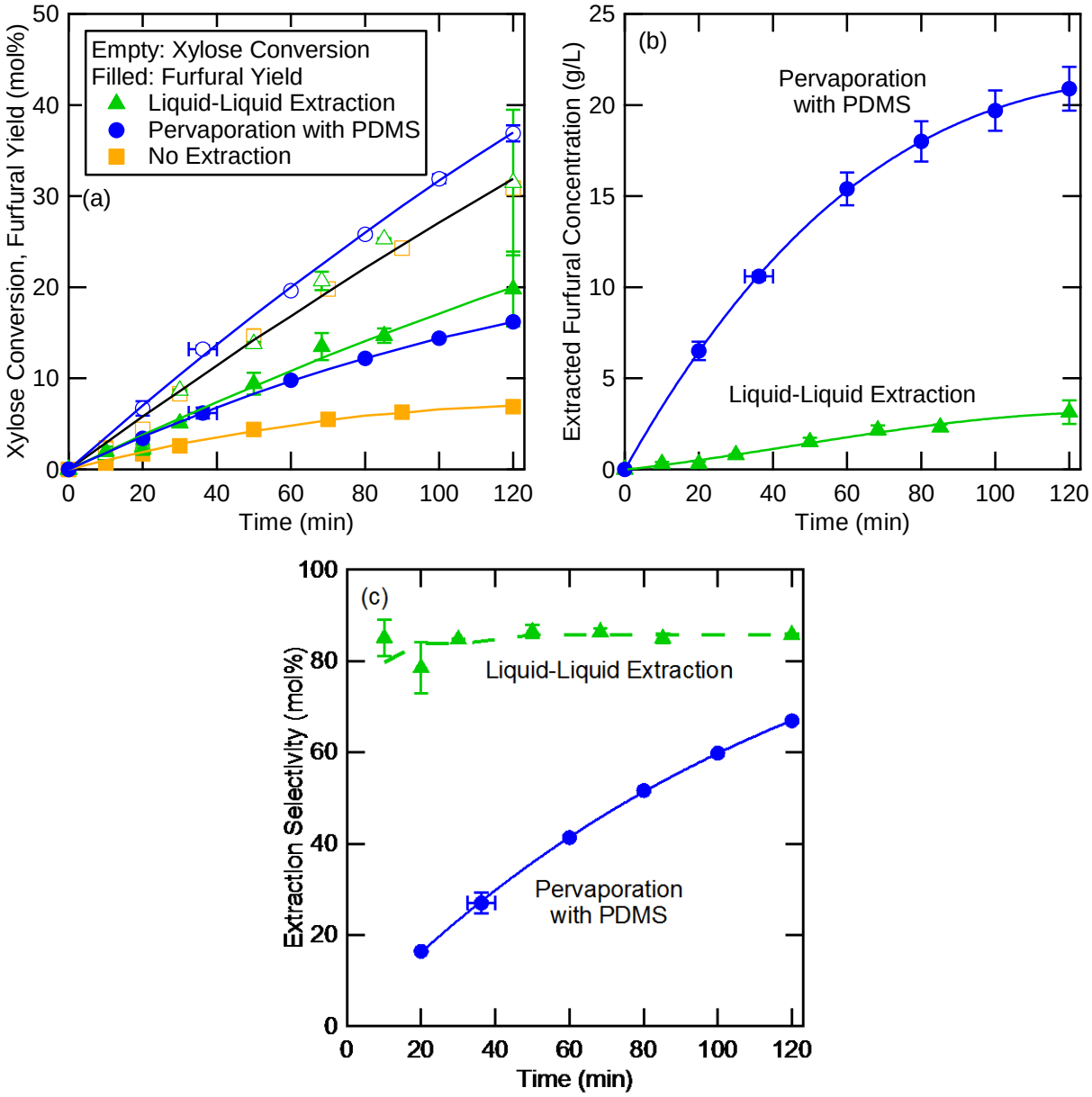

Figure 2.2. Comparison among furfural extraction configurations of (a) xylose conversion and furfural yield; (b) concentration of furfural in the extractant phase (toluene or permeate); and (c) extraction selectivity of furfural; during the conversion of 375 mM xylose to furfural at 140 °C with 133 mM H^+ from Amberlyst 70. Extraction configurations include liquid-liquid extraction (2:1 toluene:water by volume), pervaporation with a PDMS membrane, and no extraction. All curves are provided to guide the eye, with the exception of the dashed line in (c) representing the equilibrium distribution of furfural in 2:1 toluene:water by volume.

to higher concentrations of catalyst and xylose than would have been present at a given conversion in a constant-volume reactor, and consequently higher rates of xylose conversion. The furfural yield for all three systems increased monotonically over the course of 120 min, the highest yield of furfural being achieved with LLE, followed by pervaporation with PDMS membranes, and

finally the base case of no extraction. The higher furfural yield with either separation method demonstrates that both methods improve the furfural yield.

One important quantity to consider when comparing the two processes is the cumulative concentration of furfural in the extracted phase. As seen in Figure 2.2b, the furfural concentration in the permeate phase obtained by pervaporation with a PDMS membrane was 6 times higher that obtained in the extractant phase produced by LLE. The much higher furfural concentration produced by pervaporation was a consequence of using a furfural-selective membrane that more readily absorbed and transported furfural relative to water.

To quantify the effectiveness of extraction, we define an extraction selectivity in the following way:

$$\text{Extraction Selectivity} = \frac{\text{Moles of furfural extracted}}{\text{Total moles of furfural formed}} \times 100\% \qquad (2.6)$$

Extraction selectivity is bound by 0% and 100% since the denominator is composed of the extracted furfural and the furfural present in the reactive phase (*i.e.,* the aqueous phase in LLE-assisted reactions and the retentate in pervaporation-assisted reactions). We show extraction selectivity as a function of reaction time for reactions assisted by LLE and by pervaporation with a PDMS membrane in Figure 2.2c. Under the conditions employed in this study, extraction by LLE was more selective than by pervaporation; after 120 min of reaction, the extraction selectivity for LLE was 85% compared to 67% for pervaporation. Extraction selectivity in the case of LLE was constant with reaction time, whereas extraction selectivity for pervaporation increased monotonically with time.

The observed differences in extraction selectivity with reaction time can be attributed to differences in the extraction method. In the case of LLE, the aqueous and organic phases were not sampled during the reaction; the reactors were removed from the heated oil bath, quenched in an ice bath, and sampled after approximately one hour. The equality of the extraction selectivity for LLE-assisted reactions (data points in Figure 2.2c) and the measured equilibrium distribution indicates that the furfural had equilibrated between the two phases during LLE-assisted reaction at the time of sampling. What this means is that the extent of furfural partitioning into the toluene phase is governed solely by the equilibrium constant and the ratio of toluene to water volumes An increase in the toluene:water ratio would increase the LLE selectivity, but would also result in further dilution of furfural in the extracting phase. By contrast, the extraction selectivity for pervaporation increases monotonically with time, as it is governed by the rate of furfural permeation through the membrane relative to the rate of its formation by reaction.

2.3.2 Comparisons of Pervaporation Membranes

Additional pervaporation-assisted reactions were carried out using SDS triblock copolymer membranes, which have been shown previously to exhibit high furfural permeability.[34] The results achieved with these membranes are compared to those achieved using PDMS membranes in Figure 2.3. As demonstrated in Figure 2.3a, similar xylose conversions and furfural yields were obtained with either membrane type. However, both the concentration of furfural in the permeate (Figure 2.3b) and the extraction selectivity (Figure 2.3c) were higher when using SDS membranes rather than PDMS membranes. The permeate obtained using the SDS membrane reached a furfural concentration that was 62% higher than that attained using the PDMS membrane, indicating that

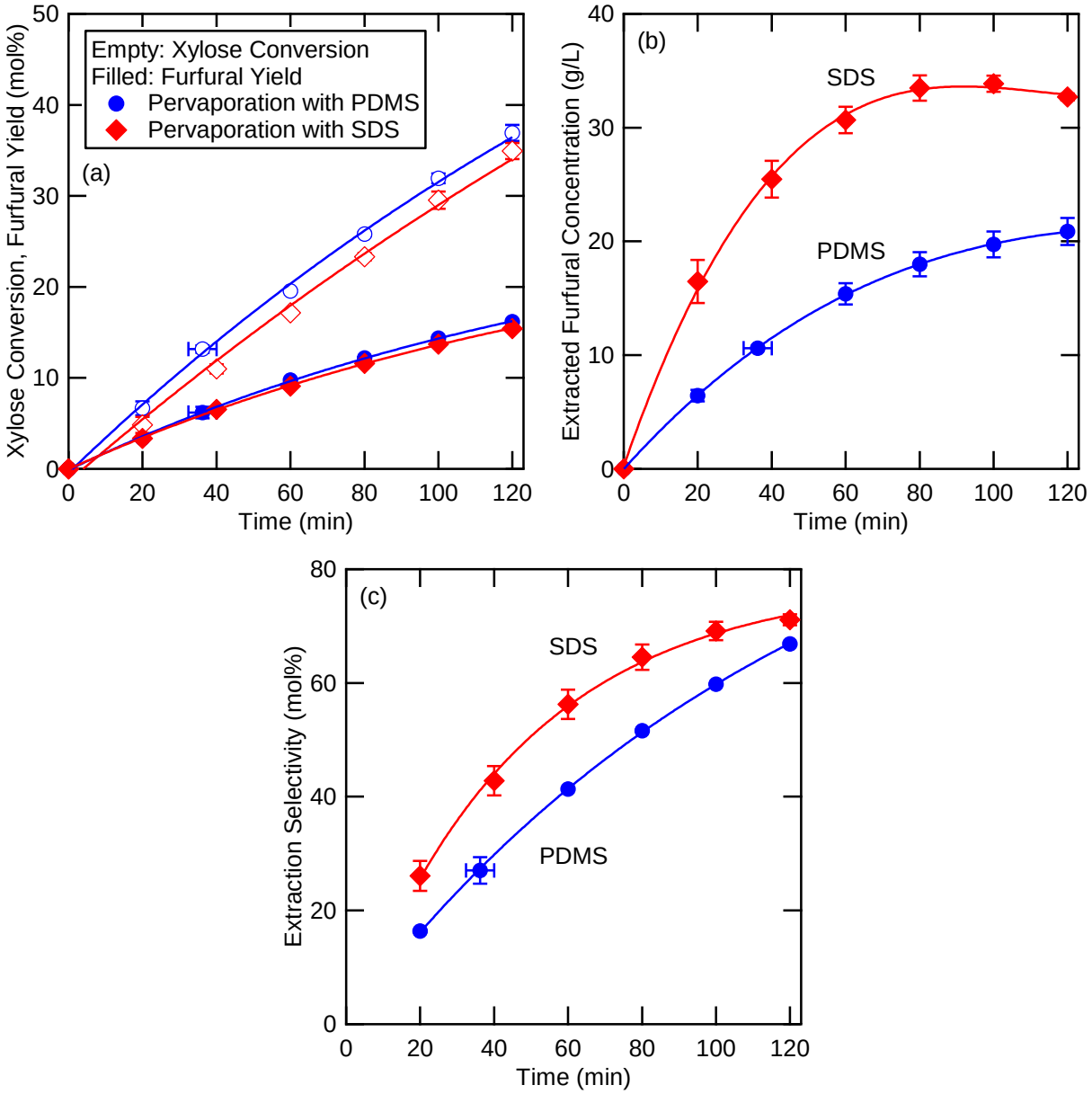

Figure 2.3. Comparison among PDMS or SDS membranes of (a) xylose conversion and furfural yield; (b) concentration of furfural in the permeate; and (c) extraction selectivity of furfural; during the pervaporation-assisted conversion of 375 mM xylose to furfural at 140 °C with 133 mM H^+ from Amberlyst 70. All curves are provided to guide the eye.

the SDS membrane has a higher selectivity for furfural over water. We also note that the extraction selectivity was 33% higher using the SDS membrane than the PDMS membrane, signifying that the rate of furfural mass transfer through the SDS membrane was higher and that a greater fraction of the furfural was transported into the permeate, leaving the concentration of furfural in the retentate lower. The reduced retentate furfural concentration reduced the formation of humins and, consequently, increased the reaction selectivity, as shown in Figure 2.3a; the furfural yields are matched across membranes, but the xylose conversion is slightly lower for the SDS membrane, resulting in a higher reaction selectivity. The observed difference is fairly minor, demonstrating

the relative insensitivity of furfural yield to changes in mass transfer coefficient. We, therefore, conclude that large improvements in furfural extraction rate are required to significantly increase the total furfural yield.

While SDS membranes exhibited better furfural permeability and selectivity than did PDMS membranes, the furfural permeability of SDS membranes decreased by nearly 50%, over the course of an experiment, whereas the furfural permeability of the PDMS membranes remained relatively constant, as is shown in Figure 2.4. In both cases, though, the water permeability remained unaffected. The decreasing furfural permeability through SDS membranes led to relatively slower furfural permeation rates at longer reaction times, resulting in a lower furfural yield and extraction selectivity compared to what could have been achieved had the furfural permeability remained constant. Since the water permeability did not change while the furfural permeability did, the permeate furfural concentration was also lower than what it could have been had the furfural permeability been constant. While the change in furfural permeability was clear, its effects on furfural yield, extraction selectivity, and permeate furfural concentration were rather subtle, reinforcing the notion that these metrics of reaction performance are relatively insensitive to changes in mass transfer rates.

It is possible that the lack of cross-links in SDS allowed the humins produced during the reaction to change its morphology, which may in turn have led to the selective decrease in furfural permeability through the membrane. Morphological changes have previously been shown to affect permeability, as was observed in PDMS-containing copolymers used for pervaporation of aqueous ethanol solutions[39,40] and in polystyrene-*block*-polybutadiene block copolymers used for permeation of CO_2 gas.[41] We intend to investigate this possibility in our systems in the future. If the PDMS cross-links were indeed responsible for maintaining constant furfural permeability, one might be able to replicate the effect in a triblock copolymer by cross-linking the structural block

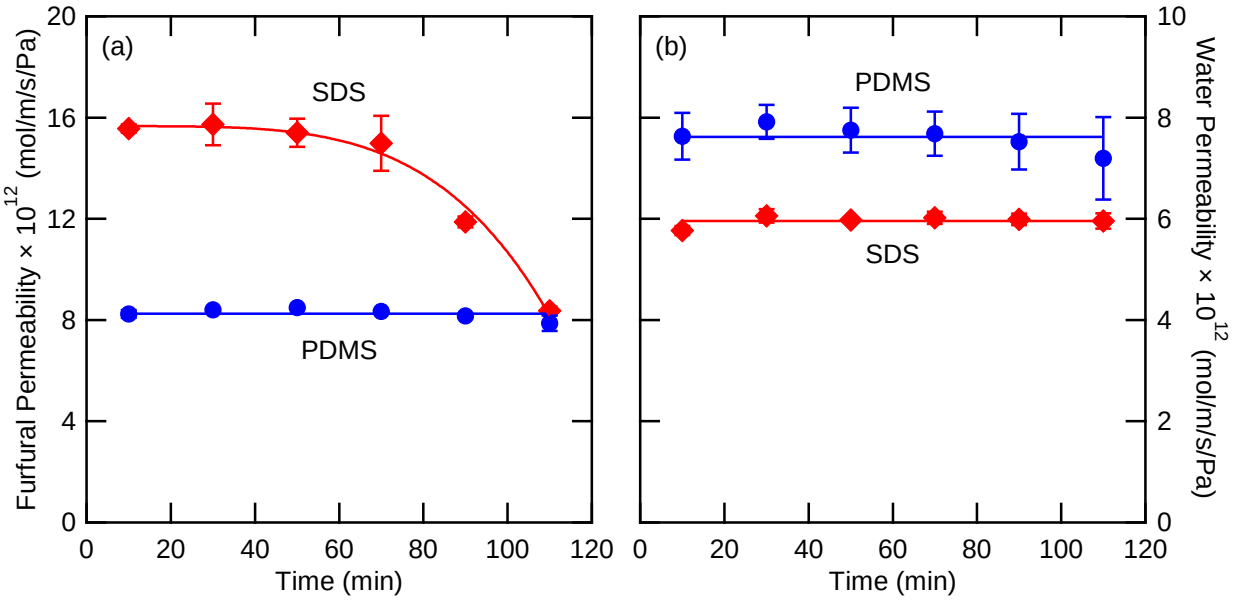

Figure 2.4. (a) Furfural and (b) water permeabilities of SDS and PDMS membranes during the pervaporation-assisted conversion of 375 mM xylose to furfural at 140 °C with 133 mM H^+ from Amberlyst 70. Each data point is representative of the 20 minute range starting 10 minutes before and ending 10 minutes after the point. All curves are provided to guide the eye.

(polystyrene in our case) while still leaving the transporting block (PDMS in our case) flexible. This may allow for the preservation of the high permeability of non-cross-linked PDMS, which was evident when comparing SDS to PDMS (see initial furfural permeabilities in Figure 2.4a), and the simultaneous incorporation of the resistance to morphological change from the cross-linked structural block.

2.3.3 Simulations of Reaction and LLE or Pervaporation

A theoretical model of simultaneous xylose dehydration and furfural extraction (by LLE or pervaporation) was developed in order to understand the effects of operating conditions on the achievable levels of furfural recovery. The set of equations we used in this model are provided in the Supporting Information. The reaction network outlined in Scheme 2.1 was used to model the reaction kinetics of the systems. It was assumed that the intermediates in the xylose-to-furfural conversion are in pseudo-steady state. For LLE-assisted reactions, only furfural was allowed to transfer between phases and the rate of mass transfer was assumed to be very rapid, resulting in an equilibrium distribution. For the pervaporation-assisted reactions, both furfural and water were allowed to permeate through the membrane. The mass transfer rate of each component was represented by Equation (2.5), with membrane permeabilities calculated from the data in Figure 2.4. Permeabilities through PDMS membranes were taken to be the mean of the data presented in Figure 2.4, while the furfural permeability of SDS membranes was taken as the first data point in Figure 2.4, and the water permeability of SDS membranes was taken as the mean of the data in Figure 2.4. These mass transfer constants and the remainder of the modeling parameters which we held constant are listed in rows 1-22 of Table 2.1. Reaction rate constants k_1, k_2, k_3, k_4, and k_5 were determined through least squares minimization of the sum of errors between the predicted and observed concentrations for reactions assisted by LLE and pervaporation with PDMS. Specifically, these were xylose and furfural concentrations in the aqueous phase for the LLE-assisted reaction, xylose concentrations in the retentate for the pervaporation-assisted reaction, and furfural concentrations in both the retentate and the permeate for the pervaporation-assisted reaction. The values of those reaction rate constants can be found in rows 23-27 of Table 2.1.

We did not include the case of reaction without extraction in the calculation of reaction rate constants. This was because the measured furfural concentration in the retentate during the pervaporation-assisted reaction was higher than that in the reactor during the reaction without extraction. One would then expect, by Reactions 3 and 5 in Scheme 2.1, that the furfural consumption would be greater during the pervaporation-assisted reaction, but that was not what we observed; pervaporation improved the furfural yield. This observation led to our exclusion of the case of reaction without extraction from these calculations and as a result, the reaction rate constants we report in rows 23-27 of Table 2.1 only represent xylose dehydration with simultaneous furfural extraction. Further analysis and explanation for this exclusion is provided in the Supporting Information.

Figure 2.5 compares the simulated results with the corresponding experimental results for the LLE-assisted, PDMS-pervaporation-assisted, and SDS-pervaporation-assisted reactions. The simulated and experimental results compare very well for all three cases, albeit less so for SDS-pervaporation data. Some of this deviation can be ascribed to the decrease in furfural permeability of SDS membranes with time of use, as discussed previously. It is also clear that the model we developed slightly underestimates both the extraction selectivity and the permeate furfural

concentration for pervaporation-assisted reactions carried out with either PDMS or SDS membranes.

Table 2.1. Parameters used for experiments, membrane calculations, and simulations

Row	Parameter	Symbol	Value
	Common parameters		
1	Proton concentration (mmol/L)	$[H^+]$	133
2	Initial xylose concentration (mmol/L)	$[X]_0$	375
	Liquid-liquid extraction parameters		
3	Equilibrium constant ($(mol/L)_{org}/(mol/L)_{aq}$)	K	2.74
4	Volume ratio (L_{org}/L_{aq})	v	2.0
	Pervaporation parameters		
5	Initial volume (mL)	V_0	180
6	Initial xylose loading (mmol)	$N_{X,0}$	67.5
7	Furfural molecular weight (g/mol)	M_f	96.08
8	Water molecular weight (g/mol)	M_w	18.02
9	Water density (g/mL)	ρ_w	1.0
10	Membrane area (cm^2)	A	37
11	Membrane temperature (°C)	T_{mem}	75
12	PDMS membrane thickness (μm)	L	4.0
13	SDS membrane thickness (μm)	L	4.8
14	Furfural permeability of PDMS (mol/m/s/Pa)	P_f	$8.3 \cdot 10^{-12}$
15	Water permeability of PDMS (mol/m/s/Pa)	P_w	$7.6 \cdot 10^{-12}$
16	Furfural permeability of SDS (mol/m/s/Pa)	P_f	$1.6 \cdot 10^{-11}$
17	Water permeability of SDS (mol/m/s/Pa)	P_w	$6.0 \cdot 10^{-12}$
18	Furfural activity coefficient	γ_f	85[a]
19	Water activity coefficient	γ_w	1[a]
20	Furfural saturation vapor pressure at T_{mem} (Pa)	p_f^{sat}	3804[b]
21	Water saturation vapor pressure at T_{mem} (Pa)	p_w^{sat}	38457[b]
22	Permeate pressure (Pa)	$p_{permeate}$	3
	Reaction rate constants		
23	Xylose dehydration (L/mol/s)	k_1	$3.4 \cdot 10^{-4}$
24	Furfural production (L/mol/s)	k_2	$7.0 \cdot 10^{-4}$
25	Furfural-intermediate condensation ($L^2/mol^2/s$)	k_3	$4.6 \cdot 10^{-3}$
26	Xylose-intermediate condensation ($L^2/mol^2/s$)	k_4	$5.7 \cdot 10^{-4}$
27	Furfural resinification (L/mol/s)	k_5	$1.3 \cdot 10^{-4}$

[a] Reference 38, activity coefficients at 75 °C estimated from vapor-liquid equilibrium data

[b] Reference 38, saturation vapor pressures (mm Hg) at 75 °C calculated by Antoine equation, $A_{furfural} = 8.402$, $B_{furfural} = 2338.49$, $C_{furfural} = 261.638$, $A_{water} = 8.07131$, $B_{water} = 1730.63$, $C_{water} = 233.426$

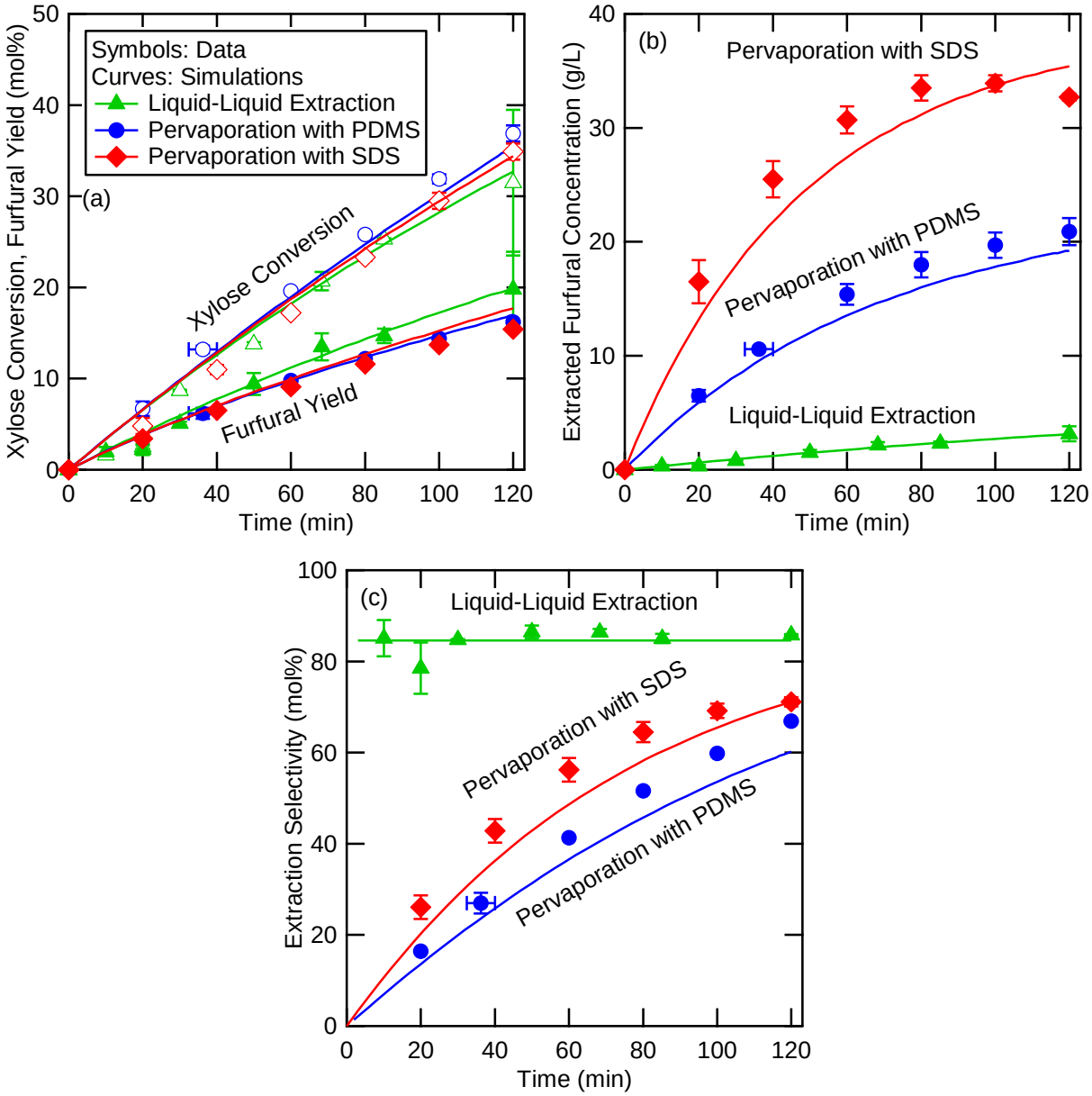

Figure 2.5. Comparison among experimental data and simulated results of (a) xylose conversion and furfural yield; (b) concentration of furfural in the extractant phase (toluene or permeate); and (c) extraction selectivity of furfural; during the conversion of 375 mM xylose to furfural at 140 °C with 133 mM H^+ from Amberlyst 70. Extraction configurations include liquid-liquid extraction (2:1 toluene:water by volume), pervaporation with a PDMS membrane, and pervaporation with an SDS membrane.

2.3.4 Predictions of Reaction and LLE or Pervaporation over Experimentally Inaccessible Durations

The model was used to predict the results of xylose dehydration with simultaneous furfural extraction for much longer reaction times than were achievable experimentally. We chose five furfural extraction configurations, using the parameters listed in Table 2.1: (1) LLE; (2)

pervaporation with a PDMS membrane; (3) pervaporation with an SDS membrane with constant, rather than decaying, furfural permeability (which we refer to as "pervaporation with SDS"); (4) pervaporation with a membrane that had five times the value of (P_iA/l) of the experimental SDS membranes, also with constant furfural permeability (which we refer to as "SDS (5x P_iA/l)"); and (5) a hypothetical configuration in which furfural extraction is instantaneous and infinite in capacity (*i.e.* extraction selectivity always equals 100%). These five configurations are summarized in Table 2.2. We note here that while the simulated results of pervaporation-assisted reactions plotted in Figure 2.5 included the effects of a decreasing reactor volume caused by water permeation, those in this analysis did not, since the water permeation was significant enough to deplete the reactor of its solvent within the time considered. To account for this, the model was modified slightly: the rate of water permeation remained the same, but the amount of water in the reactor did not change. Physically, this means that any water passing through the membrane is rapidly replaced.

We compared xylose conversions, furfural yields, extracted furfural concentrations, and extraction selectivities for different extraction configurations, as shown in Figure 2.6a-c. Xylose conversion remained unaffected by extraction method, reaching 95% after 1000 min.

Figure 2.6a shows that furfural yield increases monotonically throughout the reaction, signifying that every extraction method reduced the concentration of furfural within the reactor sufficiently so that the rates of furfural consumption (Reactions 3 and 5 in Scheme 2.1) are never able to exceed the rate of furfural production. In the infinite extraction case, the hypothetical limit of furfural yield at 95% xylose conversion is 73%. What this reveals is that Reaction 4 in Scheme 2.1, on its own, is responsible for a humins yield of 22%. When furfural separation is by LLE or when furfural separation is achieved by pervaporation through a PDMS or an SDS membrane with properties given in Table 2.1, the furfural yield decreases to between 52% and 59% – 72-82% of the hypothetical limit with infinite extraction. By increasing the value of (P_iA/l) for an SDS membrane by fivefold, it is possible to attain a furfural yield limit of 69% at a xylose conversion of 95% – a 17% increase over the case of pervaporation with SDS.

Shown in Figure 2.6b are the predicted extracted furfural concentrations for each extraction configuration over the course of the reaction, except for the case of infinite extraction. As we saw experimentally, the predicted furfural concentrations in the permeate resulting from both pervaporation using either an SDS or a PDMS membrane exceeds the predicted furfural concentration in toluene obtained by LLE. However, in the SDS (5x P_iA/l) case, the predicted furfural concentration is initially higher than that obtained by LLE, but becomes lower than that obtained by LLE at 520 min and continues to decrease thereafter.

Table 2.2. Reactor configurations simulated for experimentally inaccessible durations

Number	Name	Description
1	LLE	Liquid-liquid extraction with 2:1 toluene:water by volume
2	PDMS	Pervaporation with PDMS
3	SDS	Pervaporation with an SDS membrane with constant, rather than decaying, furfural permeability
4	SDS (5x P_iA/l)	Pervaporation with a membrane with five times the value of (P_iA/l) of the experimental SDS membranes
5	Infinite extraction	A hypothetical configuration in which furfural extraction is instantaneous and infinite in capacity

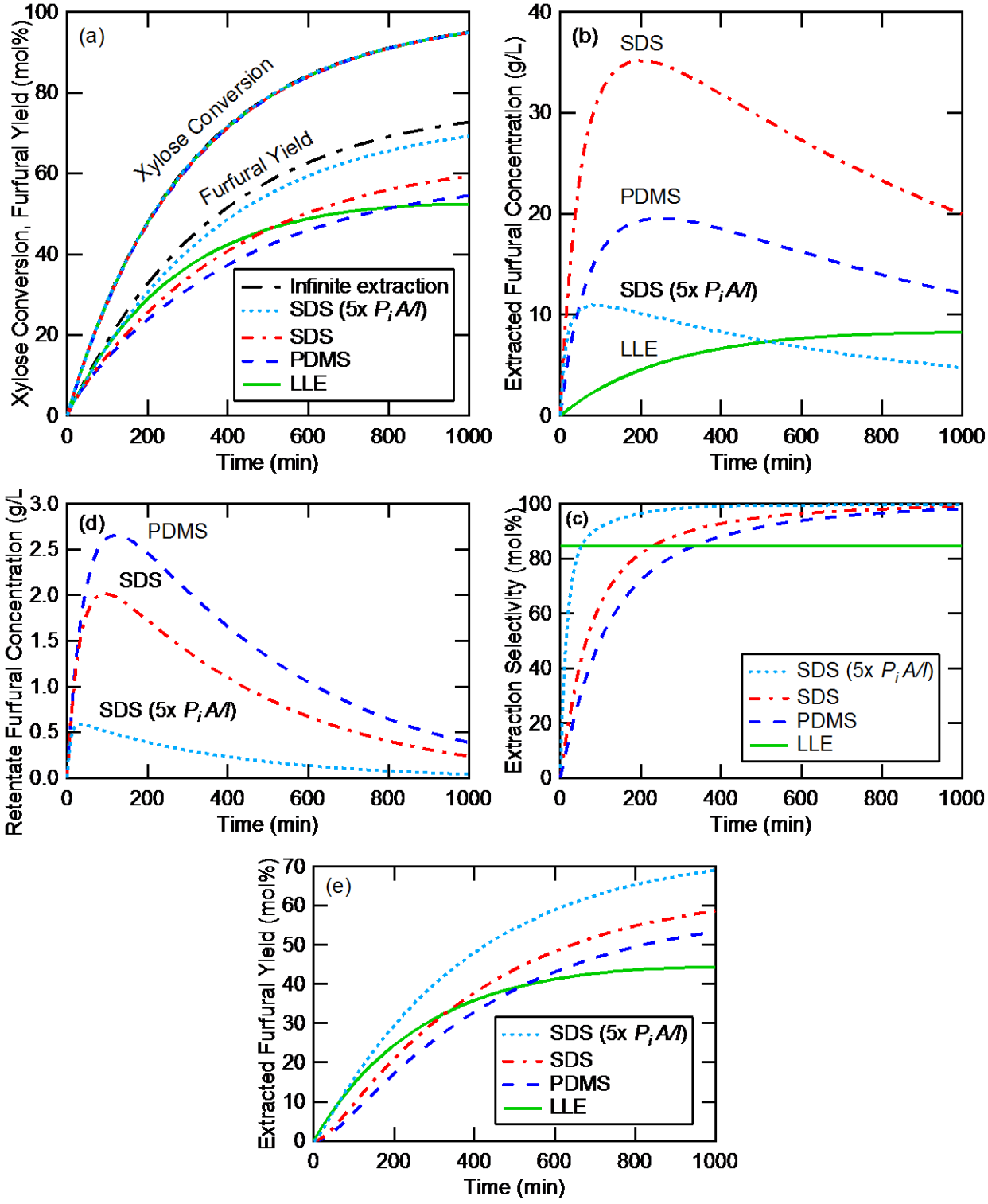

Figure 2.6. Comparison among simulated results of (a) xylose conversion and furfural yield; (b) concentration of furfural in the extractant phase (toluene or permeate); (c) extraction selectivity of furfural; (d) concentration of furfural in pervaporation-assisted reactors; and (e) furfural yield in the extractant phase (toluene or permeate) during the conversion of 375 mM xylose to furfural at 140 °C with 133 mM H^+ from Amberlyst 70. Extraction configurations are listed in Table 2.2.

It is worth noting that the change with time in the predicted furfural concentration in the extracted phase differs for LLE and pervaporation. Simulations of LLE show that the furfural concentration in the extract rises monotonically and proportionally to the furfural yield. This is a consequence of the constant extraction selectivity combined with the assumption of rapid mass transfer. In the simulations of pervaporation, the extracted furfural concentration rises rapidly initially, peaks within 260 min, and then falls. This behavior differs qualitatively from what is predicted for LLE because both furfural and water permeate the membrane during pervaporation. As shown in Figure 2.6d, the predicted furfural concentration in the reactor rises initially then decreases. This behavior stems from the changing and competing rates of furfural production versus consumption or pervaporation. Initially, the rate of furfural production is high because the xylose concentration is high. At later times, though, the furfural production rate diminishes and is overcome by the combination of pervaporation and consumption to form humins. A consequence of the trends in reactor furfural concentration is that the furfural permeation rate also rises initially and then decreases. However, since the furfural concentration is low, the water concentration and hence the water permeation rate is essentially constant. The combined result leads to the trends shown in Figure 2.6b. The times to the maximum in permeate furfural concentration and the reactor furfural concentration do not match because the permeate furfural concentration is the result of the cumulative effect of changing furfural permeation rates, and not the instantaneous permeate furfural concentration; the cumulative permeate needs time to be diluted by the increasingly dilute permeate flux in order to reach its maximum value.

The predictions shown in Figure 2.6c demonstrate by that by 360 min all three pervaporation configurations give greater extraction selectivity than LLE, ultimately exceeding 98% while LLE is limited to 85%, further underscoring the advantage of pervaporation over LLE. Multiplying the extraction selectivity by the total furfural yield gives the furfural yield in the extracted phase, or extracted furfural yield, which we plot for all four simulated extraction configurations in Figure 2.6e. The extracted furfural yield represents the yield of furfural that would be captured in the end, assuming no loss during purification. In our simulations, the extracted furfural yields of all three pervaporation configurations were 21-56% higher than that of LLE, showing an additional benefit of pervaporation over LLE.

The present study demonstrates that pervaporative separation of furfural from an aqueous solution not only reduces the loss of product due to formation of humins, but also results in a much more concentrated product than could be achieved by LLE. It is expected that further enhancements in pervaporative extraction could be achieved by improving the membrane properties, *i.e.* increasing the permeability of furfural through the film through the use of a different membrane material, increasing the membrane area, and decreasing the membrane thickness. In this study, we demonstrated an improvement in furfural permeability by changing our PDMS membranes to SDS block copolymer membranes. One could envision improving the membranes further through the use of a transporting phase with more intrinsic free volume, such as poly[1-(trimethylsilyl)-1-propyne] (PTMSP)[29,42] or by changing the volume fraction of the transporting phase, with which the permeability is expected to be proportional.[39,43] Additionally, pervaporative extraction could be improved by increasing the operating temperature of the film. Clearly, operation of the membrane separator at the temperature of the reaction (140 °C) would be desirable, since this would eliminate the need for the heat exchanger placed between the reactor and the membrane unit. An increase in the membrane temperature would also increase the saturation vapor pressure of furfural in the membrane feed 13 times,[38] which would, in turn, increase the furfural mass transfer rate by a similar magnitude (see Equation (2.5)).

2.4 Conclusions

A laboratory-scale reactor/membrane separation system was built and tested in order to assess the feasibility of using pervaporation to remove furfural from an aqueous solution as it is formed by the Brønsted-acid catalyzed dehydration of xylose. We found that LLE and pervaporation with either PDMS or SDS membranes improved the yield of furfural over the case of reaction without extraction. SDS membranes had high furfural permeabilities, offering a promising alternative to cross-linked PDMS membranes, but their furfural permeabilities declined during the course of the reaction, ultimately limiting their use. The data from reactions with simultaneous furfural extraction were simulated using a model of the system, which enabled an analysis of the benefits of pervaporation-assisted xylose dehydration at near-complete conversion to be explored more fully. When compared to LLE, pervaporation was found to produce an extractant phase of significantly greater purity and to extract a larger proportion of the furfural produced. Both of these advantages improve the potential economic viability of pervaporation-assisted xylose dehydration compared to an LLE-assisted process.

Improvements in pervaporation could come from changing the dimensions of the membrane (*i.e.* increasing the area and decreasing the thickness) and from changing the membrane material itself. As shown in rows 14 and 16 of Table 2.1, the triblock copolymer SDS membranes have a furfural permeability twice that of cross-linked PDMS, despite having a smaller volume fraction of the furfural-transporting block. Pervaporation membranes may be further improved by utilizing more-permeable block copolymer transporting units or by cross-linking the structural unit, which may lead to increased membrane resistance to changes in furfural permeability during its production.

2.5 Acknowledgments

This work was supported by the Energy Biosciences Institute at the University of California at Berkeley, funded by BP. The authors thank Dow Chemical for donating the Amberlyst 70 ion-exchange resin used as a catalyst in this study and Ying Lin Louie for her assistance in operating the GC-MS for this study.

2.6 Supporting Information

We modeled xylose dehydration with simultaneous furfural extraction by pervaporation and LLE in accordance to Scheme 2.1, using the constants provided Table 2.1. For LLE-assisted reactions, we assumed that the mass transfer rate of furfural across the two phases was very rapid, resulting in an equilibrium distribution and allowing us to write the following differential equations:

$$\frac{d[X]}{dt} = -(k_1 + k_4[I])[X][H^+] \tag{2.S1}$$

$$\frac{d[I]}{dt} = (k_1[X] - k_2[I] - k_3[I][F] - k_4[I][X])[H^+] \tag{2.S2}$$

$$\frac{d[F]^{\text{aq}}}{dt} = \left(\frac{1}{K\nu + 1}\right)(k_2[I] - k_3[I][F] - k_5[F])[H^+] \tag{2.S3}$$

$$\frac{d[F]^{\text{org}}}{dt} = \left(\frac{K}{K\nu + 1}\right)(k_2[I] - k_3[I][F] - k_5[F])[H^+] \tag{2.S4}$$

where $[X]$, $[I]$, $[H^+]$, and $[F]^{\text{aq}}$ are the concentrations of xylose, intermediate product, protons, and furfural in the aqueous phase, respectively, and $[F]^{\text{org}}$ is the concentration of furfural in the organic phase. The constants K and ν are the equilibrium constant (*i.e.* $[F]^{\text{org}}/[F]^{\text{aq}}$) and the volume ratio (*i.e.* toluene-phase volume/aqueous-phase volume), respectively. The constants k_1, k_2, k_3, k_4, and k_5 correspond to the same constants in Scheme 2.1. We invoked the pseudo-steady state assumption, *i.e.* $d[I]/dt \approx 0$, so that

$$[I] = \frac{k_1[X]}{k_2 + k_3[F] + k_4[X]} \tag{2.S5}$$

We treated the pervaporation-assisted reactions with a similar approach. We used Equation (2.5) to calculate permeation rates, but neglected the term corresponding to the permeate pressure in permeation rates because the permeate pressure was nearly zero. Mass balances were written in terms of moles, rather than concentrations, because water could permeate through the membrane and change the volume of the reactor:

$$\frac{dN_{\text{x}}}{dt} = -\left(k_1 + k_4\left(\frac{k_1 N_{\text{x}}/V}{k_2 + k_3 N_{\text{f}}^{\text{ret}}/V + k_4 N_{\text{x}}/V}\right)\right)\frac{N_{\text{x}}}{V}N_{\text{H}^+} \tag{2.S6}$$

$$\begin{aligned}\frac{dN_{\text{f}}^{\text{ret}}}{dt} = &\left[\left(k_2 - k_3\frac{N_{\text{f}}^{\text{ret}}}{V}\right)\left(\frac{k_1 N_{\text{x}}/V}{k_2 + k_3 N_{\text{f}}^{\text{ret}}/V + k_4 N_{\text{x}}/V}\right) - k_5\frac{N_{\text{f}}^{\text{ret}}}{V}\right]N_{\text{H}^+} \\ &- A\frac{P_{\text{f}}}{l}\frac{N_{\text{f}}^{\text{ret}}}{N_{\text{x}} + N_{\text{f}}^{\text{ret}} + N_{\text{w}}^{\text{ret}}}\gamma_{\text{f}}p_{\text{f}}^{\text{sat}}\end{aligned} \tag{2.S7}$$

$$\frac{dN_{\mathrm{w}}^{\mathrm{ret}}}{dt} = -A\frac{P_{\mathrm{w}}}{l}\frac{N_{\mathrm{w}}^{\mathrm{ret}}}{N_{\mathrm{x}} + N_{\mathrm{f}}^{\mathrm{ret}} + N_{\mathrm{w}}^{\mathrm{ret}}}\gamma_{\mathrm{w}}p_{\mathrm{w}}^{\mathrm{sat}} \tag{2.S8}$$

$$\frac{dV^{\mathrm{ret}}}{dt} = \frac{M_{\mathrm{w}}}{\rho_{\mathrm{w}}}\frac{dN_{\mathrm{w}}^{\mathrm{ret}}}{dt} \tag{2.S9}$$

$$\frac{dN_{\mathrm{f}}^{\mathrm{perm}}}{dt} = A\frac{P_{\mathrm{f}}}{l}\frac{N_{\mathrm{f}}^{\mathrm{ret}}}{N_{\mathrm{x}} + N_{\mathrm{f}}^{\mathrm{ret}} + N_{\mathrm{w}}^{\mathrm{ret}}}\gamma_{\mathrm{f}}p_{\mathrm{f}}^{\mathrm{sat}} \tag{2.S10}$$

$$\frac{dN_{\mathrm{w}}^{\mathrm{perm}}}{dt} = A\frac{P_{\mathrm{w}}}{l}\frac{N_{\mathrm{w}}^{\mathrm{ret}}}{N_{\mathrm{x}} + N_{\mathrm{f}}^{\mathrm{ret}} + N_{\mathrm{w}}^{\mathrm{ret}}}\gamma_{\mathrm{w}}p_{\mathrm{w}}^{\mathrm{sat}} \tag{2.S11}$$

$$\frac{dV^{\mathrm{perm}}}{dt} = \left(M_{\mathrm{f}}\frac{dN_{\mathrm{f}}^{\mathrm{perm}}}{dt} + M_{\mathrm{w}}\frac{dN_{\mathrm{w}}^{\mathrm{perm}}}{dt}\right)\frac{1}{\rho_{\mathrm{w}}} \tag{2.S12}$$

Here, the subscripts represent components and the superscripts denote phases. Thus, N_i^j is the moles of component i in phase j. The subscripts x, f, H^+, and w represent xylose, furfural, protons, and water, respectively, while the superscripts ret and perm represent the retentate and permeate, respectively. Xylose was only found in the retentate, so its phase index is neglected. V^j represents the volume of phase j, A is the area of the membrane, P_i is the permeability of component i, l is the thickness of the membrane, γ_i is the activity coefficient of i in the liquid feed, and p_i^{sat} is the saturation vapor pressure of i at the feed conditions.

We used least squares minimization of the sum of errors between experimentally observed and simulated concentrations for reactions assisted by LLE and pervaporation with PDMS. These concentrations were that of xylose and furfural in the aqueous phase for the LLE-assisted reaction, xylose concentrations in the retentate for the pervaporation-assisted reaction, and furfural concentrations in both the retentate and the permeate for the pervaporation-assisted reaction. The resultant reaction rate constants are given in rows 23-27 of Table 2.1.

Data from the reaction without extraction was not included because the measured furfural concentration in the retentate during the pervaporation-assisted reaction was higher than that in the reactor during the reaction without extraction. This observation, in conjunction with Reactions 3 and 5 in Scheme 2.1, would lead one to expect the furfural consumption to be greater during the pervaporation-assisted reaction. This expectation is inconsistent with our experimental data, which showed that pervaporation improved the furfural yield, and led us to exclude the case of reaction without extraction from the reaction-rate-constant calculations and subsequent simulations of experimentally inaccessible reaction times with those reaction rate constants (see Figure 2.6).

Figure 2.S1 shows the comparison of experimental data and simulated results for the case of reaction without extraction, using the reaction rate constants for xylose dehydration with simultaneous furfural extraction (provided in Table 2.1). We used Equations (2.S1), (2.S3), and (2.S5) while setting the volume ratio v equal to zero. The xylose conversion is predicted well, but the furfural yield is overestimated by a factor of 2. We analyzed each of the five reaction rate constants in order to improve the simulated furfural yield only in the case of reaction without extraction, assessing how sensitive the xylose conversion and furfural yield at 120 min were to changes in each parameter.

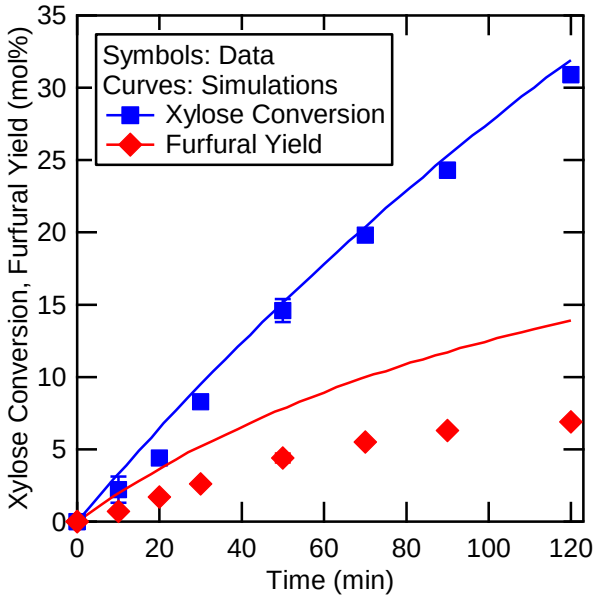

Figure 2.S1. Comparison among experimental data and simulated results of xylose conversion and furfural yield during the conversion of 375 mM xylose to furfural at 140 °C with 133 mM H^+ from Amberlyst 70 without furfural extraction. Reaction rate constants are listed in Table 2.1.

Rate constant k_1, which represents xylose dehydration, has the most significant effect on xylose conversion and, by extension, also significantly affects furfural yield. Changes in this constant do not result in proportionate changes in the xylose conversion and furfural yield at 120 min because of their exponential dependence on time and on multiple rate constants. Ultimately, k_1 should be left unchanged to ensure reasonable agreement between the experimental and predicted xylose conversions.

Rate constant k_4, which represents xylose-intermediate condensation, could be increased to increase the production of humins *via* Reaction 4. A secondary effect would be the reduction in [*I*] (see Equation (2.S5)), which would lead to less furfural production. However, the difference in xylose conversion between the reactions with LLE and without extraction is minimal (see Figure 2.2a), suggesting that k_4[*I*] is, and must remain, much smaller than k_1 (see Equation (2.S1)); k_4 should remain unchanged.

Rate constant k_5, which represents furfural resinification, could also be increased to increase the production of humins and decrease furfural yield. However, the rate of Reaction 5 is small because of the low furfural concentration, so large changes in k_5 are necessary to significantly impact the furfural yield: a 15-fold increase in k_5 results in the 2-fold decrease in furfural yield required to match the simulated and experimental furfural yields, as shown in Figure 2.S2a.

Rate constant k_2, which represents furfural production, could be decreased to decrease furfural yield. A side effect of decreasing k_2 is that [*I*] is increased slightly, leading to a minor increase in xylose conversion *via* Reaction 4, which causes the simulated and experimental xylose conversion to diverge. However, the most pronounced impact is on furfural yield, with a modest 1.8-fold decrease in k_2 leading to a 1.3-fold decrease in furfural yield.

Rate constant k_3, which represents furfural-intermediate condensation, could be increased to decrease furfural yield, as well as reduce [*I*] and consequently decrease xylose conversion *via* Reaction 4. On its own, a 1.8-fold increase in k_3 results in a 1.2-fold decrease in furfural yield.

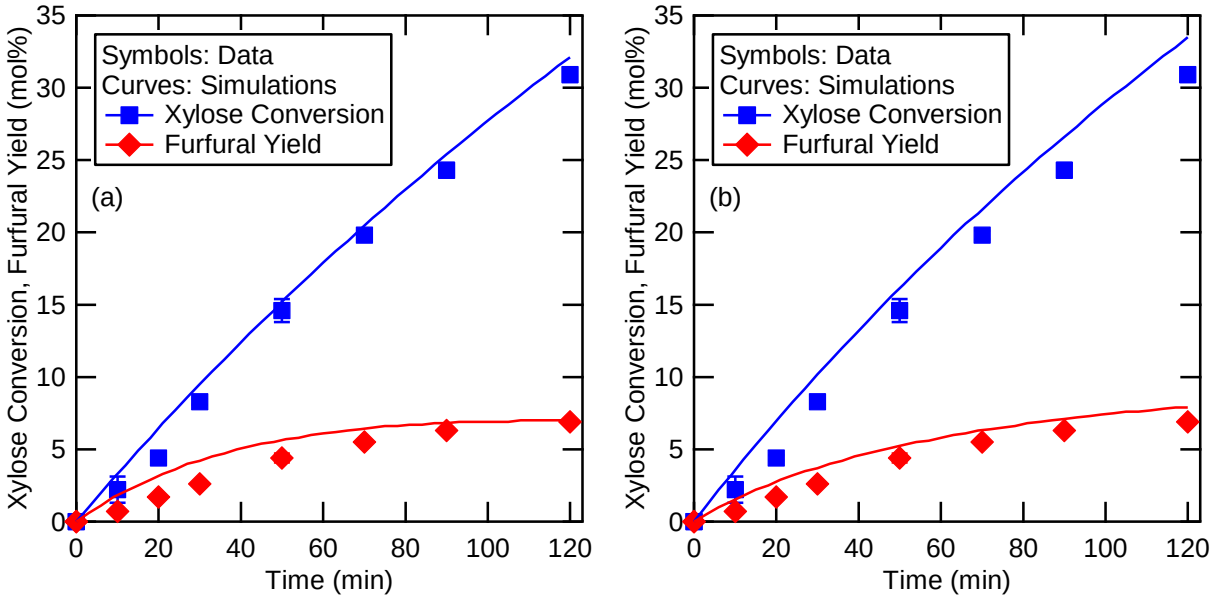

Figure 2.S2. Comparison among experimental data and simulated results of xylose conversion and furfural yield during the conversion of 375 mM xylose to furfural at 140 °C with 133 mM H^+ from Amberlyst 70 without furfural extraction. Reaction rate constants are listed in Table 2.1, except in (a) k_5 was changed to $2.0 \cdot 10^{-4}$ L/mol/s and in (b) k_2 was changed to $3.9 \cdot 10^{-4}$ L/mol/s while k_3 was changed to $8.3 \cdot 10^{-3}$ $L^2/mol^2/s$.

However, when this increase is coupled with the 1.8-fold decrease in k_2, the two effects work together to accurately predict the xylose conversion and furfural yield in the case of reaction without extraction, as shown in Figure 2.S2b.

We applied the aforementioned adjustments to k_5 and to the pair of k_2 and k_3 and simulated the extraction-assisted reactions for experimentally inaccessible durations, similarly to how we produced Figure 2.6. The results from increasing k_5 by a factor of 15 are shown in Figure 2.S3, while the results from decreasing of k_2 by a factor of 1.8 and simultaneously increasing k_3 by a factor of 1.8 are shown in Figure 2.S4. In both cases, the xylose conversion, furfural yield, and extraction selectivity trends matched what we found with our unadjusted reaction rate constants (in Figure 2.6): conversions were the same regardless of extraction method, yields increased in the order of LLE < PDMS < SDS < SDS (5x P_iA/l) < Infinite Extraction, and the LLE extraction selectivity remained constant while all pervaporation extraction selectivities approached 100%. The extracted furfural concentrations trended similarly across all three cases, except with LLE when furfural resinification was inflated (see Figure 2.S3c) because the furfural concentration rose enough that the rate of furfural resinification exceeded that of furfural production, leading to the maxima observed in both the furfural yield and the furfural concentration in toluene (see Figures 2.S3b and 2.S3c, respectively). We can conclude from this analysis that while the exact values of xylose conversion, furfural yield, and extracted furfural concentration are somewhat sensitive to the values of the reaction rate constants k_1-k_5, the trends with respect to extraction method are rather insensitive; pervaporation holds the potential to improve furfural yield, concentration of furfural in the extractant phase, and the proportion of furfural in the extractant phase.

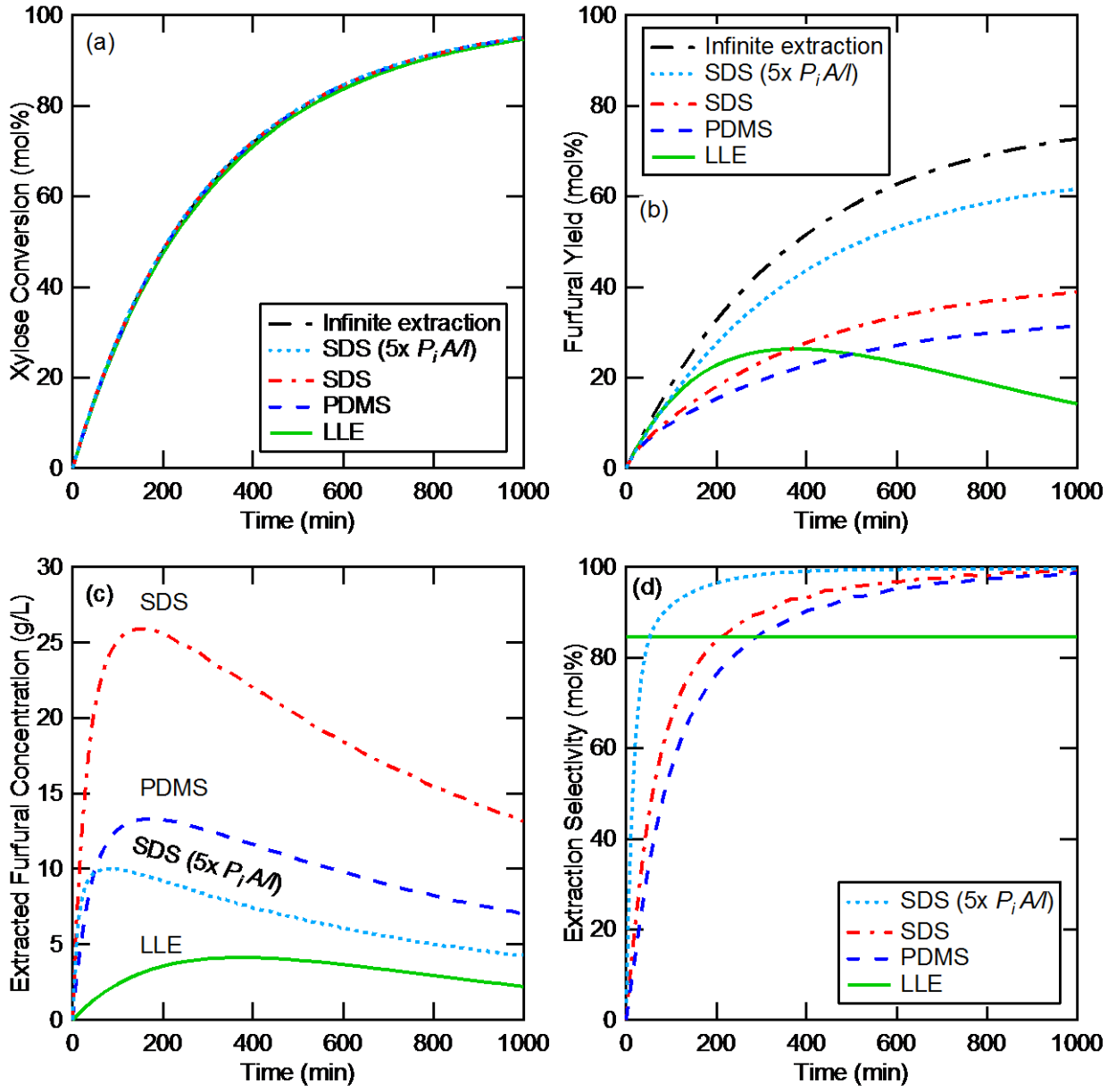

Figure 2.S3. Comparison among simulated results of (a) xylose conversion; (b) furfural yield; (c) concentration of furfural in the extractant phase (toluene or permeate); and (d) extraction selectivity of furfural during the conversion of 375 mM xylose to furfural at 140 °C with 133 mM H^+ from Amberlyst 70 with increased furfural resinification (k_5 = 2.0·10^{-3} L/mol/s). Extraction configurations are listed in Table 2.2.

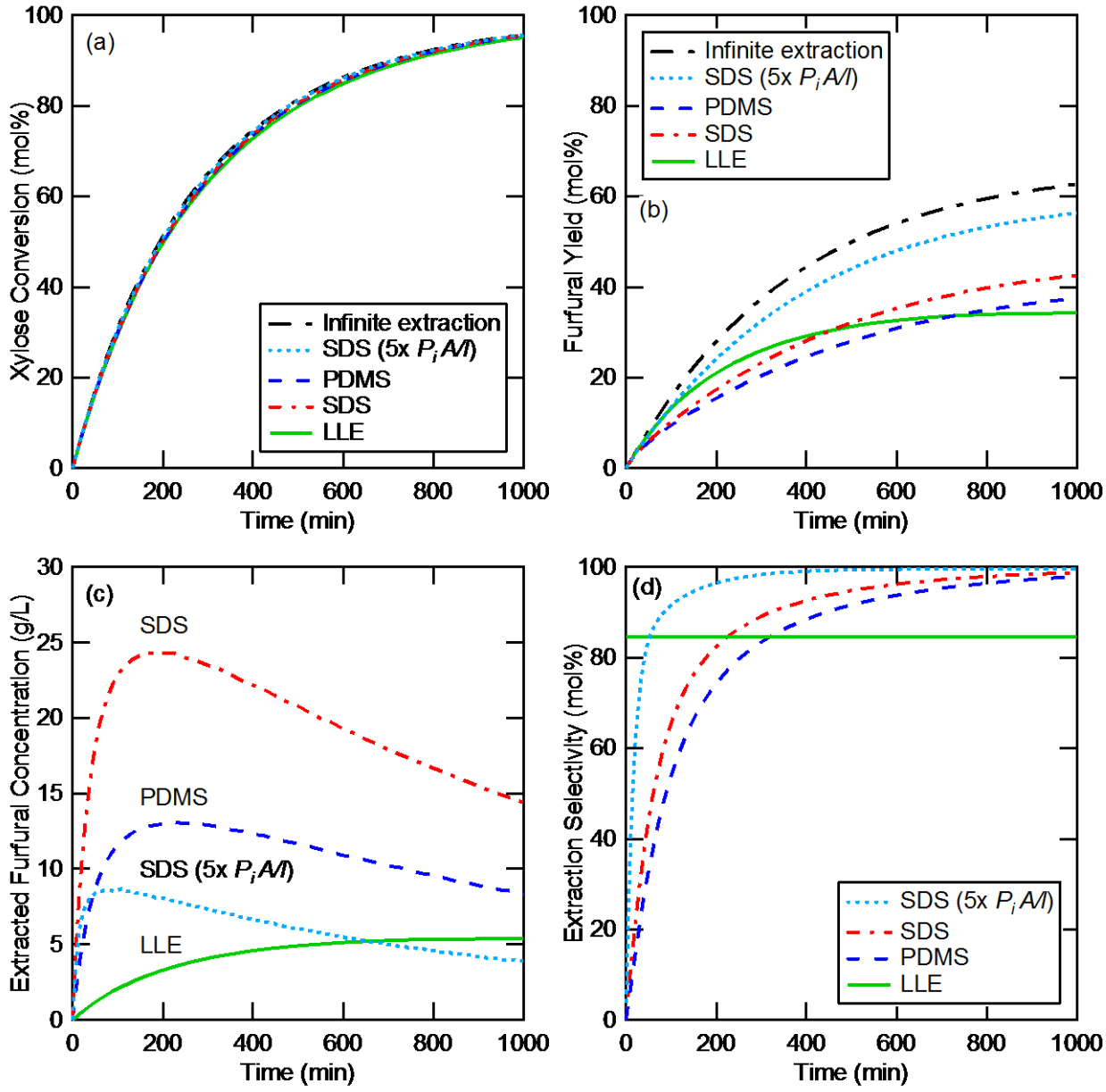

Figure 2.S4. Comparison among simulated results of (a) xylose conversion; (b) furfural yield; (c) concentration of furfural in the extractant phase (toluene or permeate); and (d) extraction selectivity of furfural during the conversion of 375 mM xylose to furfural at 140 °C with 133 mM H^+ from Amberlyst 70 with decreased furfural production (k_2 = 3.9·10^{-4} L/mol/s) and increased furfural-intermediate condensation (k_3 = 8.3·10^{-3} L^2/mol^2/s). Extraction configurations are listed in Table 2.2.

2.7 References

1. G. W. Huber, S. Iborra and A. Corma, *Chem. Rev.*, 2006, **106**, 4044-4098.
2. G. Dautzenberg, M. Gerhardt and B. Kamm, *Holzforschung*, 2011, **65**.
3. C. E. Wyman, B. E. Dale, R. T. Elander, M. Holtzapple, M. R. Ladisch and Y. Y. Lee, *Bioresour. Technol.*, 2005, **96**, 1959-1966.
4. B. Danon, G. Marcotullio and W. de Jong, *Green Chem.*, 2014, **16**, 39-54.
5. G. W. Huber, J. N. Chheda, C. J. Barrett and J. A. Dumesic, *Science*, 2005, **308**, 1446-1450.
6. D. M. Alonso, J. Q. Bond and J. A. Dumesic, *Green Chem.*, 2010, **12**, 1493.
7. A. Corma, O. de la Torre, M. Renz and N. Villandier, *Angew. Chem.*, 2011, **50**, 2375-2378.
8. M. Balakrishnan, E. R. Sacia and A. T. Bell, *ChemSusChem*, 2014, **7**, 1078-1085.
9. J. J. Bozell and G. R. Petersen, *Green Chem.*, 2010, **12**, 539.
10. J. P. Lange, E. van der Heide, J. van Buijtenen and R. Price, *ChemSusChem*, 2012, **5**, 150-166.
11. C. M. Cai, T. Zhang, R. Kumar and C. E. Wyman, *J. Chem. Technol. Biotechnol.*, 2014, **89**, 2-10.
12. K. J. Zeitsch, *The Chemistry and Technology of Furfural and its Many By-Products*, Elsevier Science, Amsterdam, 2000.
13. J. M. J. Antal, T. Leesomboon, W. S. Mok and G. N. Richards, *Carbohydr. Res.*, 1991, **217**, 71-85.
14. A. S. Dias, S. Lima, P. Brandão, M. Pillinger, J. Rocha and A. A. Valente, *Catal. Lett.*, 2006, **108**, 179-186.
15. S. Lima, A. Fernandes, M. M. Antunes, M. Pillinger, F. Ribeiro and A. A. Valente, *Catal. Lett.*, 2010, **135**, 41-47.
16. H. Gao, H. Liu, B. Pang, G. Yu, J. Du, Y. Zhang, H. Wang and X. Mu, *Bioresour. Technol.*, 2014, **172**, 453-456.
17. R. Weingarten, J. Cho, J. W. C. Conner and G. W. Huber, *Green Chem.*, 2010, **12**, 1423.
18. J. N. Chheda, Y. Román-Leshkov and J. A. Dumesic, *Green Chem.*, 2007, **9**, 342.
19. H. Amiri, K. Karimi and S. Roodpeyma, *Carbohydr. Res.*, 2010, **345**, 2133-2138.
20. R. Xing, W. Qi and G. W. Huber, *Energy Environ. Sci.*, 2011, **4**, 2193.
21. W. Wang, J. Ren, H. Li, A. Deng and R. Sun, *Bioresour. Technol.*, 2015, **183**, 188-194.
22. M. J. Campos Molina, R. Mariscal, M. Ojeda and M. Lopez Granados, *Bioresour. Technol.*, 2012, **126**, 321-327.
23. S. Le Guenic, F. Delbecq, C. Ceballos and C. Len, *J. Mol. Catal. A: Chem.*, 2015, **410**, 1-7.
24. L. M. Vane, *J. Chem. Technol. Biotechnol.*, 2005, **80**, 603-629.
25. D. Cai, T. Zhang, J. Zheng, Z. Chang, Z. Wang, P. Y. Qin and T. W. Tan, *Bioresour. Technol.*, 2013, **145**, 97-102.
26. I. Blume, J. Wijmans and R. W. Baker, *J. Membr. Sci.*, 1990, **49**, 253-286.
27. Y. He, D. M. Bagley, K. T. Leung, S. N. Liss and B. Q. Liao, *Biotechnol. Adv.*, 2012, **30**, 817-858.
28. W. Van Hecke, T. Hofmann and H. De Wever, *Bioresour. Technol.*, 2013, **129**, 421-429.
29. R. W. Baker, *Membrane Technology and Applications*, John Wiley & Sons Ltd, The Atrium, Southern Gate, Chichester, West Sussex, P19 8SQ, United Kingdom, 2012.
30. U. K. Ghosh, N. C. Pradhan and B. Adhikari, *Desalination*, 2007, **208**, 146-158.

31. U. K. Ghosh, N. C. Pradhan and B. Adhikari, *Desalination*, 2010, **252**, 1-7.
32. X. Liu, H. Jin, Y. Li, H. Bux, Z. Hu, Y. Ban and W. Yang, *J. Membr. Sci.*, 2013, **428**, 498-506.
33. F. Qin, S. Li, P. Qin, M. N. Karim and T. Tan, *Green Chem.*, 2014, **16**, 1262.
34. D. R. Greer, A. E. Ozcam and N. P. Balsara, *AIChE J.*, 2015, **61**, 2789-2794.
35. M. Sagehashi, T. Nomura, H. Shishido and A. Sakoda, *Bioresour. Technol.*, 2007, **98**, 2018-2026.
36. D. R. Greer, T. P. Basso, A. B. Ibanez, S. Bauer, J. M. Skerker, A. E. Ozcam, D. Leon, C. Shin, A. P. Arkin and N. P. Balsara, *Green Chem.*, 2014, **16**, 4206-4213.
37. J. Wijmans and R. W. Baker, *J. Membr. Sci.*, 1995, **107**, 1-21.
38. J. Gmehling, U. Onken and W. Arlt, *Vapor-liquid equilibrium data collection*, DECHEMA, Frankfurt, 1978.
39. A. E. Ozcam, N. Petzetakis, S. Silverman, A. K. Jha and N. P. Balsara, *Macromolecules*, 2013, **46**, 9652-9658.
40. T. Miyata, S. Obata and T. Uragami, *Macromolecules*, 1999, **32**, 3712-3720.
41. D. Kinning, E. Thomas and J. Ottino, *Macromolecules*, 1987, **20**, 1129-1133.
42. C. H. Lau, P. T. Nguyen, M. R. Hill, A. W. Thornton, K. Konstas, C. M. Doherty, R. J. Mulder, L. Bourgeois, A. C. Liu, D. J. Sprouster, J. P. Sullivan, T. J. Bastow, A. J. Hill, D. L. Gin and R. D. Noble, *Angew. Chem. Int. Ed.*, 2014, **53**, 5322-5326.
43. A. K. Jha, S. L. Tsang, A. E. Ozcam, R. D. Offeman and N. P. Balsara, *J. Membr. Sci.*, 2012, **401-402**, 125-131.

Chapter 3: Continuous and Batch Pervaporation-Assisted Furfural Production Catalyzed by $CrCl_3$

Abstract

Furfural is a precursor to numerous chemicals, *e.g.* fuels, solvents, polymers. It is produced by acid-catalyzed dehydration of biomass-derived C_5 sugars, namely xylose, but its selectivity is limited by side reactions which form humins, a collection of low-value byproducts. Humins production can be reduced by extracting furfural as it is produced, *e.g.* by *in situ* pervaporation. The goal of this study was to operate a pervaporation-assisted reactor continuously in order to determine how pervaporation rate, varied by changing the membrane-area-to-reactor-volume ratio *a*, affects furfural yield and permeate concentration. A laboratory-scale membrane reactor was built for this study and was used for $CrCl_3$-catalyzed xylose conversion to furfural at 90 °C. In batch reactions, pervaporation rate did not affect furfural yield, but moderate pervaporation did increase furfural concentration by an order of magnitude relative to the reaction without pervaporation. Additionally, $CrCl_3$ was fully retained in the reactor; none of it permeated. This behavior was caused by the negligible vapor pressure of $CrCl_3$–finite vapor pressure is necessary for pervaporation–and offered a simple means of separating product (furfural) from homogeneous catalyst ($CrCl_3$). This permitted continuous furfural production with no catalyst added during the reaction. Pervaporation-assisted reactions with $CrCl_3$ and H_2SO_4 at 130 °C were then simulated, based on reaction rate coefficients measured without pervaporation and extrapolations of pervaporation data from lower temperatures. Simulations of batch reactions with varying values of *a* revealed a tradeoff between furfural production and permeate concentration, *i.e.* higher *a* leads to faster production but lower permeate concentrations and *vice versa*. Simulations of continuous reactions with varying *a* showed production rate was proportional to *a*, while permeate concentration and reaction selectivity were maximized at an intermediate value of *a*.

3.1 Introduction

Furfural is a biomass-derived chemical that has a wide variety of applications.[1-3] Recent developments have demonstrated that it and its derivatives can be used for the production of fuels,[4-8] solvents,[9-12] polymers,[3,11-14] and pharmaceuticals.[1,12,15] Current furfural production reaches about 300 kton per annum and mostly comes from China, although the Dominican Republic and South Africa also produce furfural on a large scale.[3,7,16,17]

Modern furfural production is carried out in both batch and continuous reactors, which are loaded with typically about 25-33 wt% lignocellulosic biomass (*e.g.* oat hulls, corn cobs, and bagasse)[16] and 3 wt% sulfuric acid (H_2SO_4) and are heated with live steam (25-35 tons of steam per ton of furfural produced).[7,16] However, this arrangement produces only 40-70% of the theoretical furfural yield.[1,3,7,16] H_2SO_4 serves as the catalyst to promote depolymerization of polysaccharides present in the biomass to yield monosaccharides. Five-carbon monosaccharides, *e.g.* xylose, subsequently undergo dehydration promoted by the same catalyst to produce furfural. The steam not only heats the reactors, but also extracts furfural as it is produced. This steam-

stripping process mitigates the formation of low-value byproducts known as humins, which form by coupling of xylose or furfural with reaction intermediates and by resinification of furfural.[18-20]

Researchers have recently explored the use of liquid-liquid extraction (LLE) with an immiscible organic solvent, rather than steam, to reduce humins production and thus improve furfural yield in laboratory-scale biphasic reactors. Solvents include toluene,[21-23] methyl isobutyl ketone,[23-25] cyclopentylmethyl ether,[26-28] among others, and are typically used in organic:aqueous volumes ratios greater than 1 in order to increase furfural extraction. The furfural yield varies with each study (depending on solvent, catalyst, xylose loading, *etc.*), but the effect is the same as with steam stripping: furfural yield is increased relative to an equivalent reaction without extraction by as much as 100%.[24]

In Chapter 2, we examined the potential of pervaporation as an alternate means of extracting furfural during its formation from xylose in batch reactors. Pervaporation is a process in which a non-porous membrane is contacted by a liquid feed and a permeate vapor. A vacuum is used to reduce the fugacity of the permeate vapor below that of the liquid feed, thus providing the driving force for permeation.[29,30] This process is often used to perform organic-water separations,[31-34] *e.g.* selectively extracting furfural from water.[35-42] Experimental studies of batch reactors without extraction, with LLE, and with pervaporation, revealed that both reactions with extraction (LLE and pervaporation) produced more furfural than was observed in the absence of extraction, but the pervaporation-assisted reactor yielded a product phase with a much higher concentration of furfural. Additionally, our simulations of the LLE- and pervaporation-assisted reactors demonstrated that pervaporation could capture in the product phase virtually all of the furfural formed, while LLE could only extract 85%, an amount determined by phase equilibrium.

A significant drawback of our prior experimental setup (Figure 2.1) was that, in order to ensure membrane stability, liquid was continuously withdrawn from the vessel in which reaction took place, cooled, flowed past the membrane, returned to the reaction vessel, and reheated. This external flow loop accounted for one third of the reactor volume and required considerable heat transfer (both cooling and heating). Additionally, there was no system in place to replace water lost from the reactor by permeation, limiting experiment duration because of liquid volume depletion. In the present study, we constructed a new membrane reactor to address these concerns.

The reaction and pervaporation took place in a single, compact unit, eliminating the need for an external flow loop or excessive heat transfer. A reservoir was attached to add liquid to the reactor continuously, enabling us to run experiments for long durations. We conducted experiments at 90 °C (within the temperature limits of the membranes) with chromium (III) chloride ($CrCl_3$) as a catalyst, as $CrCl_3$ has previously been shown to convert xylose to furfural rapidly, even at low temperatures.[43-45] We found that pervaporation is able to retain fully the catalyst in the reactor, permitting us to operate, and thus produce furfural, continuously. Switching from batch- to continuous-mode has previously improved pervaporation reactors[46,47] and furfural production,[3,18] but has never been examined for pervaporation-assisted furfural production. We address the strengths and weaknesses of our continuous reactor and turn to simulations to study the reaction at a higher temperature catalyzed by H_2SO_4 in addition to $CrCl_3$. We vary the membrane-area-to-reactor-volume ratio, a, and use that to elucidate how pervaporation rate affects furfural production in batch and continuous reactors.

3.2 Experimental Methods

3.2.1 Materials

D-(+)-xylose (≥99%), D-(–)-lyxose (99%), D-xylulose (≥98%), furfural (99%), toluene (≥99.5%), dodecane (99%), cyclohexane (≥99%), and chromium (III) chloride hexahydrate ($CrCl_3$; ≥98.0%) were purchased from Sigma-Aldrich and used as received. Amberlyst 70, an ion-exchange resin donated by Dow Chemical Co., was washed with nanopure water until the pH of the supernatant was >5.5, then dried overnight at 80 °C in a vacuum oven. The concentration of acid sites on Amberlyst 70 was confirmed to be equal to the manufacturer's reported value of 2.55 eq H^+/kg by H^+/Na^+ exchange with NaCl solution, then titration of the resulting acidic supernatant with NaOH solution using phenolphthalein as the indicator. Sulfuric acid (H_2SO_4; 95%) was purchased from Acros Organic and was used as received. Nanopure water was used for all experiments. Cross-linked polydimethylsiloxane (PDMS) thin-film composite membranes were purchased from Pervatech and had a 130 µm-thick polyethylene terephthalate support layer, a 100 µm-thick polyisoprene intermediate ultrafiltration membrane layer, and a 3-5 µm-thick pervaporation PDMS layer (4 µm was used in all calculations requiring membrane thickness). These membranes were received as sheets and were cut to fit the membrane cell. The block copolymer polystyrene-*block*-polydimethylsiloxane-*block*-polystyrene (SDS), which was previously shown to be permeable to furfural, was purchased from Polymer Source and was used as received. The number-averaged molecular weight of the polydimethylsiloxane block was 104 kg/mol, and that of the polystyrene blocks was 22 kg/mol. The dispersity of the polymer sample was 1.3, and 86 wt% of the sample was the triblock copolymer with the balance being mostly diblock copolymer.

3.2.2 SDS Membrane Preparation

A solution consisting of 0.5-1 g of SDS dissolved in 20 mL of cyclohexane was used to prepare each solvent-cast SDS membrane. The solution was poured onto a 100 mm polytetrafluoroethylene (PTFE) evaporation dish (Fisher, 02-617-148), which was covered and allowed to dry in a fume hood for three days. The resulting membrane was then peeled off the dish, sandwiched between two filter papers, and cut to fit the pervaporation cell. The thickness of each solvent cast membrane was measured at 12 points using a micrometer and the average value was used in all calculations involving membrane thickness.

3.2.3 Furfural Production at 90 °C with or without Pervaporation

Reactions at 90 °C were carried out in a custom-built apparatus, shown schematically in Figure 3.1. This reactor was comprised of a membrane cell, a magnetic stir plate (Thermo Scientific, 88880013), two cold traps for condensing permeated vapors, a vacuum pump (Welch, 2014), a high-pressure nitrogen cylinder (Praxair, NI 2R), a gas pressure regulator (VWR, 55850-624), and an 800 mL feed reservoir (EMD Millipore, 6028). The components were connected by stainless steel (Swagelok), polyethylene (PE; EMD Millipore), polytetrafluoroethylene (PTFE; Grainger), and silicone (Cole-Parmer) tubing; and stainless steel (Swagelok), PE (EMD Millipore), and polyether ether ketone (PEEK; IDEX Health & Science) fittings and valves.

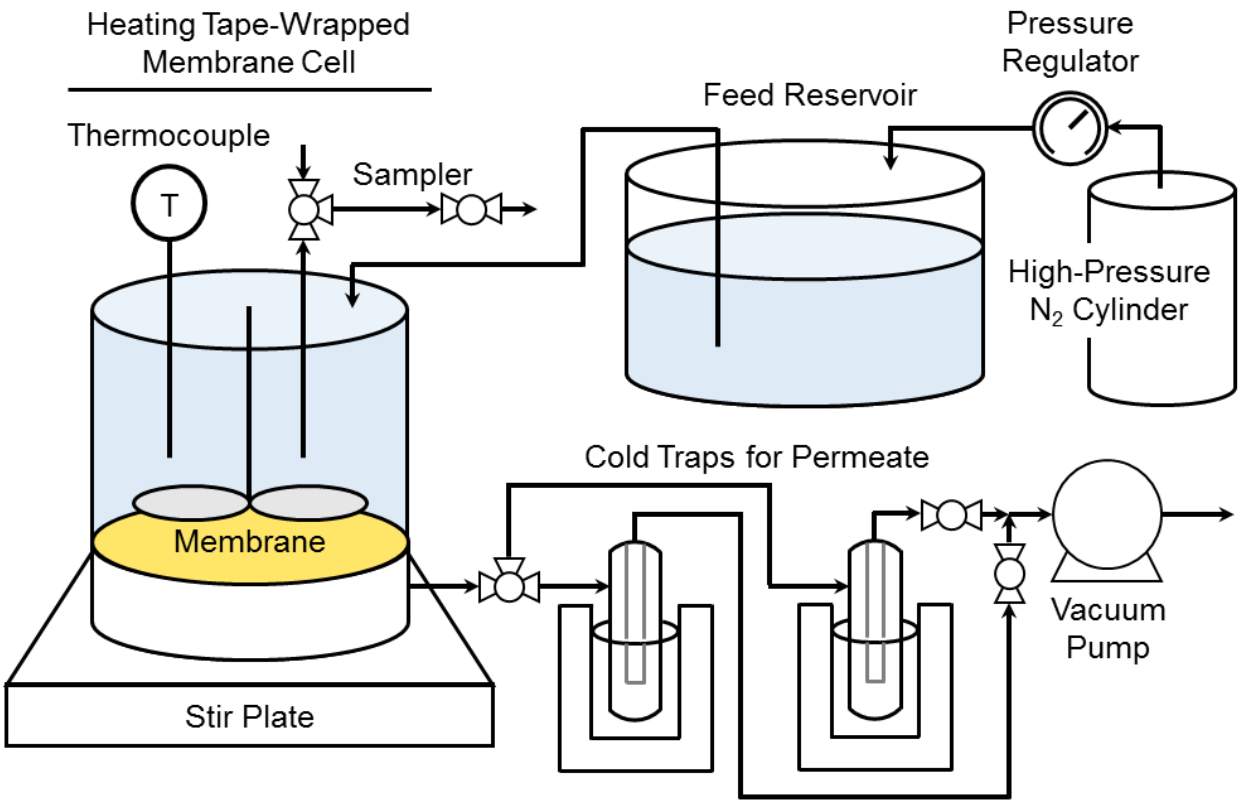

Figure 3.1. Pervaporation membrane-reactor. Reaction takes place at 90 °C in the 83-mL cell, while furfural is continuously extracted by the pervaporation membrane. The nitrogen cylinder, pressure regulator, and feed reservoir maintain constant liquid volume in the cell. The vacuum pump enables pervaporation, while the cold traps collect permeated vapors (*i.e.*, furfural and water).

The membrane cell had three main components: a head, a base, and a glass tube. The head was fabricated from PEEK and had four attachments: a thermocouple (Omega, TMTSS-062G-6), a pressure relief valve (General Air Products, ST12), a sampler, and an inlet tube from the feed reservoir. Corrosion was prevented by placing the thermocouple in a glass sheath and electroplating the relief valve with gold. Additionally, a shaft carrying a PTFE-coated magnetic stir bar and bearing extended from the head into the membrane cell, suspending the stir bar 5 mm above the membrane surface. The base is a circular piece of gold-electroplated stainless steel, containing a 4.8-cm-diameter circular recess into which the membrane is placed. The recess had grooves cut into it to facilitate permeate flow from the membrane through a silicone tube in the base that led to the cold traps. The glass tube served as the walls of the membrane cell and was a piece of borosilicate glass wrapped in heating tape (Omega, STH051-020). The temperature was controlled by a controller (Omega, CNi3233), which was connected to the thermocouple and heating tape. Viton o-rings (42 x 3 mm, McMaster-Carr, 9263K736) were placed on both ends of the glass tube, resulting in a membrane area of 13.9 cm^2. The cell was assembled by placing, from top to bottom, the head, an o-ring, the tube, an o-ring, the membrane, a piece of filter paper, and the base. The head, glass tube, and base were sealed by screwing bolts onto three posts that ran from the base to the head, providing compression to the o-rings. The cell was then placed on top

of a magnetic stir plate. The internal volume of the cell was 83 mL and it was always filled to that amount during use.

Two cold traps and a vacuum pump were located downstream of the membrane cell. Two sizes of cold traps were used to accommodate the permeation rate, depending on the membrane: small (ChemGlass, CG-4516-02) with the SDS membranes, or large (custom blown by Research & Development Glass Products & Equipment, Berkeley, CA) with the PDMS membrane. Permeate vapors were condensed in the cold traps by cooling them with a dry ice and isopropanol mixture (small) or liquid nitrogen (large). The cold traps were connected to the membrane and vacuum pump in parallel, ensuring that the membrane and vacuum pump were always connected, even when a used cold trap was exchanged for a new one. The vacuum pump was capable of pulling different pressures, depending on the cold traps: $\leq$ 3 mbar (small cold traps) or 6-15 mbar (large cold traps), as measured by a vacuum gauge (Vacuubrand, DVR 2) located between the pump and the cold traps.

A high-pressure nitrogen cylinder, gas pressure regulator, and a feed reservoir were located upstream of the membrane cell. The nitrogen cylinder and regulator were connected to the vapor headspace of the feed reservoir, while the feed reservoir was connected to the membrane cell by a dip tube submerged in the liquid of the reservoir. The regulator was used to maintain a gauge pressure of 1 bar throughout the system–a pressure in excess of the vapor pressure of the contents of the membrane cell. During operation, this system was able to sustain a constant liquid volume in the membrane cell, confirmed by measuring the volume of liquid in the cell before and after each experiment. This control mechanism operates as follows. When liquid permeates through the membrane, the cell headspace volume increases and the system pressure drops. The regulator then reacts to this pressure drop by adding more nitrogen to the reservoir headspace to raise the pressure to its setpoint, which pushes liquid through the reservoir dip tube into the cell. Ultimately, the volume of liquid passed through the membrane is replaced by the same volume of liquid from the reservoir.

At the start of each experiment, the membrane cell was assembled with a new membrane: SDS, PDMS, or 130-µm-thick impermeable PTFE for the reaction without pervaporation. The membrane and the cold traps were then connected to each other and vacuumed. The cell was filled with 83 mL of an aqueous xylose and $CrCl_3$ solution: 25 µmol/mL $CrCl_3$ and either 250 µmol/mL xylose in the batch reactions or 200 µmol/mL xylose in the continuous reaction. The feed-reservoir liquid was water in the batch reactions with pervaporation, and a solution of 100 g/L xylose in water for the continuous reaction with pervaporation. The reservoir contained only nitrogen in the batch reaction without pervaporation. The feed reservoir was connected to the cell and the system was pressurized to 1 bar (gauge). The valve connecting the membrane to the cold traps was closed at this point in the batch reaction without pervaporation. Stirring at 600 rpm then began, followed by heating to 90 °C. The cell reached 88 °C within 15 min and 90 °C within 30 min.

The membrane cell was sampled during the reaction using the sampling port, first taking a sample to flush the sampling port, then taking another for analysis. The total volume removed per sample was 800 µL. The permeate was collected at the same time as the reactor was sampled. The permeate flow was directed from the accumulating cold trap to the other installed cold trap (*e.g.*, from the left cold trap to the right trap in Figure 3.1), then the accumulated cold trap was removed, thawed, and replaced with a fresh one. The thawed permeate was a single-phase mixture under the conditions used in this study. The accumulated cold trap was weighed and an aliquot was removed for analysis.

3.2.4 Reactions at 130 °C with or without Liquid-Liquid Extraction (LLE)

Batch reactions at 130 °C were carried out in 10 mL thick-walled glass vials (Sigma-Aldrich, 27198) sealed with PTFE/silicone crimp top septa (Agilent, 8010-0420) and immersed in a silicone oil bath. Separate reactors were used for each reaction time. The temperature of the oil bath was maintained with a magnetic-stirring hotplate (Sigma-Aldrich, Z645060). Reactor contents were stirred using PTFE-coated stir bars rotating at a rate of 600 rpm.

Three sets of reactions were conducted: xylose conversion without LLE, xylose conversion with LLE, and furfural conversion. When xylose was converted without LLE, each reactor received 4 mL of a reactant solution comprising 250 μmol/mL xylose, 25 μmol/mL $CrCl_3$, and 100 μmol/mL H_2SO_4 in water. When xylose was converted with *in situ* LLE, each reactor received 2 mL of the same reactant solution and 4 mL of toluene. When furfural was converted, each reactor received 4 mL of a reactant solution of 125 μmol/mL furfural, 25 μmol/mL $CrCl_3$, and 100 μmol/mL H_2SO_4. Upon completion of the reaction, the reactors were removed from the oil bath and quenched in an ice bath. An aliquot of each phase (water and toluene, if applicable) was removed from the reactor for analysis. An internal standard (5 mg/mL dodecane in toluene) was added to toluene-phase samples prior to analysis.

3.2.5 Equilibrium Distribution of Furfural

The equilibrium distribution of furfural between water and toluene was measured by filling 10 mL thick-walled glass vials (Sigma-Aldrich, 27198) with a PTFE-coated stir bar, 4 mL of toluene, and 2 mL of aqueous furfural solution also containing 25 μmol/mL $CrCl_3$ and 100 μmol/mL H_2SO_4. Each vial was matched to a time point from the LLE-assisted reactions with the total furfural in each vial corresponding to the total furfural produced in its matched time point. The vials were then sealed with PTFE/silicone crimp top septa, shaken vigorously by hand for 10 s, then placed on a stir plate for one hour, with the stir bar rotating at 600 rpm. The vials were then opened and an aliquot of each phase was removed for analysis, with an internal standard (5 mg/mL dodecane in toluene) added to toluene-phase samples prior to analysis.

3.2.6 Pervaporation of Furfural/Water Solutions

Pervaporation experiments were conducted in two units: a catalyst-free membrane reactor, as described in 2.2.3 Xylose Dehydration, or a benchtop pervaporation unit (Sulzer Chemtech), as described in Reference 48.

The membrane reactor was used to explore the relationship between apparent furfural permeability and different feed solutions: (1) 1.5 g/L furfural in water, (2) 50 g/L xylose and 1.5 g/L furfural in water, and (3) a solution referred to as "xylose dehydration broth," retained from reaction experiments conducted as described in 2.2.3 Xylose Dehydration, containing 50 g/L xylose, 1.5 g/L furfural, and soluble humins. The SDS membranes used for this set of experiments were 2 μm in thickness, prepared and characterized by spin coating, as described in 2.2.2 SDS Membrane Preparation.

The pervaporation unit was used to examine pervaporation at temperatures of 50-90 °C. A feed solution of 20 g/L furfural was used for these measurements with SDS membranes of 121-132 μm in thickness, prepared as described in 3.2.2 SDS Membrane Preparation.

3.2.7 Product Analysis

Samples of the aqueous phase were analyzed by high-performance liquid chromatography (HPLC) using an Ultra High Performance Liquid Chromatograph system (Shimadzu). 10 µL aliquots of the samples were injected onto a 300 mm × 7.8 mm Aminex HPX-87H (Bio-Rad) column equipped with a 4.6 mm × 30 mm micro-guard Cation H guard column (Bio-Rad) and a refractive index detector. The compounds were eluted at 65 °C with an isocratic flow rate of 0.4 mL/min of 0.01 N H_2SO_4 in water. Product quantities were determined by converting integrated peak areas into concentrations using a 7-point calibration curve generated from standards created with analytical grade chemicals.

Samples of the organic phase from the LLE-assisted reactors were analyzed by gas chromatography-flame ionization detection (GC-FID) using a Varian CP-3800 Gas Chromatograph equipped with a FactorFour Capillary Column (UF-5ms 30 m, 0.25 mm, 0.25 µm, P/N CP8944) connected to a Varian quadrupole-mass spectrometer (MS) and flame ionization detector (FID). Product concentrations were determined from integrated FID peak areas using a 7-point calibration curve generated from standards created with analytical grade chemicals.

Permeate samples were analyzed by inductively coupled plasma optical emission spectrometry (ICP-OES) using an Optima 7000 DV instrument with yttrium as an internal standard to determine the presence of chromium. The instrument had a detection limit of 0.25 µg/L (ppb).

3.2.8 Calculations

Conversions and yields are reported as molar percentages relative to the initial moles of reactant. $CrCl_3$ was capable of isomerizing xylose to form lyxose and xylulose, and of dehydrating all three xylose isomers to form furfural. Conversion of all three isomers in aggregate was reported ("xylose isomer conversion"), rather than the conversion of xylose alone, *i.e.*

$$\text{Xylose Isomer Conversion} = \frac{N^0_{\text{xylose}} - \left(N_{\text{xylose}} + N_{\text{lyxose}} + N_{\text{xylulose}}\right)}{N^0_{\text{xylose}}} \times 100\% \qquad (3.1)$$

where N denotes the moles, the superscript 0 denotes initial value, and the subscript denotes the compound. Similarly, for the reactions which assessed the rate of furfural conversion without any sugars present, furfural conversion was calculated as follows:

$$\text{Furfural Conversion} = \frac{N^0_{\text{furfural}} - N_{\text{furfural}}}{N^0_{\text{furfural}}} \times 100\% \qquad (3.2)$$

The product of interest in this study was furfural and its yield was defined as

$$\text{Furfural Yield} = \frac{N_{\text{furfural}}}{N^0_{\text{xylose}}} \times 100\% \qquad (3.3)$$

The moles of xylose and furfural were calculated by multiplying the molar concentration of each species in a given phase by that phase's volume. For every phase, except for the permeate phase in pervaporation-assisted experiments, the phase volumes were assumed to be equal to their

initial values. For the permeates, the volumes were calculated by converting the total permeated mass to volume by assuming a solution density of 1 g/mL.

For reactions conducted at 90 °C with the custom-built apparatus, initial moles were determined from a sample taken from the membrane cell when heating began. For reactions conducted at 130 °C in 10 mL glass vials, initial moles were determined by preparing and analyzing extra reactors as stated previously, but without heating in an oil bath.

The equilibrium distribution of furfural is reported as the proportion of the total furfural loaded that was present in the toluene phase, *i.e.*

$$\text{Equilibrium distribution} = \frac{\text{Moles of furfural in toluene phase}}{\text{Total moles of furfural loaded in vial}} \times 100\% \qquad (3.4)$$

The equilibrium distribution is related to the equilibrium constant K, defined as the ratio of furfural concentration in the toluene phase to the aqueous phase, and the toluene:water volume ratio v, as follows:

$$\text{Equilibrium distribution} = \frac{Kv}{Kv + 1} \times 100\% \qquad (3.5)$$

The extraction selectivity of a given process is defined as the fraction of furfural that has been extracted, *i.e.*

$$\text{Extraction Selectivity} = \frac{\text{Moles of furfural extracted}}{\text{Total moles of furfural formed}} \times 100\% \qquad (3.6)$$

The molar permeation rate of component i, $\dot{n}_i$, in pervaporation is described as follows:[29,30]

$$\dot{n}_i = \frac{\Delta m_i}{M_i \Delta t} = A \cdot J_i = A \cdot \frac{P_i}{l}\left(x_i \gamma_i p_i^{\text{sat}} - y_i p_{\text{permeate}}\right) \qquad (3.7)$$

where Δm_i is the change in mass of the permeate during the length of time Δt, M_i is the molecular weight, A is the area of the membrane, J_i is the molar flux, P_i is the permeability, l is the thickness of the membrane, x_i is the mole fraction in the liquid feed, γ_i is the activity coefficient in the liquid feed, p_i^{sat} is the saturation vapor pressure at the feed conditions, y_i is the mole fraction in the vapor permeate, and p_{permeate} is the total permeate pressure. Activity coefficients at 90 °C and 75 °C of water (1 and 1) and furfural (66 and 85, respectively) were assumed to be constant, and were estimated from binary water-furfural vapor-liquid equilibrium data. Saturation vapor pressures were determined by the Antoine equation, using constants calculated from binary water-furfural vapor-liquid equilibrium data. Equation (3.7) was then used to calculate the membrane permeabilities of water and furfural at 90 °C and 75 °C. Each data point of permeability plotted with respect to time represents the time from that data point to the prior one. For a data set with points at 20 min and every 20 min thereafter, the 20-min point represents the time from 0 to 20 min, the 40-min point represents the time from 20-40 min, and so on.

Error bars are provided for all reactions performed at 130 °C and for furfural/water pervaporation at 50-90 °C. The reactions at 130 °C were duplicated and each resulting figure with experimental data was constructed using the mean values for each time point, with the error bars

representing the range of the two trials. The pervaporation experiments at 50-90 °C were conducted with two membranes per temperature, and three measurements taken per membrane. The resulting plots report the average value at each temperature, while the error bars represent the standard deviation of the six measurements. Some error bars are not visible because the ranges for those time points are smaller than the symbols used in the plots.

3.3 Results and Discussion

3.3.1 Experimental Studies of Pervaporation-Assisted Furfural Production at 90 °C

Xylose was converted in the presence of $CrCl_3$ at 90 °C in water. The temporal conversion of xylose isomers (xylose, lyxose, xylulose) and furfural yield are shown in Figure 3.2a for three cases: no pervaporation, moderate rate of pervaporation, and rapid rate of pervaporation. A moderate rate of pervaporation refers to use of a 69-μm-thick SDS membrane with a moderate furfural permeance (*i.e.* permeability divided by membrane thickness) of 1.16 mmol/m^2/h/Pa, whereas a rapid rate of pervaporation refers to pervaporation with a 4-μm-thick PDMS membrane with a furfural permeance of 5.59 mmol/m^2/h/Pa. It is apparent that at 90 °C the rate of pervaporation has no effect on the xylose conversion or the furfural yield. This is likely due to the low reaction temperature for which the reaction of furfural to humins does not occur. Therefore, it appears that Reactions 3 and 5 in Scheme 3.1 are suppressed at low temperatures, but increase in relative significance to other reactions at higher temperatures, suggesting that the reactions that consume furfural have relatively high activation energies.

While pervaporation does not lead to an improvement in furfural yield, the use of pervaporation still has merits. Figure 3.2b shows the cumulative concentration of furfural in the product phase over time for the three experiments. The permeate furfural concentration collected from the SDS membrane exceeds that of the reaction without extraction by approximately an order of magnitude, showing a clear improvement in product concentration. Conversely, the permeate furfural concentration obtained using the PDMS membrane is roughly half of what was obtained without extraction. This result has two causes. The first is the difference in membrane selectivity (*i.e.*, the ratio of furfural-to-water permeabilities). The selectivity of the SDS membrane is 6.3 while that of the PDMS membrane is 1.1; the higher selectivity of SDS allows it to permeate more furfural relative to water than PDMS, leading to a more concentrated permeate. The second is a less obvious cause, which reveals a fundamental tradeoff of *in situ* furfural extraction: extraction reduces the furfural concentration in the retentate, which adversely affects the pervaporation rate of furfural and permeate furfural purity.

The tradeoff between pervaporation rate and permeate concentration is explained by the data in Figures 3.2c and 3.2d, which show the extraction selectivity and concentration of furfural remaining in the reactor, respectively, as a function of time. Figure 3.2c shows that both membranes extract most of the furfural produced, with the PDMS membrane reaching 97% by 24 h and the SDS membrane reaching 82% in the same time. Conversely, the extraction selectivity of the reaction without pervaporation is zero, by definition. The result for the permeate concentration is best explained with Figure 3.2d, which shows the concentration of furfural remaining in the reactor. As expected from the extraction selectivities of the three reaction configurations shown in Figure 3.2c, the concentrations of furfural decrease in the order of no extraction > SDS > PDMS. The permeate concentration of furfural (Figure 3.2b) is determined not only by the membrane

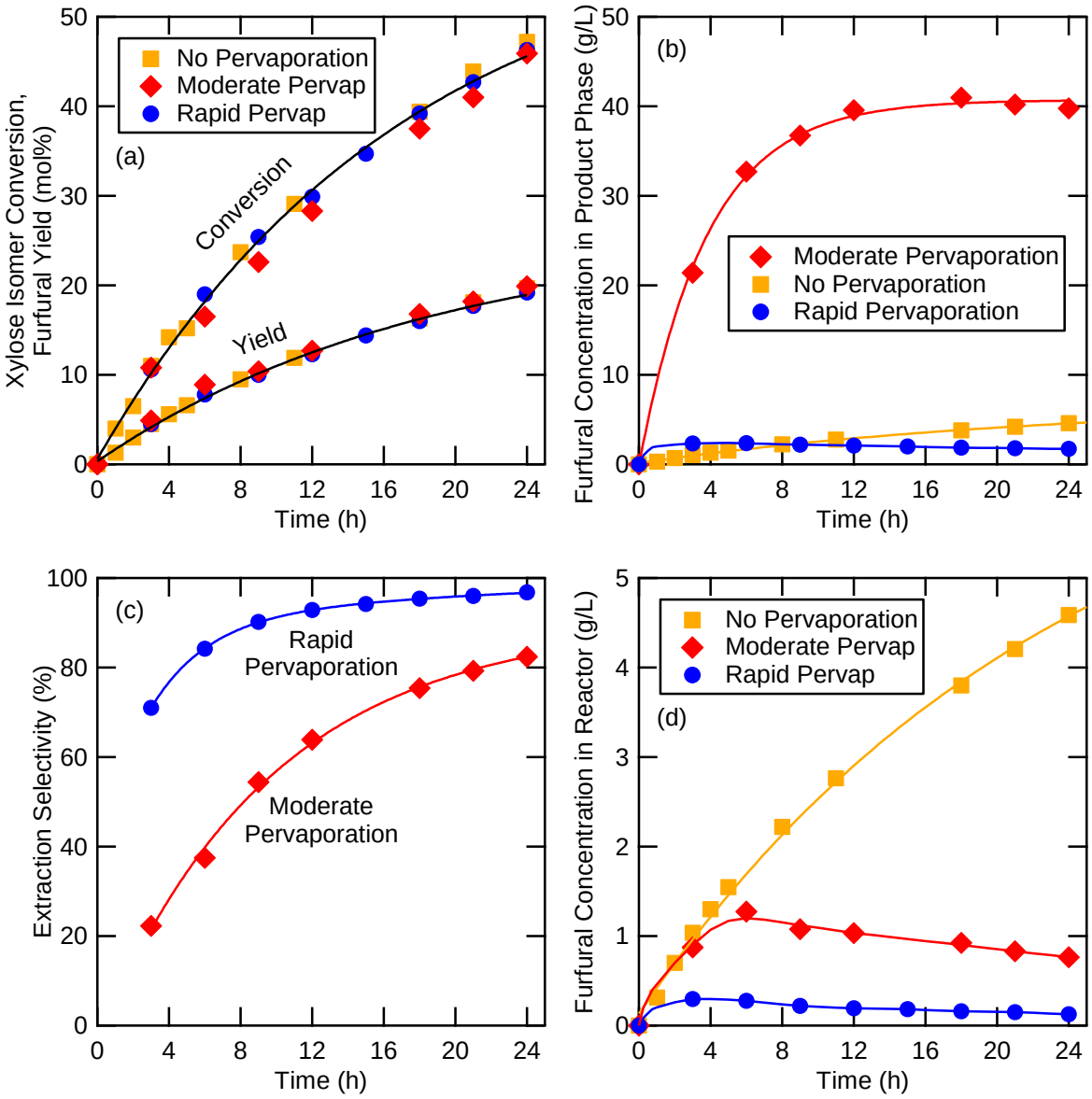

Figure 3.2. Batch-mode xylose conversion to furfural at 90 °C with 25 mM $CrCl_3$ with varying rates of pervaporation: none, moderate (69-µm-thick SDS membrane), and rapid (4-µm-thick PDMS membrane). (a) Xylose isomer conversion and furfural yield. (b) Furfural concentration in product phase (permeate if applicable, otherwise reactor). (c) Fraction of furfural extracted by pervaporation. (d) Concentration of furfural remaining in the reactor. All curves are provided to guide the eye.

properties, but also the concentration of furfural in the reactor (Figure 3.2d). For a given membrane, the permeate furfural concentration is determined by the following equation:

$$c_{\mathrm{f}}^{\mathrm{perm}} \propto \frac{J_{\mathrm{f}}}{J_{\mathrm{f}}+J_{\mathrm{w}}} \approx \frac{J_{\mathrm{f}}}{J_{\mathrm{w}}} \approx \frac{P_{\mathrm{f}}}{P_{\mathrm{w}}} \frac{x_{\mathrm{f}}\gamma_{\mathrm{f}}p_{\mathrm{f}}^{\mathrm{sat}}}{x_{\mathrm{w}}\gamma_{\mathrm{w}}p_{\mathrm{w}}^{\mathrm{sat}}} \tag{3.8}$$

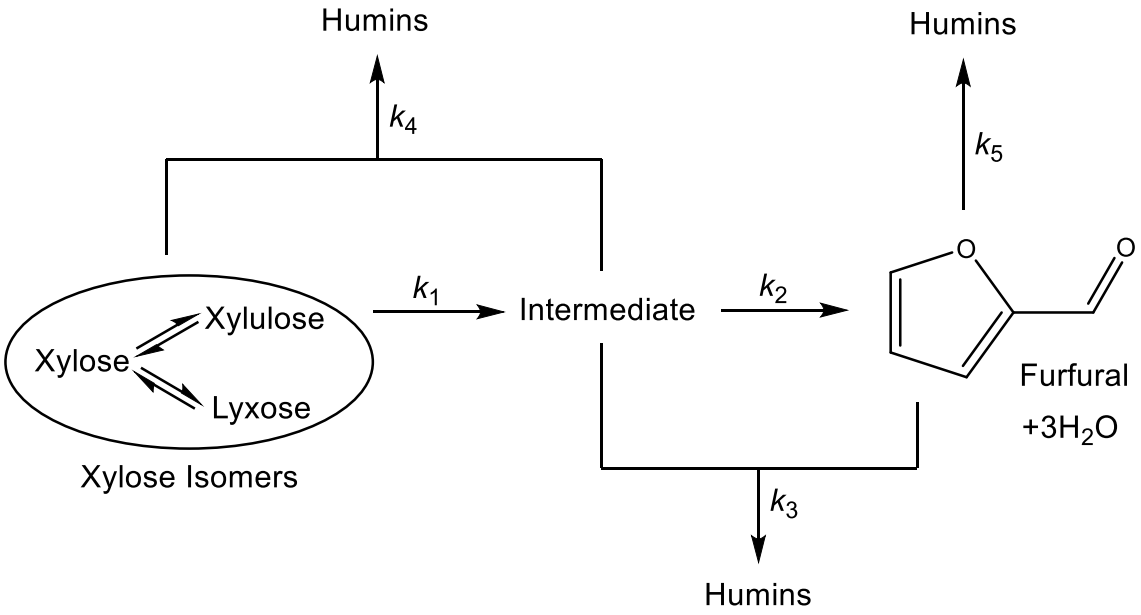

Scheme 3.1. Reaction network for furfural production from xylose. Isomerization is catalyzed by Lewis acids, while furfural production is catalyzed by Brønsted acids.

A lower furfural concentration in the reactor (x_f) diminishes the numerator and increases the denominator by increasing x_w. In the dilute scenario, as is the case in these experiments (1 g/L of furfural in water is equivalent to 0.02 mol%), x_w is effectively constant and, barring significant changes in activity coefficients, the furfural concentration in the permeate is proportional to the furfural concentration in the reactor. High permeate concentrations are achievable through favorable thermodynamics (ratio of activity coefficients and saturation vapor pressures) and favorable membrane properties (membrane selectivity). The SDS membrane outperforms the PDMS membrane in permeate concentration because of the higher reactor concentration and more favorable membrane selectivity: 6.3 for SDS, compared to 1.1 for PDMS.

Perhaps the most interesting finding from these experiments concerns the composition of species crossing the pervaporation membranes. The HPLC and ICP-OES analyses of the permeate samples revealed that only two chemicals were present in the permeate: furfural and water. Neither xylose isomers nor $CrCl_3$ were found in the permeate above the detection limit (HPLC: ~1 mg/L, ICP-OES: 0.25 µg/L), meaning that the membranes were infinitely selective for the product (furfural) over the reactant (xylose isomers) and the catalyst ($CrCl_3$). This phenomenon can be explained by examining Equation (3.9), which is a simplification of Equation (3.7) that describes the permeation rate of a material through a pervaporation membrane:

$$\dot{n}_i = A\frac{P_i}{l}\left(\gamma_i x_i p_i^{\text{sat}} - y_i p_{\text{permeate}}\right) \approx A\frac{P_i}{l}\gamma_i x_i p_i^{\text{sat}} \tag{3.9}$$

Passage of a material through the membrane is approximately proportional to the saturation vapor pressure of that material. However, neither xylose nor $CrCl_3$ have any significant saturation vapor pressure and are thus not expected to pervaporate. Therefore, pervaporation offers a simple way to separate a product from a homogeneous catalyst. In the context of furfural production from

xylose, this finding enables the continuous production of furfural with only a small, initial charge of homogeneous catalyst.

Figure 3.3a compares the amount of furfural produced over time with two reactor configurations: batch and continuous. Both reactions were carried out with the same amount of catalyst. The batch reaction was conducted without furfural extraction for 72 h (the results were identical to those achieved with extraction, as shown in Figure 3.2a). The continuous reaction was conducted by feeding a solution of 100 g/L xylose in water at a volumetric flow rate matching the pervaporation rate, using a 49-µm-thick SDS membrane. Furfural production rate is initially rapid in the batch reaction, but slows significantly after 30 h. Conversely, furfural production rate is fairly constant throughout the continuous reaction and the amount of furfural produced surpasses that of the batch reaction after about 30 h, even when considering only the permeated furfural, which constitutes about 90% of all of the furfural formed. The furfural produced in the continuous reaction beyond that point demonstrates the advantage gained by running the reaction continuously.

Additionally, the smaller amount of furfural produced in the continuous reaction compared to the batch reaction in the beginning can be attributed to the differing initial xylose concentrations for the two reactions. The batch reaction started with 250 mM xylose, while the continuous reaction started with 200 mM xylose. We chose to start the continuous reaction with a different concentration of xylose because our preliminary calculations showed that, with a 100 g/L xylose feed solution, the reactor would reach a steady-state xylose isomer concentration of approximately 200 mM; by starting the reaction at a concentration close to the expected steady-state value, the time required to reach steady state could be minimized. Starting one reaction with more xylose (*i.e.* the batch reaction) would lead to more furfural formed, at least initially. When multiplying the furfural formed in the continuous reaction by 250/200 to account for the difference in initial xylose

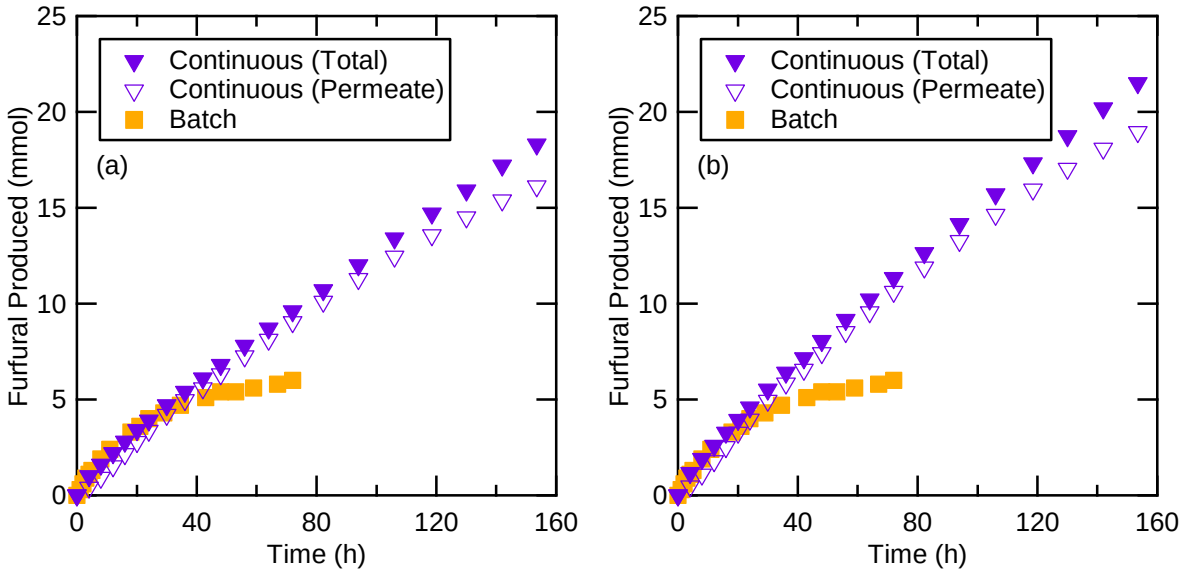

Figure 3.3. Continuous-mode furfural production compared to batch-mode production at 90 °C with 25 mM $CrCl_3$. Continuous-mode reaction assisted by 49-µm-thick SDS membrane. Batch-mode reaction conducted without pervaporation. Pervaporation resulted in complete catalyst retention, permitting lack of catalyst addition during continuous reaction. (a) As-measured results. (b) Continuous-mode results multiplied by 250/200 to account for difference in initial xylose concentration.

concentration, as is done in Figure 3.3b, the results are similar up to 12 h, at which point the continuous reaction surpasses the batch reaction.

3.3.2 Shortcomings of Pervaporation-Assisted Furfural Production at 90 °C

A significant drawback of the continuous, pervaporation-assisted reaction is shown in Figure 3.4a, which presents the furfural and water permeabilities of the SDS membrane over time. The water permeability remains constant throughout, while the furfural permeability starts high, increases in the first 24 h, then decreases steadily and significantly over time. This decrease in furfural permeability leads to a decrease in the furfural pervaporation rate and permeate concentration, as well as an increase in furfural concentration within the reactor. Left unsolved, this problem would limit the use of pervaporation for continuous furfural production.

A possible solution to the decreasing furfural permeability would be to cross-link the polymer membranes prior to use. Figure 3.4b shows the furfural permeabilities of SDS and cross-linked PDMS membranes for a reaction carried out at 90 °C. The SDS permeability varies somewhat during the 24-h reaction, but the PDMS permeability remains much more constant, demonstrating a possible relative stability of cross-linked PDMS to the reaction conditions. Furthermore, in a previous study we conducted of pervaporation-assisted furfural production at 140 °C catalyzed by solid Amberlyst 70, we found that furfural permeability for SDS membranes decreased during the course of reaction while that of the cross-linked PDMS membrane remained constant, as shown in Figure 3.4c.

We also performed pervaporation experiments with membranes using the same methods used to collect the data shown in Figure 3.4c, except that the catalyst was removed and three different feed solutions were used: (1) furfural in water, (2) xylose and furfural in water, and (3) xylose dehydration broth. The starting concentrations for Solutions 1 and 2 were similar to those in the reaction in Figure 3.4c. Solution 3, the xylose dehydration broth, was the liquid that remained in the reactor after pervaporation-assisted furfural production which contained xylose, furfural, and soluble humins (all solids, including the solid Amberlyst 70 catalyst, were removed by vacuum filtration). The results of these experiments are shown in Figure 3.4d. Furfural permeability of the SDS membranes remains constant with Solutions 1 and 2, but decreases with the xylose dehydration broth (Solution 3) in a manner similar to that observed during the reaction (Figure 3.4c). This indicates that the cause of the furfural permeability decrease is likely the soluble humins formed during the reaction. These humins clearly affect the SDS membranes, but do not appear to have an impact on the cross-linked PDMS membranes.

The relatively slow reaction rate and the lack of impact of furfural extraction on furfural yield, as seen in the batch reactions (Figure 3.2a), are consequences of carrying out at the reaction at 90 °C. This temperature was selected because membrane stability precluded operation above 100 °C. While prior work by Shin[49] shows that cross-linking of block copolymer pervaporation membranes improves thermal stability while retaining the permeability and selectivity of the non-cross-linked membrane, we were unable to synthesize and cross-link membranes for use at higher temperatures for this study. Consequently, we explored what would happen were it possible to operate at temperature of 130 °C, which is more characteristic of the temperatures used for the dehydration of xylose in other studies.[21-28,43,44]

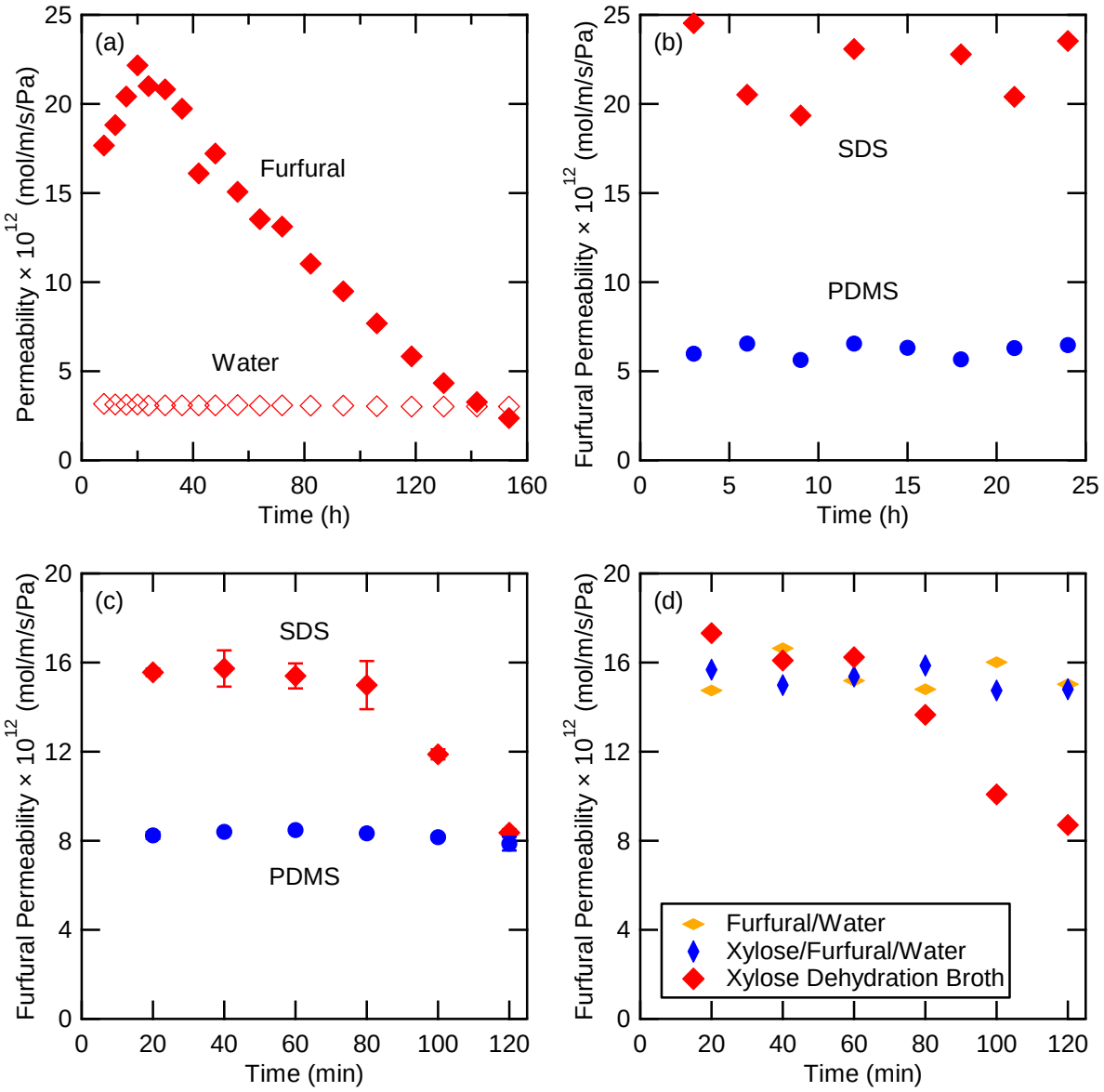

Figure 3.4. Permeability (furfural or water) of membranes (SDS or PDMS) during various experiments. (a) Permeability of SDS membrane during continuous-mode, $CrCl_3$-catalyzed furfural production. (b) Furfural permeability during batch-mode, $CrCl_3$-catalyzed furfural production. (c) Furfural permeability during batch-mode, Amberlyst-70-catalyzed furfural production. (d) Furfural permeability of SDS membranes with varying feed solutions.

3.3.3 Simulations of Pervaporation-Assisted Furfural Production at 130 °C

To determine the impact of furfural pervaporation at 130 °C, we measured the kinetics of xylose consumption and furfural formation at this temperature with and without *in situ* furfural extraction by LLE. For this experiment, we added 100 mM H_2SO_4 to the 25 mM $CrCl_3$, as the addition of a Brønsted acid to $CrCl_3$ has previously been found to improve both the reaction rate and the selectivity to furfural.[43] The conversion and yield for these reactions are shown as a

function of time in Figures 3.5a and 3.5b. The xylose isomer conversion reached 97% after 6 h, while the furfural yield reached 40-57% in the same time. Importantly, in contrast to what we found at 90 °C without H_2SO_4 (Figure 3.2a), *in situ* furfural extraction did affect the furfural yield, leading to a 43% increase in yield. Therefore, we expect *in situ* furfural pervaporation to have a similar effect on furfural yield.

Since the membranes used in this study were not stable at 130 °C, we examined the benefit of pervaporation at that temperature through simulations. The first step in this approach was to obtain the rate coefficients governing the dehydration of xylose to furfural and the conversion of both xylose and furfural to humins. We used the reaction network shown in Scheme 3.1 to represent the kinetics of the reaction catalyzed by 25 mM $CrCl_3$ and 100 mM H_2SO_4 at 130 °C. We assumed that all reactions are first-order in xylose isomers, furfural, and intermediates, when applicable, and assumed the intermediates to be at pseudo-steady state. The resulting differential equations describing the mole balances of each species are given in the Supporting Information. We calculated the reaction rate constant for furfural resinification, k_5, by fitting first-order kinetics of furfural conversion to data from a reaction starting with furfural as the substrate, in the absence of any sugars (Figure 3.5c). We calculated the remaining reaction rate constants k_1, k_2, k_3, and k_4 from data obtained without extraction (Figure 3.5b). All five reaction rate constants can be found in Table 3.1.

The simulated results are plotted alongside the experimental data from $CrCl_3$- and H_2SO_4-catalyzed reactions at 130 °C in Figure 3.5. The symbols are the experimental data, while the curves are the simulated results. Figures 3.5b and 3.5c show the data used to calculate the reaction rate constants k_1-k_5. Figure 3.5a shows the simulated results for LLE-assisted furfural production, which were calculated independently of the data. In order to simulate this scenario, we assumed that the mass transfer of furfural between the two phases was very rapid, resulting in an equilibrium distribution. We measured this distribution to be 89.6%±1.0%, *i.e.* the toluene phase contained an average 89.6% of the furfural across the measured concentration range (the error is the standard deviation of the 16 measurements). The agreement between all the simulated and experimental results is excellent, demonstrating that the calculated reaction rate constants can be used to represent reactions with varying degrees of furfural extraction.

We could not measure the permeability of SDS membranes at 130 °C because the membranes could not be used above 100 °C. We also could not measure the activity coefficient of furfural/water solutions at our concentrations of interest at that temperature. However, we found that a simplification allowed us to combine the two parameters in order to predict the system performance for reaction with pervaporation.

The driving force for pervaporation is maximized by minimizing the permeate partial pressure of all components, resulting in the simplification shown in Equation (3.9):

$$\dot{n}_i = A\frac{P_i}{l}\left(\gamma_i x_i p_i^{\text{sat}} - y_i p_{\text{permeate}}\right) \approx A\frac{P_i}{l}\gamma_i x_i p_i^{\text{sat}} \tag{3.9}$$

Equation (3.9) can then be rearranged to separate measurable quantities from those that we desire, as shown in Equation (3.10):

$$\frac{\dot{n}_i l}{A x_i p_i^{\text{sat}}} \approx (P\gamma)_i \tag{3.10}$$

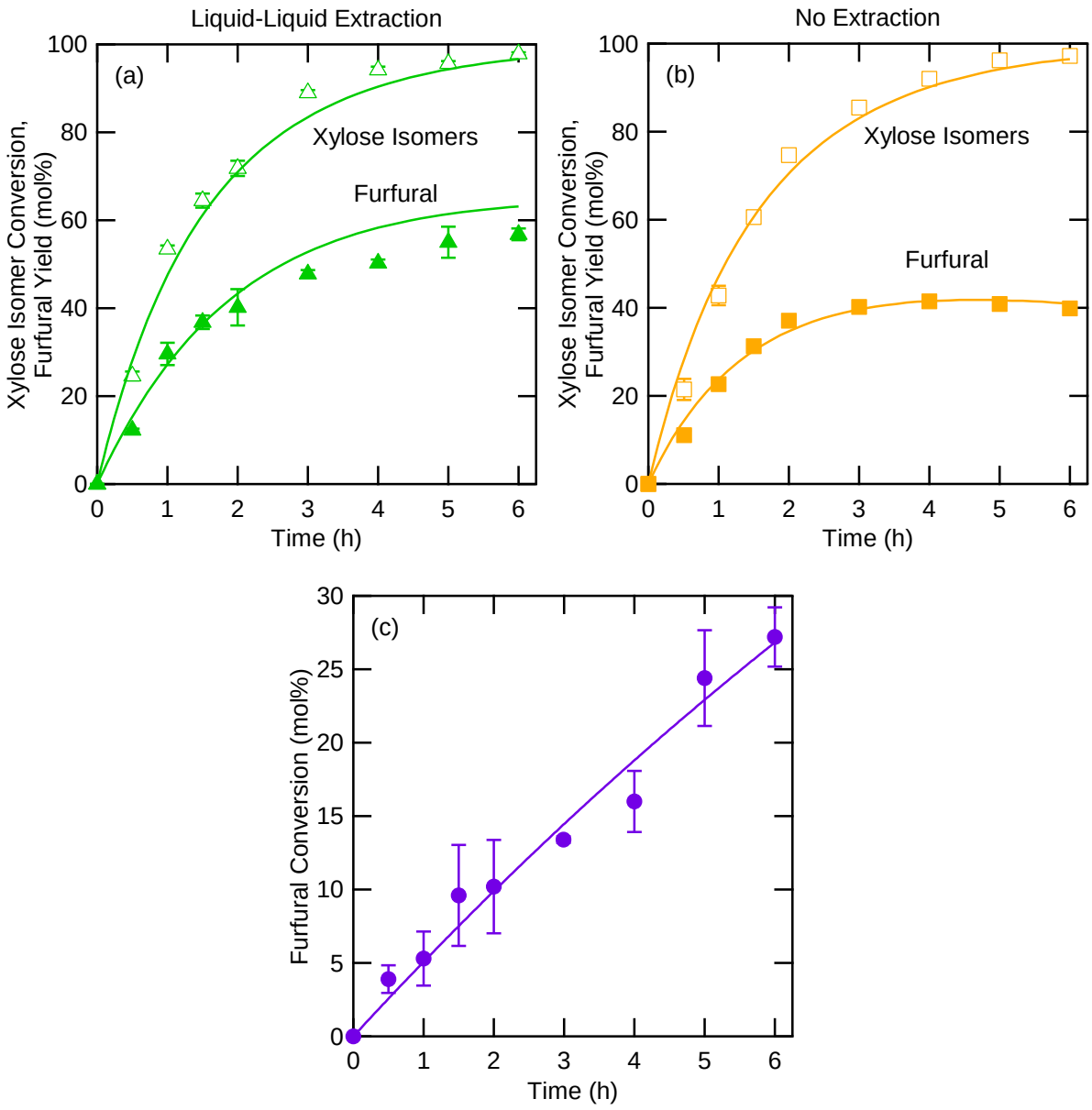

Figure 3.5. Batch-mode reactions at 130 °C with 25 mM $CrCl_3$ and 100 mM H_2SO_4. Data points represent experimental data, curves represent simulated results. (a) Conversion of 250 mM xylose with liquid-liquid extraction (2:1 toluene:water by volume). (b) Conversion of 250 mM xylose with no furfural extraction. (c) Conversion of 125 mM furfural.

Table 3.1. Parameters used in this study for membrane calculations and simulations.

Row	Parameter	Symbol	Value
	Thermodynamic parameters used to calculate permeabilities in Figure 3.4		
1	Furfural activity coefficient at 90 °C	γ_f	66[a]
2	Water activity coefficient at 90 °C	γ_w	1[a]
3	Furfural saturation vapor pressure at 90 °C (kPa)	p_f^{sat}	7.53[b]
4	Water saturation vapor pressure at 90 °C (kPa)	p_w^{sat}	70.0[b]
5	Furfural activity coefficient at 75 °C	γ_f	85[a]
6	Water activity coefficient at 75 °C	γ_w	1[a]
7	Furfural saturation vapor pressure at 75 °C (kPa)	p_f^{sat}	3.80[b]
8	Water saturation vapor pressure at 75 °C (kPa)	p_w^{sat}	38.5[b]
	Reaction rate constants at 130 °C		
9	Xylose isomer dehydration (h^{-1})	k_1	$5.1 \cdot 10^{-1}$
10	Furfural production (h^{-1})	k_2	$6.1 \cdot 10^{-1}$
11	Furfural-intermediate condensation (L/mmol/h)	k_3	$1.4 \cdot 10^{-3}$
12	Xylose-isomer-intermediate condensation (L/mmol/h)	k_4	$1.2 \cdot 10^{-3}$
13	Furfural resinification (h^{-1})	k_5	$5.2 \cdot 10^{-2}$
	Additional parameters for simulations at 130 °C		
14	Permeability × activity coefficient for furfural (mol/m/s/Pa)	$(P\gamma)_f$	$7.9 \cdot 10^{-10}$
15	Permeability × activity coefficient for water (mol/m/s/Pa)	$(P\gamma)_w$	$5.3 \cdot 10^{-12}$
16	Furfural saturation vapor pressure at (kPa)	p_f^{sat}	36.0[b]
17	Water saturation vapor pressure at (kPa)	p_w^{sat}	272[b]
18	Equilibrium constant of furfural in 2:1 toluene:water by volume	K	4.31
19	Membrane thickness (μm)	l	69
20	Reactor volume (mL)	V	83
21	Xylose concentration of feed solution in continuous-mode reactions (g/L)	$[X]_{in}$	100
22	Xylose isomer molecular weight (g/mol)	M_x	150.13
23	Furfural molecular weight (g/mol)	M_f	96.08
24	Water molecular weight (g/mol)	M_w	18.02
25	Solution density (g/mL)	ρ	1

[a] Reference 50, activity coefficients at 75 °C estimated from vapor-liquid equilibrium data

[b] Reference 50, saturation vapor pressures (mm Hg) at 75 °C calculated by Antoine equation, $A_{furfural} = 8.402$, $B_{furfural} = 2338.49$, $C_{furfural} = 261.638$, $A_{water} = 8.07131$, $B_{water} = 1730.63$, $C_{water} = 233.426$

We can measure permeation rate ($\dot{n}_i$), membrane thickness (l), membrane area (A), and the mole fractions of water and furfural (x_i), and we can calculate the saturation vapor pressures of water and furfural (p_i^{sat}) by the Antoine equation, allowing us to calculate the product of permeability and activity coefficient $(P\gamma)_i$.

Using Equation (3.10), we determined $(P\gamma)_i$ for furfural and water for SDS membranes from 50 to 90 °C, as shown in Figure 3.6. We then applied an exponential fit of the data, which we could extrapolate to 130 °C to represent a hypothetical SDS membrane that could operate at that temperature. $(P\gamma)_i$, especially for furfural, decreased as temperature increased, suggesting that the furfural flux should decrease with increasing temperature. However, since flux also depends on the saturation vapor pressure, which increases dramatically with temperature as dictated by the Antoine equation, the combined result is a significant increase in the furfural flux with temperature.

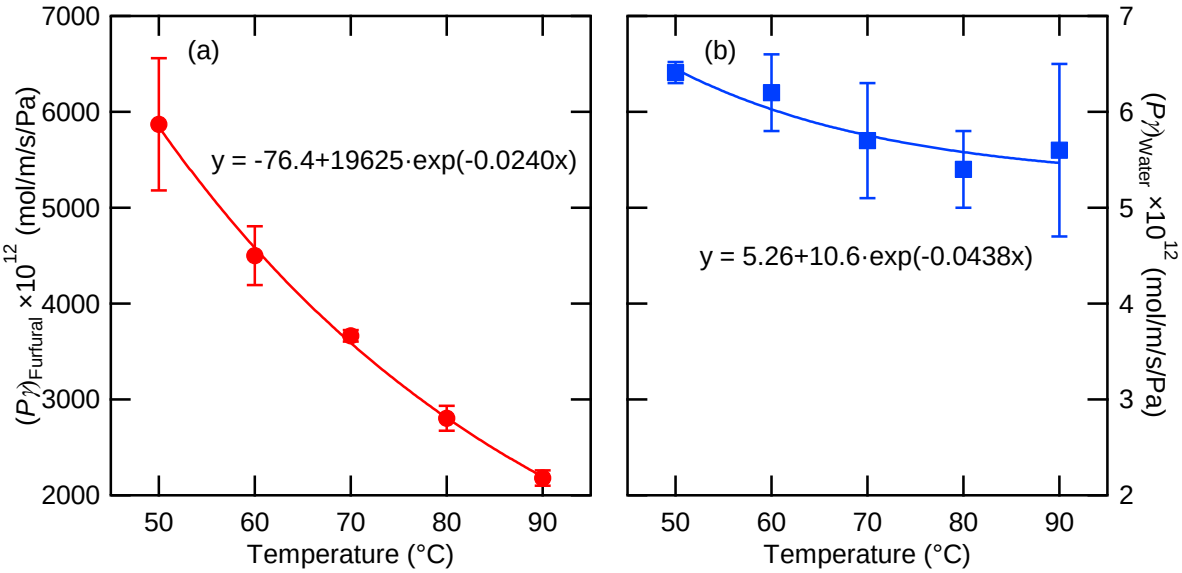

Figure 3.6. Change in the product of permeability and activity coefficient with temperature for SDS membranes for (a) furfural and (b) water. Equations describe the exponential fit (curves) to the data (symbols).

The first simulation undertaken was reaction in the batch mode with furfural extraction by LLE with toluene or pervaporation using an SDS membrane (a membrane thickness of 69 µm was used together with varying membrane-area-to-reactor-volume ratios, a). The differential equations used for these simulations are given in the Supporting Information while $(P\gamma)_i$, saturation vapor pressures, and other constants relevant to the simulations are reported in Table 3.1. The results of these calculations are presented in Figure 3.7.

A value of a = 0.17 cm^{-1} corresponds to the geometry of our experimental setup: 13.9 cm^2 of membrane area with 83 mL of reactor volume. For a = 1.3 cm^{-1}, the furfural yield obtained by pervaporation-assisted reaction is equivalent to that for LLE-assisted reaction after 6 h, and for a = 0.58 cm^{-1} furfural yield reaches 95% of that for LLE-assisted reaction. As shown in Figure 3.7a, the xylose isomer conversions for all five degrees of furfural extraction are identical, while the furfural yields follow the expected trend, increasing in order of no extraction < pervaporation with a = 0.17 cm^{-1} < a = 0.58 cm^{-1} < a = 1.3 cm^{-1} ≈ LLE.

Figure 3.7b, which shows the furfural concentration in the product phase (toluene for the LLE-assisted reaction, permeate for the pervaporation-assisted reactions), highlights a serious disadvantage of LLE and a significant advantage of pervaporation. When compared to the case of no extraction, LLE diminishes the furfural concentration in the extracted phase for three reasons. The first is that LLE is conducted with a 2:1 volume ratio of toluene:water; this reduces the furfural concentration by increasing the volume of solvent. Second, not all of the furfural formed in the aqueous phase is transferred to the toluene phase (only 89.6%), thereby reducing the furfural concentration further. While LLE increases the furfural yield by 54% relative to the value without extraction (40%), this gain in furfural yield does not compensate for the reduction in furfural concentration resulting from the use of a 2:1 ratio of toluene:water.

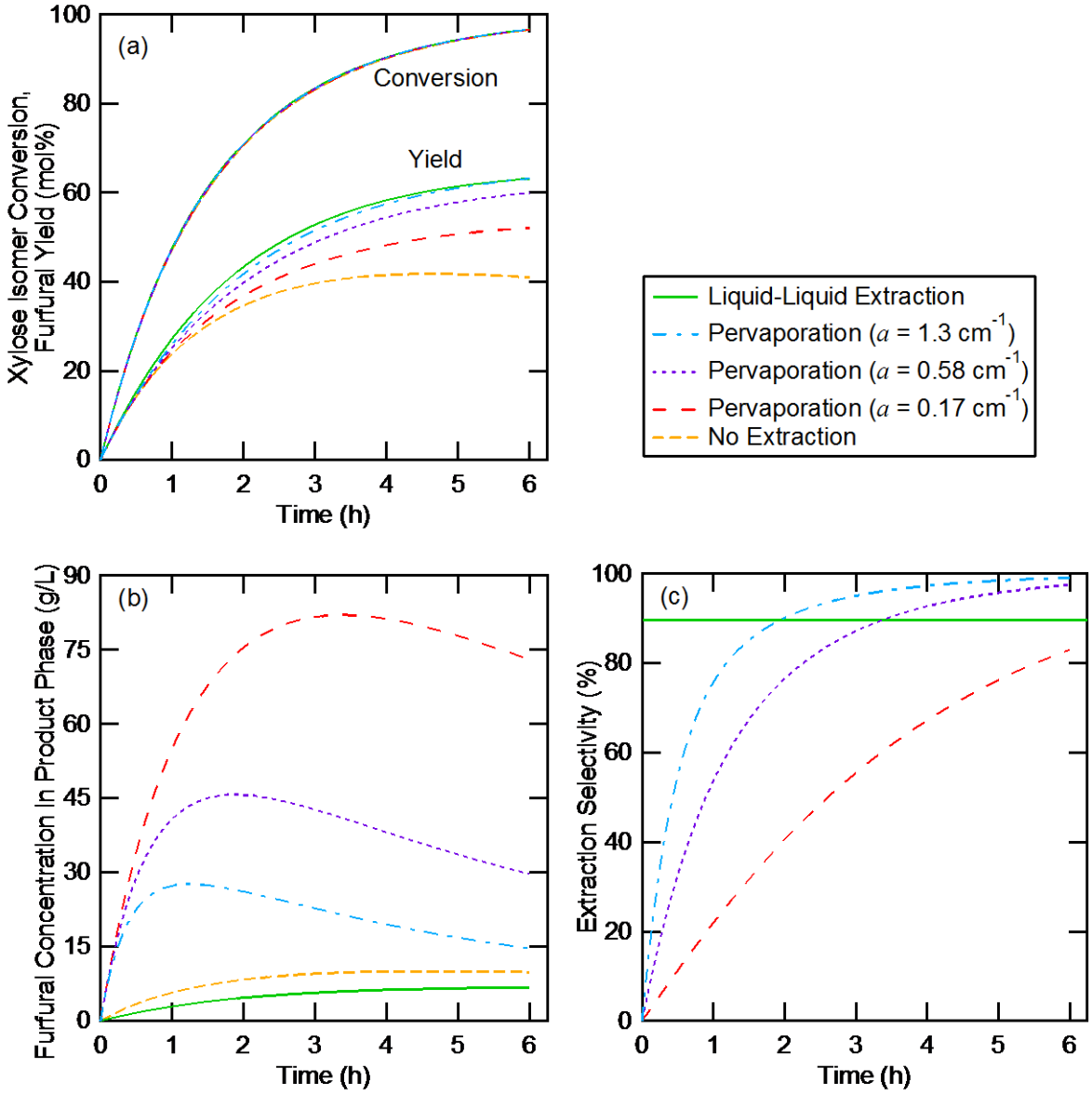

Figure 3.7. Simulations of batch-mode xylose conversion to furfural at 130 °C with 25 mM $CrCl_3$ and 100 mM H_2SO_4 with varying degrees of extraction: none, liquid-liquid extraction (2:1 toluene:water by volume), or pervaporation with a 69-µm-thick SDS membrane of varying area-to-volume ratios, *a*. (a) Xylose isomer conversion and furfural yield. (b) Furfural concentration in product phase (permeate or toluene if applicable, otherwise reactor). (c) Fraction of furfural extracted.

All three values of *a* considered result in higher concentrations of furfural in the product than that achievable by LLE, and for a = 0.17 cm^{-1} concentration of furfural in the permeate approaches the solubility limit of furfural in water at room temperature. This is because the combination of $(P\gamma)_i$ and saturation vapor pressure is an order of magnitude higher for furfural than water, allowing the permeate to be significantly more concentrated than in the reactor. The pervaporation product concentrations decrease with increasing *a* because of the decrease in

furfural concentration in the reactor, as discussed previously (3.3.1 Experimental Studies of Pervaporation-Assisted Furfural Production at 90 °C, Figure 3.2).

Similar reasoning explains the maximum in permeate concentration with time of reaction. The furfural production rate is initially very high in batch-mode reactions and exceeds the pervaporation and consumption rates, allowing the furfural concentration in the reactor to increase. The increase in furfural concentration in the reactor leads to an increase in furfural concentration in the permeate. As the reaction continues, the furfural pervaporation and consumption rates exceed the production rate, leading to a decline in furfural concentration in the reactor. This results in a more dilute permeate stream coming out of the membrane, which reduces the cumulative concentration of the permeate, as shown in Figure 3.7b.

Figure 3.7c shows the extraction selectivity, or fraction of furfural present in the product phase, for the LLE-assisted reaction and each pervaporation-assisted reaction. The LLE value remains constant (89.6%) throughout the reaction because we found that process to be rapid and equilibrium-limited. Increasing the toluene:water ratio would improve the extraction selectivity, but further reduce the furfural concentration in the toluene. The extraction selectivities of all three pervaporation-assisted reactions increase monotonically with time. The two higher rates of pervaporation achieve near-complete furfural extraction by the end, reaching 97.5% and 99.1% for a = 0.58 cm^{-1} and 1.3 cm^{-1}, respectively. This result, when combined with the results of Figures 3.7a and 3.7b, presents a tradeoff between quantity of furfural produced and concentration of furfural in the permeate.

At first glance, one might assume that the best way to produce furfural in a batch-mode reactor would be to maximize the membrane area, as that would lead to a maximized pervaporation rate and thus a minimized furfural concentration in the reactor and minimized furfural consumption by side reactions. However, this is not the case, as shown in Figure 3.7 (and Figure 3.2, to an extent). For the case of a = 0.58 cm^{-1}, the permeate furfural yield (product of furfural yield and extraction selectivity) is 58.4% and the permeate concentration is 29.7 g/L after 6 h. For a = 1.3 cm^{-1}, the permeate furfural yield is 62.6% and the permeate concentration is 14.6 g/L after 6 h. The benefit of the extra 4.2% permeate furfural yield must be weighed against the cost of purifying a permeate with a 50.8% reduction in concentration and using 124% more membrane area. The same cost-benefit analysis could be conducted comparing a = 0.58 cm^{-1} to 0.17 cm^{-1}, paying for 15.1% more permeate furfural yield with a 59.4% drop in concentration and 241% more membrane area.

3.3.4 Simulations of Continuous, Pervaporation-Assisted Furfural Production at 130 °C

We also simulated continuous reaction and pervaporation at 130 °C. The differential equations describing this process can be found in the Supporting Information. We used the same initial conditions as we employed in our continuous-mode setup: the reactor started with 30 g/L xylose (200 mM) in water and the feed reservoir contained 100 g/L xylose (666 mM) in water. The steady-state results of these simulations are plotted as a function of a in Figure 3.8. Steady state was reached within 50 h of reaction for all values of a considered (0.033 to 1.3 cm^{-1}). The main results of interest are the steady-state values of concentration of xylose isomers in the reactor, the permeation rate of furfural, the concentrations of furfural in the reactor and in the permeate, and the selectivity of the reaction.

Figure 3.8a shows how the steady-state concentration of xylose isomers and furfural permeation rate vary with a. The concentration of xylose isomers increases proportionally with a

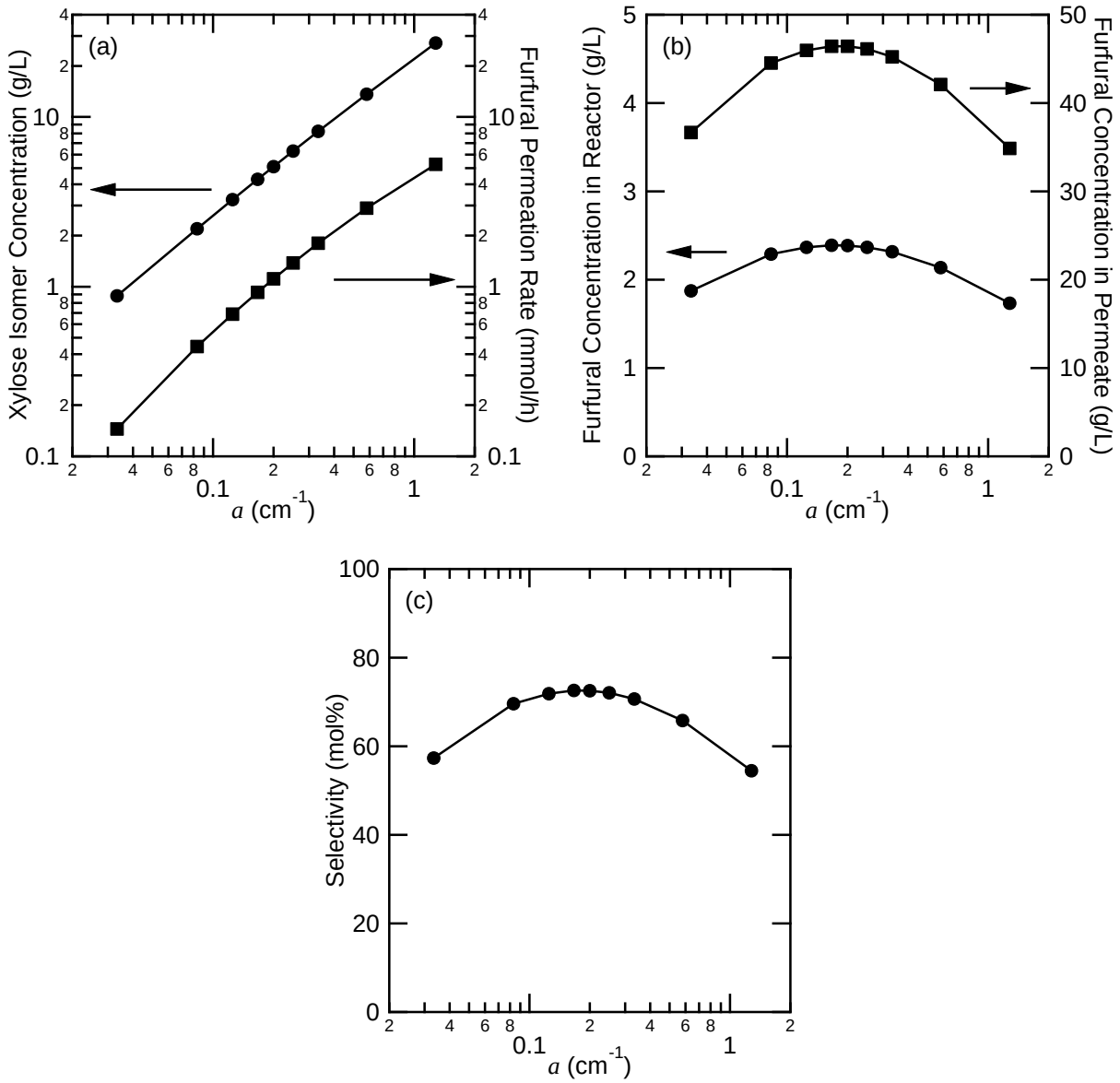

Figure 3.8. Simulations of continuous-mode xylose conversion to furfural at 130 °C with 25 mM $CrCl_3$ and 100 mM H_2SO_4 with varying membrane-area-to-reactor-volume ratio, a. Plots show steady-state values of (a) xylose isomer concentration in the reactor and furfural permeation rate. (b) Furfural concentration in the reactor and in the permeate. (c) Reaction selectivity.

because the rate of xylose addition must be balanced by the rate of xylose isomer consumption, as shown in Equation (3.11):

$$\frac{[X]_{\text{in}}}{V}\frac{dV^{\text{perm}}}{dt} = (k_1 + k_4[I])[X] \tag{3.11}$$

where $[X]_{\text{in}}$ is the concentration of xylose solution entering the reactor, V is the reactor volume, dV^{perm}/dt is the volumetric permeation rate (which is equal to the volumetric addition rate of xylose

solution), [I] is the concentration of an assumed pseudo-steady-state reaction intermediate, and [X] is the concentration of xylose isomers.

For the ranges of a and the resulting ranges of furfural concentrations in the reactor considered, the rate of xylose addition, dictated by the combined permeation rate of water and furfural, is proportional to a. Similarly, the rate of xylose isomer consumption is proportional to xylose isomer concentration. However, these proportionalities are approximations since the permeation rate depends on concentrations of furfural and water in the reactor and the xylose isomer consumption rate depends on concentration of an assumed pseudo-steady-state reaction intermediate; these concentrations are not proportional to a, thus the xylose isomer concentration is not strictly proportional to a. Steady-state furfural permeation rate exhibits a similar trend with a as that seen for xylose isomer concentration, but its dependence on a is somewhat less linear. Linearity would be expected, based on Equation (3.7), but the furfural permeation rate also depends on furfural concentration in the reactor, which varies with a, as shown in Figure 3.8b.

Figure 3.8b shows a relatively weak correlation between steady-state furfural concentration in the reactor and a, rising by 28% with an order-of-magnitude increase in a and falling by 27% with another order-of-magnitude increase in a, resulting in a maximum in furfural concentration. This occurs because of the balance in furfural production (by Reaction 2 of Scheme 3.1) with furfural consumption (by Reactions 3 and 5 of Scheme 3.1) and pervaporation, as shown in Equation (3.12):

$$k_2[I] = k_3[I][F] + k_5[F] + a\frac{P_\mathrm{f}}{l}\gamma_\mathrm{f}x_\mathrm{f}p_\mathrm{f}^\mathrm{sat} \tag{3.12}$$

where [F] is the concentration of furfural in the reactor. Furfural production is proportional to the concentration of the reactive intermediate, which is approximately proportional to xylose isomer concentration (see Equation (3.S4)), which is proportional to a; thus, furfural production is approximately proportional to a. On the other side of the mole balance is furfural consumption and pervaporation, the combination of which varies from being largely determined by pervaporation to nearly-completely determined by pervaporation. Pervaporation is proportional to a, so the combination of furfural production, consumption, and pervaporation is the fairly insensitive function of a shown in Figure 3.8b.

Figure 3.8b also shows the permeate furfural concentration. This concentration is the instantaneous concentration, rather than the cumulative concentration. We chose to report the instantaneous concentration because it is a figure that is representative of steady state; it is time-invariant. Conversely, the cumulative concentration depends on arbitrary factors, namely the initial concentration of xylose in the reactor and the time elapsed since the reaction began; however, the cumulative and instantaneous concentrations equalize if given enough time. The permeate furfural concentration is proportional to the furfural concentration in the reactor, as shown in Equation (3.8), and is 20 times greater. Just as an intermediate value of a leads to a maximum in reactor furfural concentration, an intermediate value of a leads to a maximum in the permeate concentration of furfural.

Figure 3.8c examines the dependence of steady-state selectivity on a. We define selectivity as:

$$\text{Selectivity} = \frac{\text{Molar permeation rate of furfural}}{\text{Molar addition rate of xylose}} \times 100\% \tag{3.13}$$

The molar addition rate of xylose is determined by the permeation rates of furfural and water; all permeated volume is replaced by the same volume of 100 g/L xylose solution. The changes in selectivity with *a* are significant, rising from 57% to 73% then falling to 54%. The reason for this pattern stems from the difference in how the rates of furfural and water permeation are affected by *a*. Furfural permeation rate, as discussed previously, depends on furfural concentration in the reactor, which leads to the slightly non-linear behavior shown in Figure 3.8a. Water permeation rate is relatively linear because the concentration of water in the reactor is essentially constant with respect to *a*; the reaction is fairly dilute, especially on a molar basis. Additionally, as seen in Figure 3.8b, the permeate is mostly water, indicating that the total permeation rate is controlled by that of water and not furfural. Combining the trends of the furfural and total permeation rates results in the behavior seen in Figure 3.8c.

It is unclear how to produce furfural most economically using a continuous-mode, pervaporation-assisted reactor. The trends presented in Figures 3.8b and 3.8c suggest that using $a = 0.17$ cm^{-1}, coincidentally the value we had experimentally, yields the best result as that is where the selectivity and product (permeate) concentration are maximized. However, Figure 3.8a shows that the furfural production (permeation) rate continually increases with increasing *a*; one can produce significantly more furfural per reactor volume simply by increasing *a*. Considering all the trends in Figure 3.8, the optimal value of *a* might not be 0.17 cm^{-1}, but slightly higher, *e.g.* 0.2 cm^{-1}, as that provides a 20% increase in furfural production rate with no significant loss in selectivity or product concentration. Perhaps, with more insight into the economics of furfural production and pervaporation, one would conclude that $a = 1.3$ cm^{-1} is better than 0.2 cm^{-1}, because the 374% increase in production rate is worth the 25% decrease in both selectivity and product concentration.

3.4 Conclusions

A specially built 83-mL membrane-reactor was used to investigate the dynamics of xylose dehydration and the concurrent removal of furfural from the reaction mixture by pervaporation. Both batch and continuous operation of the reactor were considered. For both modes of operation, $CrCl_3$ was used as the catalyst and the reaction was carried out in the aqueous phase at 90 °C. We found that while the catalyst was capable of maintaining its activity at such a low temperature, *in situ* extraction of furfural had no impact on furfural yield in a batch reactor. Pervaporation could be used to increase the concentration of furfural in the extracted phase by as much as an order of magnitude, but permeating furfural too rapidly led to dilution of furfural. Additionally, pervaporation was infinitely selective for the permeation of the product (furfural) compared to the reactants (xylose isomers) and the catalyst ($CrCl_3$), which enabled us to produce furfural continuously by feeding an aqueous xylose solution to the reactor. Doing so allowed us to produce furfural in higher quantities and for longer times than in batch-mode operation of the reactor with the same amount of catalyst.

Continuous, pervaporation-assisted furfural production is promising, but hampered by two main issues: loss of furfural permeability with time and the limitation to operation at low temperatures due to membrane stability. Both issues could be solved by cross-linking the membranes. By varying pervaporation feed solutions, we found that the likely cause of the changing furfural permeability was the soluble humins produced during reaction. Experiments conducted with cross-linked membranes led to stable permeabilities, suggesting that cross-linking

could inhibit the loss in permeability with time on stream. This could be due to cross-links preventing the polymer chains from rearranging and changing morphology in the presence of humins, which could lead to a change in permeability. Cross-linking was also previously found to improve thermal stability of pervaporation membranes without sacrificing transport properties.[49]

Pervaporation-assisted furfural production was simulated at 130 °C in order to assess the advantages of higher temperature operation. For this effort, the reaction rate coefficients for the elementary steps shown in Scheme 3.1 were measured at 130 °C and the membrane permeabilities for furfural and water for an SDS membrane were extrapolated from data measured at lower temperatures. The simulations of batch-mode operation revealed significant changes in system performance with changes in the membrane-area-to-reactor-volume ratio, *a*. Increasing *a* led to increased furfural yield and extraction selectivity, but also to reductions in permeate concentration. Simulations of continuous-mode operation showed that changes in *a* lead to maximum in the permeate concentration and reaction selectivity, for a value of $a = 0.17$ cm^{-1}. However, since the furfural permeation rate is approximately proportional to *a*, an analysis of the effects of *a* on the permeate concentration, reaction selectivity, and permeation rate do not reveal an optimal value for *a*. This means that the choice of *a* must depend on and an analysis of the process economics.

Future work on continuous, pervaporation-assisted furfural production should focus on increasing the temperature of the reaction in order to increase reaction rates. The liquid hourly space velocity (LHSV) of the simulated reaction at 130 °C is approximately 0.001 h^{-1} (assuming $a = 0.17$ cm^{-1} and furfural permeation rate = 1 mmol/h) and reactor capital costs could be reduced with a higher LHSV. This effort should begin with further development of furfural-selective pervaporation membranes for use at typical furfural production temperatures of at least ~150 °C,[21-28,43,44] *e.g.* cross-linked block polymer pervaporation membranes studied by Shin.[49] Additionally, more-furfural-selective membranes should be researched to produce permeates of higher furfural purity and reduce water usage, and thus energy usage of the process (pervaporation requires evaporation of all permeating components). Finally, effort should be placed on identifying reaction conditions (*i.e.*, temperature, solvent, catalyst, *etc.*) that approach 100% furfural selectivity. Doing so would minimize the formation of humins and their accumulation in the reactor.

3.5 Acknowledgments

This work was supported by the Energy Biosciences Institute at the University of California at Berkeley, funded by BP. The authors thank Dow Chemical for donating the Amberlyst 70 ion-exchange resin used as a catalyst in this study, Adam Grippo for his assistance in operating the GC-FID for this study, and Eric Granlund and Jim Breen of the University of California at Berkeley College of Chemistry machine and glass shops, respectively, for their assistance in constructing the membrane reactor used in this study (Figure 3.1).

3.6 Supporting Information

We used a simplified reaction network for furfural production catalyzed by 25 mM $CrCl_3$ and 100 mM H_2SO_4 at 130 °C as shown in Scheme 3.1. All reactions were assumed to be first-order in concentrations of xylose isomers, reaction intermediate, and furfural, *i.e.*

$$\frac{d[X]}{dt} = -(k_1 + k_4[I])[X] \tag{3.S1}$$

$$\frac{d[I]}{dt} = k_1[X] - k_2[I] - k_3[I][F] - k_4[I][X] \tag{3.S2}$$

$$\frac{d[F]}{dt} = k_2[I] - k_3[I][F] - k_5[F] \tag{3.S3}$$

where [*X*], [*I*], and [*F*] are the molar concentrations of xylose isomers, reaction intermediate, and furfural, respectively. The constants k_1, k_2, k_3, k_4, and k_5 correspond to the same constants in Scheme 3.1. We assumed that the intermediate exists in a pseudo-steady state, *i.e.* $d[I]/dt \approx 0$ and

$$[I] = \frac{k_1[X]}{k_2 + k_3[F] + k_4[X]} \tag{3.S4}$$

We measured k_1-k_5 by running two reactions without furfural extraction. Both occurred at 130 °C in water and were catalyzed by 25 mM $CrCl_3$ and 100 mM H_2SO_4. We used least squares minimization of the sum of errors between experimental and simulated concentrations of xylose isomers and furfural. We measured k_5 on its own by reacting 125 mM furfural. In this case, the only relevant reaction is furfural resinification, or Reaction 5 in Scheme 3.1, and the expected time-dependence of [*F*] is

$$[F] = [F]_0 \exp(-k_5 t) \tag{3.S5}$$

where $[F]_0$ is the initial concentration of furfural (125 mM). The comparison between experimental data and this fitting equation is shown in Figure 3.5a. We measured k_1-k_4 by reacting 250 mM xylose and using the value of k_5 measured previously. The comparison between the data and the simulation is shown in Figure 3.5b and all five kinetic rate constants are shown in Table 3.1.

Next, we validated the rate constants by comparing experimental and simulated data for furfural production with furfural extraction by liquid-liquid extraction (LLE) using a 2:1 volume ratio of toluene:water. We assumed that the mass transfer rate of furfural across the two phases was very rapid, resulting in an equilibrium distribution and allowing us to rewrite the furfural mole balance as follows:

$$\frac{d[F]^{aq}}{dt} = \left(\frac{1}{K\nu + 1}\right)(k_2[I] - k_3[I][F] - k_5[F]) \tag{3.S6}$$

$$\frac{d[F]^{org}}{dt} = \left(\frac{K}{K\nu + 1}\right)(k_2[I] - k_3[I][F] - k_5[F]) \tag{3.S7}$$

where $[F]^{aq}$ and $[F]^{org}$ are the concentrations of furfural in the aqueous and toluene phases, respectively, K is the equilibrium constant (*i.e.* $[F]^{org}/[F]^{aq}$, measured to be 4.31 across the concentration range relevant to the reaction), and v is the volume ratio (*i.e.* toluene-phase volume/aqueous-phase volume = 2). The experimental and simulated data for LLE-assisted furfural production are in good agreement and are shown in Figure 3.5c.

We then used the kinetic rate constants and extrapolated pervaporation data to predict pervaporation-assisted furfural production in water with 25 mM $CrCl_3$ and 100 mM H_2SO_4 at 130 °C. The mole balances for this approach were modified slightly.

For batch-mode reactions, a term was added to the mole balance of furfural in the reactor to represent pervaporation:

$$\frac{d[F]^{ret}}{dt} = k_2[I] - k_3[I][F] - k_5[F] - \frac{Ap_f^{sat}(P\gamma)_f}{Vl}\frac{[F]^{ret}}{[F]^{ret} + [X] + [W]} \tag{3.S8}$$

where $[F]^{ret}$ is the molar concentration of furfural in the retentate (reactor), A is the membrane area, p_f^{sat} is the saturation vapor pressure of furfural at 130 °C, $(P\gamma)_f$ is the product of furfural permeability and furfural activity coefficient obtained from Figure 3.6a, V is the reactor volume, l is the membrane thickness, and $[W]$ is the molar concentration of water. $[W]$ was calculated by assuming a constant solution density of 1 g/mL, such that

$$[W] = (1\ \text{g/mL} - [F]M_f - [X]M_x)/M_w \tag{3.S9}$$

where M_f, M_x, and M_w are the molecular weights of furfural, xylose isomers, and water, respectively. In addition to the change to the furfural mole balance (Equation (3.S8)), we added equations describing the moles of furfural in the permeate and the volume of the permeate:

$$\frac{dN_f^{perm}}{dt} = \frac{Ap_f^{sat}(P\gamma)_f}{l}\frac{[F]^{ret}}{[F]^{ret} + [X] + [W]} \tag{3.S10}$$

$$\frac{dV^{perm}}{dt} = \frac{A}{l}\left(\frac{p_f^{sat}(P\gamma)_f[F]^{ret}M_f + p_w^{sat}(P\gamma)_w[W]M_w}{[F]^{ret} + [X] + [W]}\right)(1\ \text{mL/g}) \tag{3.S11}$$

where N_f^{perm} is the moles of furfural in the permeate and V^{perm} is the volume of the permeate. Equation (3.S10) matches the pervaporation term in Equation (3.S8), but is opposite in sign and is multiplied by V. Equation (3.S11) considers the permeated mass of both furfural and water and converts it to volume by assuming a solution density of 1 g/mL.

For continuous-mode reactions, we used the same differential equations as we did for the batch-mode reactions, with one more term added to the xylose isomer mole balance to describe the input of xylose:

$$\frac{d[X]}{dt} = -(k_1 + k_4[I])[X] + \frac{[X]_{in}}{V}\frac{dV^{perm}}{dt} \tag{3.S12}$$

$[X]_{in}$ is the concentration of xylose in the solution fed to the reactor. The volume of the reactor is kept constant so that the volumetric flow rate of xylose solution into the reactor matches the

volumetric permeation rate. The steady-state results presented in Figure 3.8 were obtained from simulations of 50 h of reaction, at which point all the metrics in Figure 3.8 were time-invariant.

3.7 References

1. R. Mariscal, P. Maireles-Torres, M. Ojeda, I. Sádaba and M. López Granados, *Energy Environ. Sci.*, 2016, **9**, 1144-1189.
2. M. J. Biddy, C. Scarlata and C. Kinchin, *Chemicals from Biomass: A Market Assessment of Bioproducts with Near-Term Potential*, Report NREL/TP-5100-65509, National Renewable Energy Laboratory, Golden, CO, 2016.
3. A. S. Mamman, J.-M. Lee, Y.-C. Kim, I. T. Hwang, N.-J. Park, Y. K. Hwang, J.-S. Chang and J.-S. Hwang, *Biofuels, Bioprod. Bioref.*, 2008, **2**, 438-454.
4. G. W. Huber, S. Iborra and A. Corma, *Chem. Rev.*, 2006, **106**, 4044-4098.
5. D. M. Alonso, J. Q. Bond and J. A. Dumesic, *Green Chem.*, 2010, **12**, 1493.
6. A. Corma, O. de la Torre, M. Renz and N. Villandier, *Angew. Chem.*, 2011, **50**, 2375-2378.
7. J. P. Lange, E. van der Heide, J. van Buijtenen and R. Price, *ChemSusChem*, 2012, **5**, 150-166.
8. G. A. Tompsett, N. Li and G. W. Huber, in *Thermochemical Processing of Biomass: Conversion into Fuels, Chemicals and Power*, ed. R. C. Brown, John Wiley & Sons, Ltd, Chichester, UK, First edn., 2011, ch. 8, pp. 232-279.
9. J. J. Bozell and G. R. Petersen, *Green Chem.*, 2010, **12**, 539.
10. L. Bui, H. Luo, W. R. Gunther and Y. Roman-Leshkov, *Angew. Chem. Int. Ed.*, 2013, **52**, 8022-8025.
11. D. M. Alonso, S. G. Wettstein and J. A. Dumesic, *Green Chem.*, 2013, **15**, 584.
12. K. Yan, G. Wu, T. Lafleur and C. Jarvis, *Renewable Sustainable Energy Rev.*, 2014, **38**, 663-676.
13. F. B. Oliveira, C. Gardrat, C. Enjalbal, E. Frollini and A. Castellan, *J. Appl. Polym. Sci.*, 2008, **109**, 2291-2303.
14. A. Gandini and M. N. Belgacem, *Prog. Polym. Sci.*, 1997, **22**, 1203-1379.
15. M. Hronec, K. Fulajtarová and T. Liptaj, *Appl. Catal., A*, 2012, **437-438**, 104-111.
16. C. M. Cai, T. Zhang, R. Kumar and C. E. Wyman, *J. Chem. Technol. Biotechnol.*, 2014, **89**, 2-10.
17. I. Agirrezabal-Telleria, I. Gandarias and P. L. Arias, *Catal. Today*, 2014, **234**, 42-58.
18. K. J. Zeitsch, *The Chemistry and Technology of Furfural and its Many By-Products*, Elsevier Science, Amsterdam, 2000.
19. B. Danon, G. Marcotullio and W. de Jong, *Green Chem.*, 2014, **16**, 39-54.
20. J. M. J. Antal, T. Leesomboon, W. S. Mok and G. N. Richards, *Carbohydr. Res.*, 1991, **217**, 71-85.
21. N. K. Gupta, A. Fukuoka and K. Nakajima, *ACS Catal.*, 2017, **7**, 2430-2436.
22. C. García-Sancho, J. M. Rubio-Caballero, J. M. Mérida-Robles, R. Moreno-Tost, J. Santamaría-González and P. Maireles-Torres, *Catal. Today*, 2014, **234**, 119-124.
23. S. Peleteiro, V. Santos and J. C. Parajo, *Carbohydr. Polym.*, 2016, **153**, 421-428.
24. R. Weingarten, J. Cho, J. W. C. Conner and G. W. Huber, *Green Chem.*, 2010, **12**, 1423.
25. H. Li, A. Deng, J. Ren, C. Liu, W. Wang, F. Peng and R. Sun, *Catal. Today*, 2014, **234**, 251-256.
26. M. J. Campos Molina, R. Mariscal, M. Ojeda and M. Lopez Granados, *Bioresour. Technol.*, 2012, **126**, 321-327.
27. S. Le Guenic, F. Delbecq, C. Ceballos and C. Len, *J. Mol. Catal. A: Chem.*, 2015, **410**, 1-7.

28. Y. Wang, F. Delbecq, W. Kwapinski and C. Len, *Mol. Catal.*, 2017, **438**, 167-172.
29. J. Wijmans and R. W. Baker, *J. Membr. Sci.*, 1995, **107**, 1-21.
30. R. W. Baker, *Membrane Technology and Applications*, John Wiley & Sons Ltd, The Atrium, Southern Gate, Chichester, West Sussex, P19 8SQ, United Kingdom, 2012.
31. Y. He, D. M. Bagley, K. T. Leung, S. N. Liss and B. Q. Liao, *Biotechnol. Adv.*, 2012, **30**, 817-858.
32. Y. K. Ong, G. M. Shi, N. L. Le, Y. P. Tang, J. Zuo, S. P. Nunes and T.-S. Chung, *Prog. Polym. Sci.*, 2016, **57**, 1-31.
33. D. Cai, T. Zhang, J. Zheng, Z. Chang, Z. Wang, P. Y. Qin and T. W. Tan, *Bioresour. Technol.*, 2013, **145**, 97-102.
34. W. Van Hecke, T. Hofmann and H. De Wever, *Bioresour. Technol.*, 2013, **129**, 421-429.
35. U. K. Ghosh, N. C. Pradhan and B. Adhikari, *Desalination*, 2007, **208**, 146-158.
36. U. K. Ghosh, N. C. Pradhan and B. Adhikari, *Desalination*, 2010, **252**, 1-7.
37. X. Liu, H. Jin, Y. Li, H. Bux, Z. Hu, Y. Ban and W. Yang, *J. Membr. Sci.*, 2013, **428**, 498-506.
38. S. S. Gaykawad, Y. Zha, P. J. Punt, J. W. van Groenestijn, L. A. van der Wielen and A. J. Straathof, *Bioresour. Technol.*, 2013, **129**, 469-476.
39. M. Sagehashi, T. Nomura, H. Shishido and A. Sakoda, *Bioresour. Technol.*, 2007, **98**, 2018-2026.
40. F. Qin, S. Li, P. Qin, M. N. Karim and T. Tan, *Green Chem.*, 2014, **16**, 1262.
41. D. R. Greer, T. P. Basso, A. B. Ibanez, S. Bauer, J. M. Skerker, A. E. Ozcam, D. Leon, C. Shin, A. P. Arkin and N. P. Balsara, *Green Chem.*, 2014, **16**, 4206-4213.
42. D. R. Greer, A. E. Ozcam and N. P. Balsara, *AIChE J.*, 2015, **61**, 2789-2794.
43. V. Choudhary, S. I. Sandler and D. G. Vlachos, *ACS Catal.*, 2012, **2**, 2022-2028.
44. K. R. Enslow and A. T. Bell, *Catal. Sci. Technol.*, 2015, **5**, 2839-2847.
45. J. B. Binder, J. J. Blank, A. V. Cefali and R. T. Raines, *ChemSusChem*, 2010, **3**, 1268-1272.
46. C. Shin, Z. C. Baer, X. C. Chen, A. E. Ozcam, D. S. Clark and N. P. Balsara, *J. Membr. Sci.*, 2015, **484**, 57-63.
47. Y. Shabtai, S. Chaimovitz, A. Freeman, E. Katchalski-Katzir, C. Linder, M. Nemas, M. Perry and O. Kedem, *Biotechnol. Bioeng.*, 1991, **39**, 869-876.
48. A. E. Ozcam, N. Petzetakis, S. Silverman, A. K. Jha and N. P. Balsara, *Macromolecules*, 2013, **46**, 9652-9658.
49. C.-y. Shin, PhD Dissertation, University of California, Berkeley, 2016.
50. J. Gmehling, U. Onken and W. Arlt, *Vapor-liquid equilibrium data collection*, DECHEMA, Frankfurt, 1978.

Chapter 4: Production of Hydroxyl-Rich Acids from Xylose and Glucose Using Sn-BEA Zeolite

Abstract

Sn-BEA zeolite is known to catalyze the aldose-to-ketose isomerization of xylose and glucose; however, the selectivity to pentose and hexose isomers is not stoichiometric, suggesting the formation of other products. In the present study, we have observed near-complete conversion of all pentose and hexose isomers when xylose and glucose were reacted in the presence of Sn-BEA at 140 °C and 200 °C, respectively. The previously unidentified products were identified by nuclear magnetic resonance and mass spectrometry to be hydroxyalkanoic acids and their derivatives. The hydroxyl-rich acids comprise a significant fraction of the converted sugars and are potential monomers for the synthesis of hyper-crosslinked, biodegradable polymers.

4.1 Introduction

Lignocellulosic biomass is an attractive and renewable feedstock for producing chemicals.[1,2] The two major components of lignocellulosic biomass are cellulose and hemicellulose, which together comprise as much as 80 dry wt% of this feedstock.[3] These carbohydrates can be hydrolyzed to their constituent pentose and hexose sugars, xylose and glucose. Subsequent dehydration of xylose and glucose produces furfural and 5-(hydroxymethyl)furfural (HMF), respectively, products that can be further converted to fuels, lubricants, and other commodity chemicals.[2,4,5] The selective dehydration of pentoses and hexoses to furanics has been shown to be best carried out using a combination of Lewis acid and Brønsted acid catalysts.[6,7] Brønsted acids catalyze the dehydration of sugars to furanics, whereas Lewis acids catalyze the isomerization of the most prevalent aldoses (xylose and glucose) to their ketose forms (xylulose and fructose),[8-13] which are much more susceptible to dehydration than their respective aldoses.[14]

One of the most promising Lewis acid catalysts for the aldose-to-ketose isomerization of xylose and glucose is Sn-BEA, a Beta zeolite containing framework Sn atoms.[7-10,13] The hydrophobicity of this catalyst is an attractive feature that enables isomerization of pentose and hexose sugars to be carried out in aqueous solution. However, prior studies have shown that while complete consumption of xylose and glucose can be achieved at temperatures of 100 °C and above, the selectivity to the isomers of the two sugars is incomplete, suggesting the formation of additional products.[7-9] The objective of the present study was to identify the products not accounted for in previous investigations and to suggest the reaction pathways by which they might be formed.

This chapter was reported in *ChemistrySelect*, 2016, **1**, 4167-4172 and is adapted with permission from co-authors Hsiang-Sheng Chen, Hagit Sorek, Jennifer D. Lewis, Yuriy Román-Leshkov, and Alexis T. Bell.

4.2 Experimental Methods

4.2.1 Materials

D-(+)-xylose (≥99%), D-(−)-lyxose (99%), D-xylulose (≥98%), furfural (99%), toluene (≥99.5%), pyridine anhydrous (99.8%), 1,6-hexanediol (97%), and dodecane (≥99%) were purchased from Sigma-Aldrich; D-(−)-fructose (99%), inositol (≥98%), and 5-(hydroxymethyl)furfural (98%) were purchased from Acros Organics; D-glucose anhydrous was purchased from Fisher Chemical; and D-(+)-mannose (≥99%) and 1-trymethylsilyl-imidazol (≥98%) were purchased from Fluka Analytical. All chemicals were used as received.

Sn-BEA used in this study was synthesized as follows using chemicals purchased from Sigma-Aldrich: 26.735 g aqueous tetraethylammonium hydroxide (35 wt%) and 24.069 g tetraethylorthosilicate (≥99%) were added to a Teflon® (polytetrafluoroethylene, [PTFE]) dish, which was magnetically stirred at room temperature for 90 min and then cooled in an ice bath. Then, 0.261 g Sn(II) chloride dihydrate (≥98%) dissolved in 15 mL cold deionized water (DI H_2O) was added dropwise. Sn(II), which oxidizes to Sn(IV) in water, was used instead of $SnCl_4$•$5H_2O$ and resulted in Sn-BEA consistently free of extraframework SnO_2. The solution was left uncovered on a stir plate for 12 h to reach a total mass of 35 g. Next, 2.600 g of aqueous hydrofluoric acid (50 wt%) was added dropwise and the mixture was homogenized using a PTFE spatula, resulting in a thick gel. Then, 0.358 g of purely siliceous BEA (Si-BEA) was suspended in 2 mL of DI H_2O and seeded into the mixture, which was allowed to evaporate to 33.776 g. This mixture corresponds to a final molar composition of SiO_2/0.01 $SnCl_2$/0.55 TEAOH/0.54 HF/7.52 H_2O. The thick paste was transferred to a 45 mL PTFE-lined stainless steel autoclave and heated to 140 °C for 40 days under static conditions. The solids were recovered by filtration, washed with DI H_2O and ethanol, and dried at 100 °C. Si-BEA seeds were synthesized using the following dry-gel method: 0.050 g sodium hydroxide was dissolved in 5.259 g of aqueous tetraethylammonium hydroxide (35 wt%). 3.75 g of colloidal silica (Ludox® AS-40) was added, and the mixture was stirred at 80 °C until the gel was dry (about 15 h). The solids were ground and placed into a PTFE cup inside a PTFE liner that held 2 g of DI H_2O. The liner was held in a stainless steel autoclave at 160 °C for 1 day. The solids were washed with DI H_2O and calcined using the same procedure that was used for Sn-BEA.

The experimental methods for Sn-BEA characterization and the associated results (Figures 4.S1-4.S4) can be found in the Supporting Information.

Before use in reactions, about 2 g of Sn-BEA were washed in multiple 30 mL batches of nanopure water until the pH of the water before and after the wash were equal. The Sn-BEA was then dried under vacuum overnight at 105 °C, then calcined under dry air flow (100 mL/min) at 580 °C for 10 h with a 1 °C/min ramp and 1 h stops at 150 and 350 °C.

4.2.2 Reactions

In a typical reaction, 0.3 mL of a 750 mM aqueous solution of sugar and 46 mg of Sn-BEA (yielding a sugar/Sn ratio of 30) were added to a thick-walled glass vial (Wheaton W986219NG for temperatures up to 140 °C, Sigma-Aldrich Z567701 for temperatures above 140 °C). In biphasic reactions, vials additionally received 0.6 mL of toluene. Reactions were carried out at 100 °C, 120 °C, and 140 °C when the substrate was xylose and 150 °C, 175 °C, and 200 °C when the substrate was glucose. Separate reaction vials were used for each time point and were immersed in a temperature-controlled silicone oil bath for their respective reaction times and mixed using

PTFE-coated stir bars at a rate of 750 rpm, then quenched in an ice bath. Heating and stirring were maintained by a digital stirring hotplate (Sigma-Aldrich Z645060). After quenching, each vial was diluted with 0.6 mL of water, centrifuged at 14000 rcf for 5 min, and sampled for analysis. Biphasic reaction vials additionally received 30 μL of 20.22 mg/mL of dodecane in toluene prior to centrifugation. Aqueous-phase samples were analyzed by high-performance liquid chromatography (HPLC) or gas chromatography-mass spectrometry (GC-MS) to determine their compositions or by liquid chromatography-mass spectrometry (LC-MS) to determine the molecular weights of unidentified compounds. Toluene-phase samples were analyzed by gas chromatography-flame ionization detection (GC-FID) to determine their furfural compositions.

4.2.3 High-Performance Liquid Chromatography Analysis

HPLC was used to determine the composition of aqueous-phase samples. HPLC samples were prepared by mixing an aliquot of the solution with aqueous 1,6-hexanediol (12.02 g/L) in a 2:1 volume ratio. The samples were analyzed using an Ultra High Performance Liquid Chromatograph system (Shimadzu, Kyoto, Japan). 10 μL aliquots of the samples were injected onto a 300 mm × 7.8 mm Aminex HPX-87H (Bio-Rad, Richmond, CA) column equipped with a 4.6 mm × 30 mm micro-guard Cation H guard column (Bio-Rad) and a refractive index detector. The compounds were eluted at 65 °C with an isocratic flow rate of 0.4 mL/min of 0.01 N sulfuric acid in water. Product quantities were determined by converting integrated peak areas to concentrations using a 7-point calibration curve. Concentration standards were not available for the hydroxyalkanoic and hydroxyalkenoic acids, so their concentrations were estimated by assuming those compounds and the sugars from which they were derived had equal refractive indices. The chromatograms corresponding to reaction of xylose over Sn-BEA at 140 °C and glucose over Sn-BEA at 200 °C are shown in Figures 4.1 and 4.2, respectively.

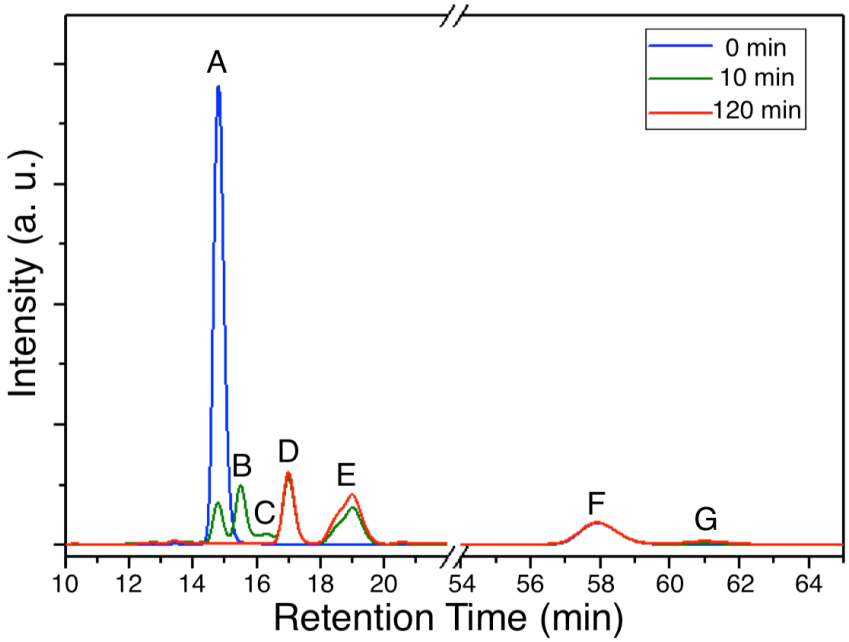

Figure 4.1. HPLC chromatogram of products after reacting xylose with Sn-BEA at 140 °C for 0, 10, and 120 min (A: xylose, B: lyxose, C: xylulose, D: 2,5-dihydroxypent-3-enoic acid, E: racemic 2,4,5-trihydroxypentanoic acid and lactic acid, F: 1,6-hexanediol as internal standard, G: furfural).

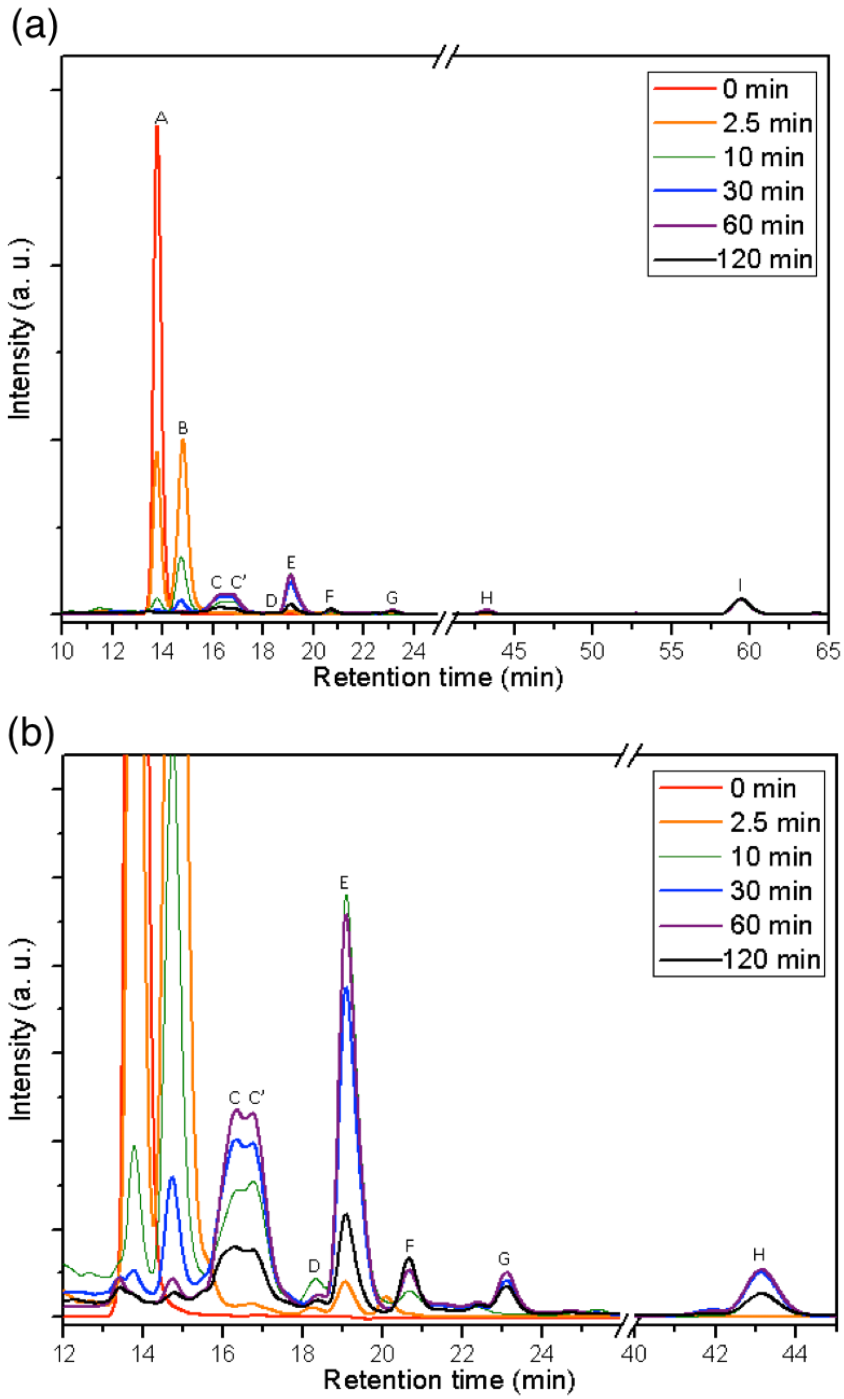

Figure 4.2. (a) HPLC chromatogram and (b) zoomed-in chromatogram of products after reacting glucose with Sn-BEA at 200 °C for 0 to 120 minutes (A: glucose, B: fructose and mannose, C & C': 2,4,5,6-tetrahydroxyhexanoic acid and 5-(1,2-dihydroxyethyl)-3-hydroxydihydrofuran-2(3*H*)-one, D: 2-hydroxybut-3-enoic acid, E: lactic acid, F: formic acid, G: levulinic acid, H: HMF, I: 1,6-hexanediol as internal standard).

4.2.4 Liquid Chromatography-Mass Spectrometry Analysis

LC-MS was used to determine the molecular weights of unidentified compounds. LC-MS samples were prepared by mixing an aliquot of the solution with aqueous 1,6-hexanediol (12.02 g/L) in a 2:1 volume ratio. The samples were analyzed using a 1200 Series liquid chromatography system (Agilent Technologies, Santa Clara, CA) coupled to a 6520 Accurate-Mass Q-TOF mass spectrometer (Agilent Technologies, Santa Clara, CA) equipped with a dual-spray electrospray ionization source. 2 μL aliquots of the diluted samples were injected onto a Phenomenex (Torrance, CA) Rezex™eROA-Organic Acid H^+ (8%) (150 mm × 4.6 mm) column equipped with a Phenomenex (Torrance, CA) Carbo-H^+ (4 mm × 3 mm) guard column. The compounds were eluted at 55 °C with an isocratic flow rate of 0.3 mL/min of 0.5% (v/v) formic acid in water (132.5 mM formic acid in water). The negative ion mode mass spectrometry conditions were: gas temperature = 285 °C, fragmentor = 75 V and capillary = 3,000 V, scan range m/z 50 to 1100, 1 scan/s. Internal mass reference ions m/z 112.9856 and m/z 1033.9881 were used to keep the mass axis calibration stable during the analysis.

4.2.5 Gas Chromatography Analysis

GC-MS was used to determine, separately, the concentrations of xylose, lyxose, xylulose, glucose, mannose, and fructose. GC-MS samples were prepared by heating 50 μL of previously diluted solution with 200 μL inositol solution (0.47 mg/mL) at 40 °C for 12 h under vacuum. Each sample then received 0.3 mL of pyridine and 0.2 mL of 1-trimethylsilyl-imidazol and was heated to 60 °C for 1 h for complete trimethyl-silation.

GC-FID was used to determine the composition of furfural in toluene-phase samples from biphasic reactions. GC-FID samples were prepared by diluting a 200 μL aliquot of the toluene phase with an additional 1 mL of toluene.

GC-MS and GC-FID samples were analyzed by the same instrument, which injected 1 μL of the sample in split mode onto a VF5-MS capillary column (30 mm × 0.25 mm × 0.25 μm, Agilent, Santa Clara, CA, USA). An Agilent Varian CP-3800 gas chromatograph coupled to a Varian 320-MS triple quadrupole mass spectrometer was used for analysis with the following settings: injector and transfer line temperature, 280 °C; carrier gas, helium at 1 mL/min; temperature program, 160 °C for 2 min isocratic, 5 °C/min to 240 °C, 30 °C/min to 320 °C. Ions were detected in full scan mode m/z 35-500. Identification of compounds was achieved by comparing measured mass spectra with the National Institute of Standards and Technology (NIST) database entries (NIST/EPA/NIH mass spectral database, version 2.0f) or by interpretation of the mass spectra and comparison to literature data. Manual fragmentation analysis was done for molecules that did not exist in NIST database. The molecular weights were confirmed by the M peak and the M-15 peak, which was the signature peak for the loss of a methyl group from derivatization by 1-trimethylsilyl-imidazol. Product quantities for sugar isomer analysis (by GC-MS) and furfural quantities from biphasic reactions (analyzed by GC-FID) were determined by converting integrated peak areas to concentrations using a 7-point calibration curve. The GC-MS spectra of 2,4,5-trihydroxypentanoic acid, 2,5-dihydroxypent-3-enoic acid, 3-hydroxy-5-(hydroxymethyl)dihydrofuran-2(3*H*)-one, 2,4,5,6-tetrahydroxyhexanoic acid, and 5-(1,2-dihydroxyethyl)-3-hydroxydihydrofuran-2(3*H*)-one after derivatization with excess 1-trimethylsilyl-imidazol are shown in Figure 4.S5.

4.2.6 Nuclear Magnetic Resonance Spectroscopy Analysis

Nuclear magnetic resonance (NMR) experiments were performed to determine the molecular structure of the reaction products. HPLC was used to purify the reaction products, splitting the reaction solution into fractions each representing 15 s of retention time in the column, yielding approximately 5 mg of the reaction products for NMR analysis. The collected samples were dried by evaporation and then dissolved in 500 μL D_2O (^1H chemical shifts are referenced to internal acetone at δ_H 2.22 and ^{13}C chemical shifts to δ_C 30.9). All spectra were collected at 298 K. NMR experiments were acquired on a Bruker Avance 600 MHz spectrometer equipped with a cryoprobe or on a Bruker Avance 800 MHz spectrometer. The pulse sequences for COSY, ^1H-^{13}C HSQC and ^1H-^{13}C HMBC experiments, were standard Bruker library sequences, acquired with 2 K data points over a 14 ppm spectral width. The spectra are provided in the Supporting Information in Figures 4.S6-4.S12 and the spectroscopic data are detailed in Tables 4.S1 and 4.S2.

The 2,4,5-trihydroxypentanoic acid we produced were identified as 2 stereoisomers and the ratio of them is about 4:3. We also calculated the ratio of 2,4,5-trihydroxypentanoic acid to lactic acid using the peak integral of protons from methyl group of lactic acid to that of 3a and 3'a. The calculated molar ratio of 2,4,5-trihydroxypentanoic acid to lactic acid was about 7:3.

4.2.7 Calculations

Conversions and yields are reported as molar percentages as follows:

$$\text{Pentose Conversion} = \frac{c^0_{\text{xylose}} - \left(c_{\text{xylose}} + c_{\text{lyxose}} + c_{\text{xylulose}}\right)}{c^0_{\text{xylose}}} \times 100\% \tag{4.1}$$

$$\text{Hexose Conversion} = \frac{c^0_{\text{glucose}} - \left(c_{\text{glucose}} + c_{\text{mannose}} + c_{\text{fructose}}\right)}{c^0_{\text{glucose}}} \times 100\% \tag{4.2}$$

$$\text{Yield of } i = \frac{c_i}{c^0_{\text{substrate}}} \times 100\% \tag{4.3}$$

where c denotes molar concentration, the superscript 0 denotes initial value, and the subscript denotes the compound (with the exception of hexose-derived lactic acid). Since one molecule of fructose can split into two molecules of lactic acid, the yield of lactic acid from hexose was defined as

$$\text{Yield of lactic acid from hexose} = \frac{1}{2} \times \frac{c_{\text{lactic acid}}}{c^0_{\text{glucose}}} \times 100\% \tag{4.4}$$

The yield of humins was calculated as the difference between the pentose or hexose conversion and the sum of the yields of identified products. When xylose was the substrate, the yield of humins was the difference between the pentose conversion, as calculated by Equation

(4.1), and the sum of the yields of HPAs, furfural, and lactic acid, as calculated by Equation (4.3). When glucose was the substrate, the yield of humins was the difference between the hexose conversion, as calculated by Equation (4.2), and the sum of the yields of HHAs, formic acid, HMF, 2-hydroxybut-3-enoic acid, and lactic acid, as calculated by Equations (4.3) and (4.4).

We assume that the formation of glycolaldehyde exists as a consequence of retro-aldol splitting of pentoses or aldohexoses, and its concentration should be equal to that of lactic acid from pentoses and 2-hydroxybut-3-enoic acid from hexoses. Similarly, we assume that α-angelica lactone forms from levulinic acid, whose concentration should be equal to that of formic acid from hexoses. Neither glycolaldehyde nor α-angelica lactone were detected and their yields, as well as the yield of levulinic acid, were not included in the calculation of the yield of humins. These assumptions and exclusions warrant the use of Equation (4.3), which does not consider the number of carbon atoms in a molecule, for calculating the yields of lactic acid from pentoses, 2-hydroxybut-3-enoic acid, and formic acid and consequently, for our calculation of the yield of humins.

Selectivity towards HHAs, furanics (*i.e.* formic acid and HMF), retro-aldol products (*i.e.* 2-hydroxybut-3-enoic acid and lactic acid), and humins were calculated as follows:

$$\text{Selectivity of } i = \frac{\text{Yield of } i}{\text{Hexose Conversion}} \times 100\% \tag{4.5}$$

The distributions of pentose and hexose isomers were calculated as follows:

$$\text{Fraction of pentose } i = \frac{c_i}{c_{\text{xylose}} + c_{\text{lyxose}} + c_{\text{xylulose}}} \times 100\% \tag{4.6}$$

$$\text{Fraction of hexose } i = \frac{c_i}{c_{\text{glucose}} + c_{\text{mannose}} + c_{\text{fructose}}} \times 100\% \tag{4.7}$$

4.3 Results and Discussion

Near-complete conversion (>98% in both case) of all isomers of pentose and hexose sugars was observed when xylose and glucose were reacted in the presence of Sn-BEA for 1 h at 140 °C and 200 °C, respectively. The products are divided into four categories: hydroxyalkanoic acids and their derivatives, furanics and their derivatives, products of retro-aldol splitting of the sugars, and humins. For xylose, the products were 2,4,5-trihydroxypentanoic acid and its derivatives (46%), furfural (3%), lactic acid (9%), and humins (40%). For glucose, the products were 2,4,5,6-tetrahydroxyhexanoic acid and its derivative (14%); HMF, levulinic acid, and formic acid (27%); lactic acid and 2-hydroxybut-3-enoic acid (24%); and humins (33%).

A representative high-performance liquid chromatography (HPLC) chromatogram of the products of xylose reaction after 0, 10, and 120 min over Sn-BEA in water at 140 °C is shown in Figure 4.1. Peaks A, B, and C are attributable to xylose, lyxose, and xylulose. In addition to these expected products, two peaks, labeled D and E, were observed. Product analysis by liquid chromatography-mass spectrometry (LC-MS) showed the $[M\text{-}H]^-$ m/z ratios for these peaks to be 149.0457 and 131.0348, respectively. The m/z ratio of the first peak (D) is identical to that of the

pentose isomers: xylose, lyxose, and xylulose, indicating that product D and these pentose isomers have the same molecular weight. The m/z ratio of peak E is 18.0109 lower than that of peak D, suggesting that the product represented by peak E results from losing one molecule of water from an isomer of xylose. HPLC was used to divide the solution of reaction products into fractions each representing 15 s of retention time in the column. These fractions were then analyzed by heteronuclear single quantum coherence two-dimensional nuclear magnetic spectroscopy (HSQC 2D-NMR), and by this means peak D was identified as 2,4,5-trihydroxypentanoic acid and peak E as 2,5-dihydroxypent-3-enoic acid. Gas chromatography-mass spectrometry **(**GC-MS) analysis also revealed a trace amount of 3-hydroxy-5-(hydroxymethyl)dihydrofuran-2(3H)-one, which was not observed by HPLC. We refer to these three products (*i.e.*, the hydroxypentanoic acid and its two observed derivatives) collectively as HPAs. Similar products were formed upon reaction of glucose over Sn-BEA at 200 °C, as shown in Figure 4.2. In this case the new products were 2,4,5,6-tetrahydroxyhexanoic acid and its derivative 5-(1,2-dihydroxyethyl)-3-hydroxydihydrofuran-2(3H)-one (also known as 3-deoxy-γ-lactones, or DGL),[15] which we refer to collectively as HHAs. The last of these products was recently discovered during the reaction of glucose over Sn-BEA in methanol.[15]

The formation of the hydroxyalkanoic acids in water resembles the $SnCl_4$-catalyzed formation of methyl-4-methoxy-2-hydroxybutanoate (MMHB) from erythrulose in methanol.[16] The formation of C_6 hydroxyalkanoates during Sn-BEA catalyzed reaction of glucose in methanol has also been reported recently.[15] These findings, together with our observations, suggest that cationic Sn centers in the zeolite facilitate the replacement of the hydroxyl group in aldoses by a hydrogen atom on the β carbon and the subsequent conversion of the aldehyde group to a carboxylic acid or ester, depending on the solvent, as illustrated in Scheme 4.1.[15,16] The hydroxyalkanoic acids can then undergo dehydration to form either alkenoic acids or furanone esters. Figure 4.3 shows the conversion of pentoses and the yields of all identifiable products (*i.e.*, HPAs, lactic acid, and furfural) as a function of reaction time for the reaction of xylose over Sn-BEA at 100 °C, 120 °C, and 140 °C. We report the yields of HPAs collectively in Figure 4.3 for conciseness; separate plots of components of this group are shown in Figure 4.S13. A small amount of furfural (less than 3% yield) was observed in these reactions, despite the absence of any added Brønsted acid.

It was hypothesized that the formation of furfural could be catalyzed by the acids formed in the reactions (*i.e.*, HPAs and lactic acid).[17] To test this idea, an aqueous solution of xylose was heated in the presence of either lactic acid or HPAs at 140 °C, using the same concentrations of those acids that were observed in the reactions using Sn-BEA. Very little furfural (less than 1%) was observed, suggesting that the formation of furfural is not catalyzed by the HPAs or the lactic acid formed in the reaction. Therefore, it is more likely that furfural formation is

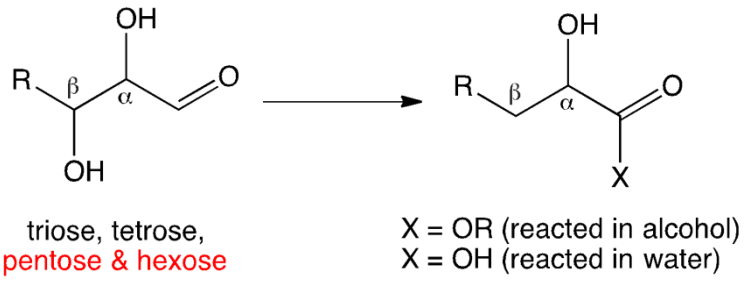

Scheme 4.1. Isomerization of C_3-C_6 aldoses to acids or esters.

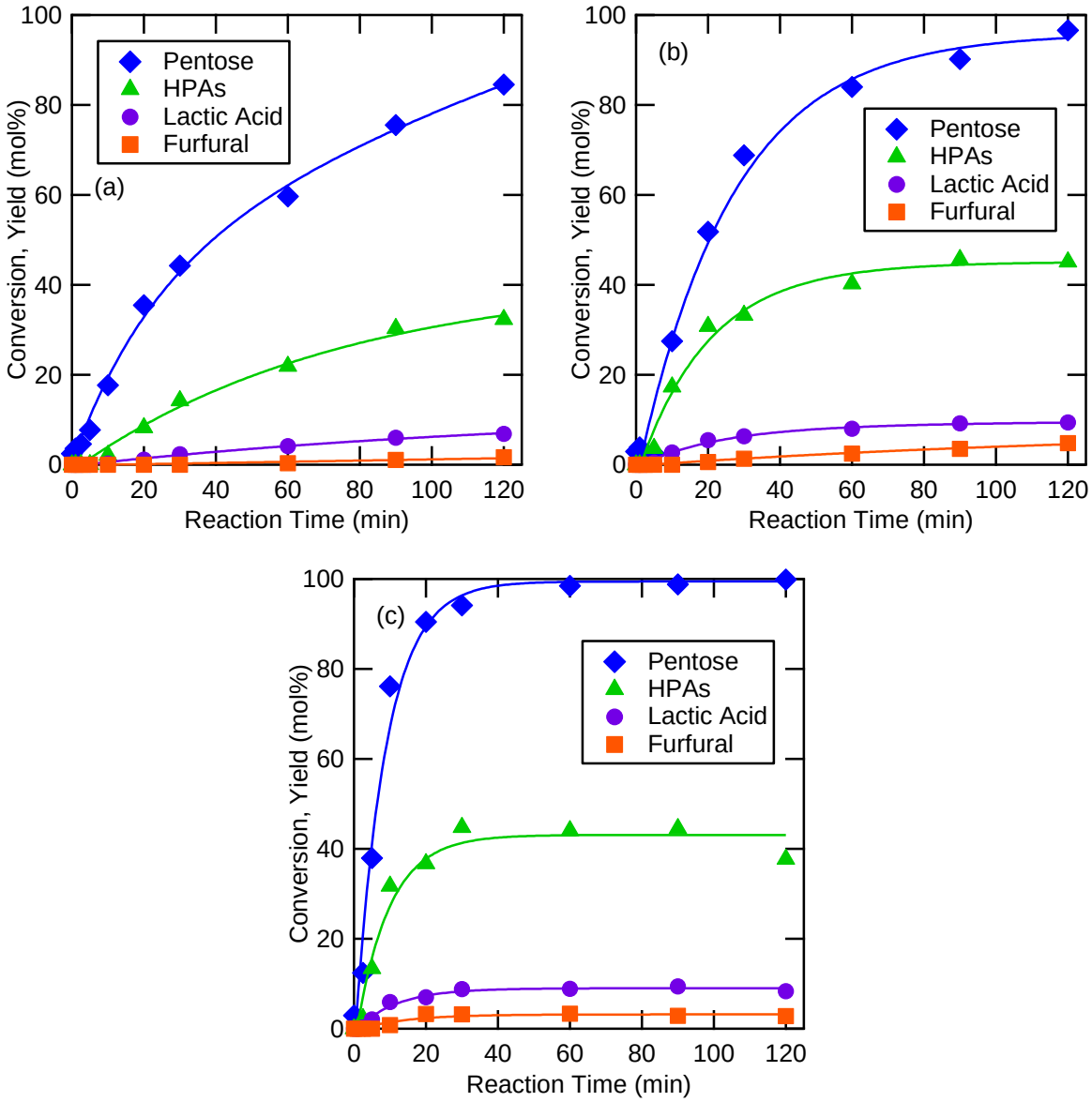

Figure 4.3. Conversion of pentose and yields of identified products at (a) 100 °C, (b) 120 °C, and (c) 140 °C.

catalyzed by the weak Brønsted-acid ≡Sn–OH and/or silanol groups of open Sn sites in the zeolite framework, which have been shown to form upon hydrolysis of a ≡Sn–O–Si≡ linkage.[18,19] In support of this conclusion, we note that weak Brønsted-acid sites were observed in our samples of Sn-BEA by Fourier transform infrared spectroscopy (FTIR) of adsorbed pyridine and 2,6-ditertbutylpyridine (see Supporting Information). It should be noted that while strong Brønsted-acid sites are most often used to catalyze the formation of furfural, weak Brønsted acids have also been shown to catalyze this reaction.[20,21] We also carried out reactions of HPAs with 3 equivalents of HCl to see whether additional Brønsted acidity would convert the HPAs to furfural. We heated xylose over Sn-BEA at 140 °C for 2 h to produce HPAs, removed the zeolite and solid waste by centrifuging the resulting solution, and added HCl to the supernatant, which we then heated to

140 °C for 3 h. This experiment showed negligible change in the concentration of HPAs, demonstrating that the HPAs are stable to the level of HCl used and do not form furfural after 3 h at 140 °C.

We found that under similar conditions, hexoses did not convert as readily as pentoses, and consequently experiments with hexoses were carried out at higher temperatures: 150 °C, 175 °C and 200 °C. The conversion of hexoses and the yields of identifiable products (*i.e.*, HHAs, lactic acid, HMF, and formic acid) are given in Figure 4.4 as functions of reaction time. We show the yields of HHAs together in Figure 4.4 because the peaks corresponding to the two molecules overlapped significantly in the HPLC chromatograms and we were unable to resolve them (see

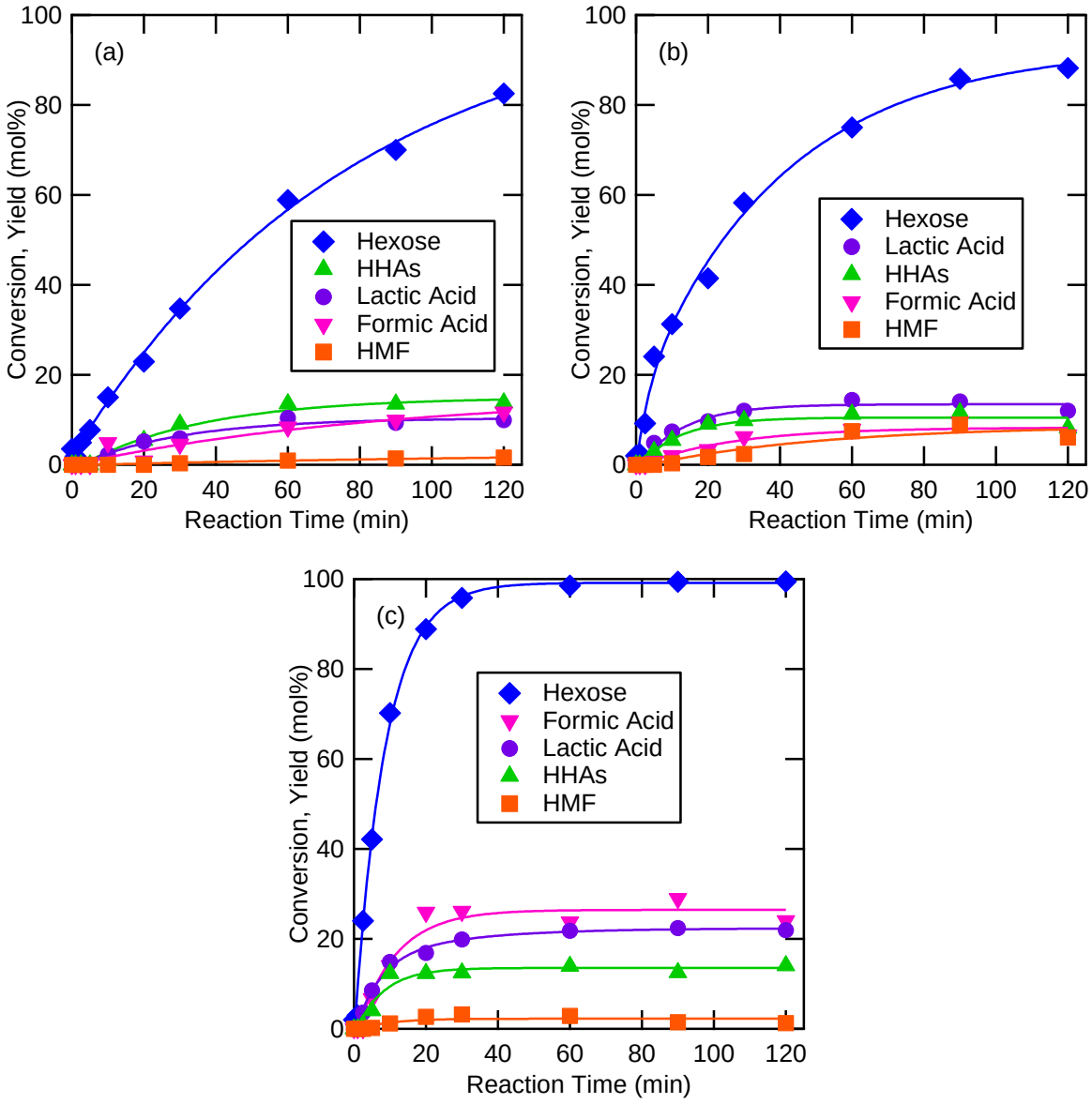

Figure 4.4. Conversion of hexose and yields of identified products at (a) 150 °C, (b) 175 °C, and (c) 200 °C. Yields of levulinic acid and 2-hydroxybut-3-enoic acid are not shown because their relatively low magnitude, reaching maximum values of 3.0% and 2.6% at 200 °C.

Figure 4.2). Our estimates for separated yields of HHAs are plotted in Figure 4.S14. In addition to the products shown, small amounts of levulinic acid and 2-hydroxybut-3-enoic acid were detected. The yields of these products are not shown in Figure 4.4 because they are very low, reaching maximum values of 3.0% and 2.6%, respectively, at 200 °C. The imbalance between the yields of levulinic acid and formic acid observed in this study has been observed before and was attributed to the tendency of levulinic acid to undergo cyclization to form α-angelica lactone.[22] However, no evidence was found in the present study for the formation of α-angelica lactone. An interesting observation is that for reactions carried out at 150 °C, 175 °C, and 200 °C, the selectivity to HHAs measured after 2 h is lowest at 175 °C (see Figure 4.S15). Conversely, the selectivity to humins reaches a maximum at the same temperature. We do not understand the reason for this pattern but suspect that it may have to do with the concentration and reactivity of various components present in the reaction mixture and the way in which these factors contribute to the formation of humins. Considerably more work would need to be carried out in order to determine the whether this hypothesis is correct.

In contrast with the results for the reactions of pentoses presented in Figure 4.3, in which HPAs were the leading products, Figure 4.4 does not show a clearly predominant hexose-derived product. However, it is worth noting that formic acid forms *via* hydrolysis of HMF, so the yield of formic acid plus HMF should represent the total yield of furanics. As mentioned above, furanics form *via* a reaction pathway that is different from that by which other products form. We conducted an additional experiment with xylose at 200 °C, to compare the yield of furfural from pentoses to that of HMF and formic acid from hexoses under the same conditions. After 2 h, we observed that the yield of furfural (11%) was much lower than the combined yield of HMF and formic acid (25%). For both pentoses and hexoses, the ketose form (xylulose and fructose, respectively) undergoes dehydration more readily to form furanics.[23,24] We also observed a lower proportion of ketoses among the pentose isomers than the hexose isomers (see Figure 4.S16) consistent with our observation of a lower yield of furfural from pentoses than HMF and its degradation products from hexoses.

The use of an extracting agent increased the yield of HPAs and furfural. The experiments presented in Figure 4.3c were repeated but with toluene used as an extracting agent in a 2:1 toluene:water volume ratio. The yield of HPAs after 2 h increased from 40% to 58% (the yield of 2,4,5-trihydroxypentanoic acid increased from 21% to 27%, while the yield of 2,5-dihydroxypent-3-enoic acid increased from 19% to 31%), while the yield of furfural increased from 3% to 17%, the yield of humins decreased from 49% to 11%, and the yield of lactic acid slightly increased from 8% to 13%. Previous studies have suggested that *in situ* extraction of furfural prevents its further reaction with intermediates derived from sugars to form humins.[22,25-27] The production of HPAs also benefits from the furfural extraction because fewer pentose molecules are converted to humins, allowing more of the pentose to be converted to HPAs.

Scheme 4.2 illustrates the proposed pathways by which xylose and glucose are converted to the observed products in water when catalyzed by Sn-BEA. We hypothesize, based on the current literature,[15-17,28-30] that Sn-BEA isomerizes the sugars between their aldose and ketose forms, and then converts them into smaller molecules *via* retro-aldol splitting. Pentoses are fragmented into glycolaldehyde and a triose (either glyceraldehyde or dihydroxyacetone).[28] A very similar pathway applies to hexoses: fructose is split into two trioses (glyceraldehyde and dihydroxyacetone) while glucose and mannose form glycolaldehyde and a tetrose (2,3,4-trihydroxybutanal).[16,17] The trioses can be interconverted by Sn-BEA and can also be dehydrated and rehydrated to produce lactic acid (see Scheme 4.1).[28] Likewise, the tetrose fragmented from

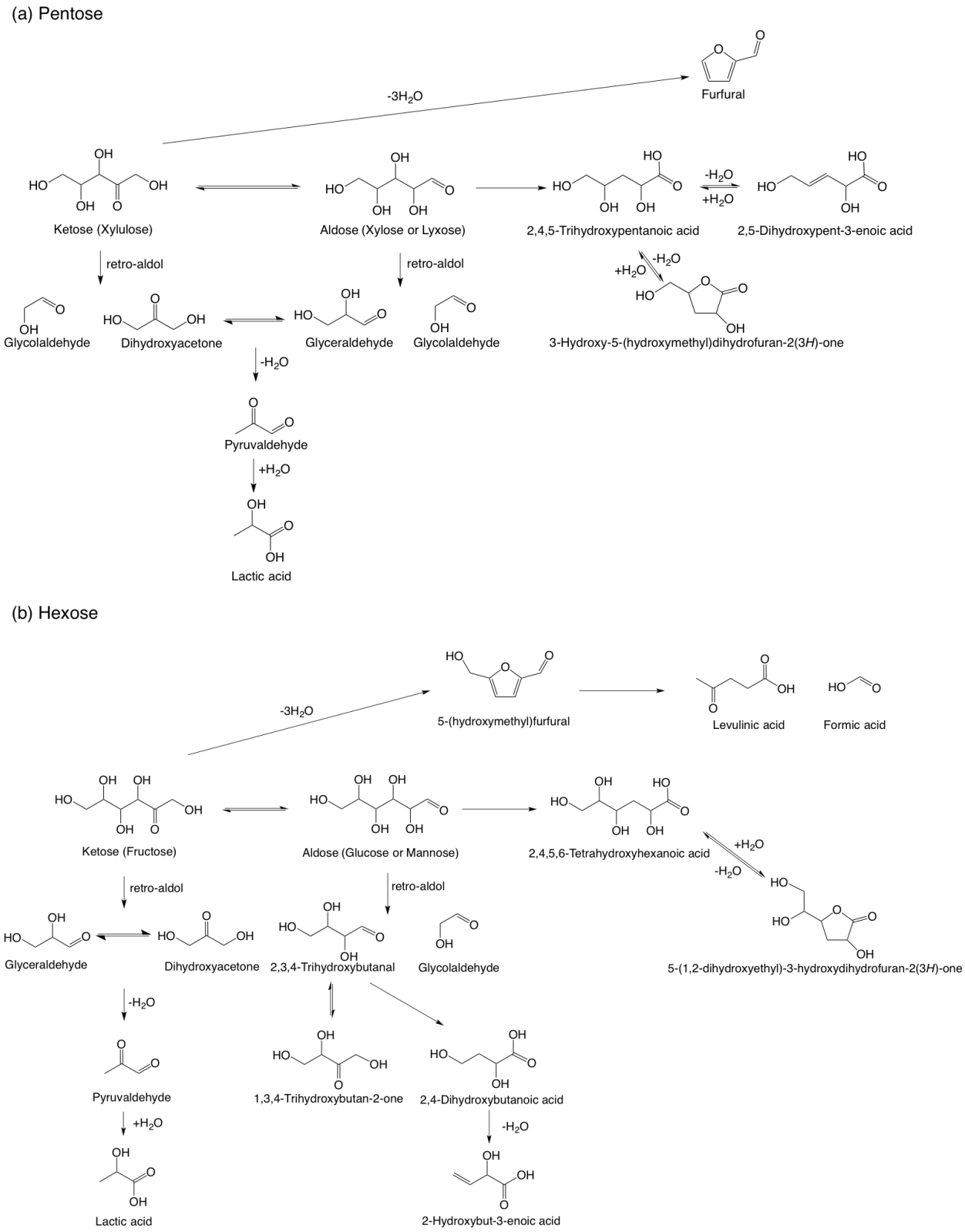

Scheme 4.2. Proposed pathways for the reactions of (a) pentoses and (b) hexoses over Sn-BEA

glucose and mannose can be dehydrated and rehydrated (see Scheme 4.1) to form 2,4-dihydroxybutanoic acid, which is further dehydrated to form 2-hydroxybut-3-enoic acid.[16,17] The work reported here suggests that HPAs and HHAs are formed by dehydration and rehydration of C_5 or C_6 aldoses without retro-aldol splitting and subsequent dehydration to form hydroxyalkenoic acids or saturated furanone esters.

4.4 Conclusions

In summary, we have identified new xylose- and glucose-derived products: 2,4,5-trihydroxypentanoic acid, 2,5-dihydroxypent-3-enoic acid, and 3-hydroxy-5-(hydroxymethyl)dihydrofuran-2(3H)-one from xylose; and 2,4,5,6-tetrahydroxyhexanoic acid and 5-(1,2-dihydroxyethyl)-3-hydroxydihydrofuran-2(3H)-one from glucose. By using toluene as an extracting agent, we were able to increase the yield of HPAs and furfural. By analogy to trioses and tetroses, this work suggests that pentoses and hexoses can also undergo a dehydration and rehydration to form carboxylic acids.

It should be noted that the HPAs and HHAs discovered in this study could be used as monomers for the synthesis of hyperbranched polymers. Typical degradable polyesters, *e.g.* poly(lactic acid-co-glycolic acid)s (PLAGAs), are commonly used for sutures, bone prostheses, and drug delivery systems.[31-36] Because these polyesters are hydrophobic, their biocompatabilty can be improved by copolymerizing them with functionalized molecules such as gluconic acid.[31,32,35-39] The hydroxyalkanoic acids and hydroxypentenoic acid reported here should be similarly useful as co-monomers, since they bear very similar molecular structures to gluconic acid. Additionally, the hydroxypentenoic acid has a C=C bond, which increases its flexibility for further functionalization and cross linking. We note as well that the furanone esters observed in this study could also be used as monomers for polymer synthesis. These observations suggest that further work on the synthesis of HPAs and HHAs is warranted given their potential use as monomers for the synthesis of hydrophilic, biodegradable polymers.

4.5 Acknowledgments

This work was supported by the Energy Biosciences Institute funded by BP. The authors acknowledge the assistance of Stefan Bauer with GC-MS, LC-MS and HPLC analysis of reaction products and with the interpretation of the results.

4.6 Supporting Information

4.6.1 Sn-BEA Characterization

The metal content of Sn-BEA was determined by inductively coupled plasma mass spectroscopy (ICP-MS) using an Agilent 7900 ICP-MS in helium mode. Samples were prepared by dissolving Sn-BEA in aqueous hydrofluoric acid (50%) at ten times the stoichiometric requirement. The resulting liquid was sequentially diluted in 2 vol% aqueous nitric acid until the Sn concentration was approximately 400 ppb. Results show that the Sn-BEA has a Si/Sn ratio of 97 ± 2, which is in good agreement with the ratio in the synthesis gel (Si/Sn = 100).

Powder X-ray diffraction (PXRD) patterns were collected with a Bruker D8 diffractometer using CuKα radiation (Figure 4.S1).

N_2 adsorption-desorption isotherms were measured on a Quantachrome Autosorb iQ at -196 °C (Figure 4.S2). Samples were degassed under vacuum prior to use (623 K, 12 h). Micropore volume was calculated to be 0.195 cm^3/g by the t-plot method. Materials were calcined under dry air flow (100 mL/min) at 580 °C for 10 h with a 1 °C/min ramp and 1 h stops at 150 and 350 °C prior to characterization.

Diffuse reflectance UV-Visible (DRUV) spectra were obtained on a Varian Cary 5000 spectrometer equipped with a Praying Mantis diffuse reflectance accessory. Samples were dehydrated by heating at 170 °C under vacuum for at least 15 h. The material was then loaded into a Praying Mantis high temperature reaction chamber with quartz windows in a dry N_2 environment to prevent adsorption of water onto the sample. The Sn-BEA spectrum was referenced to a

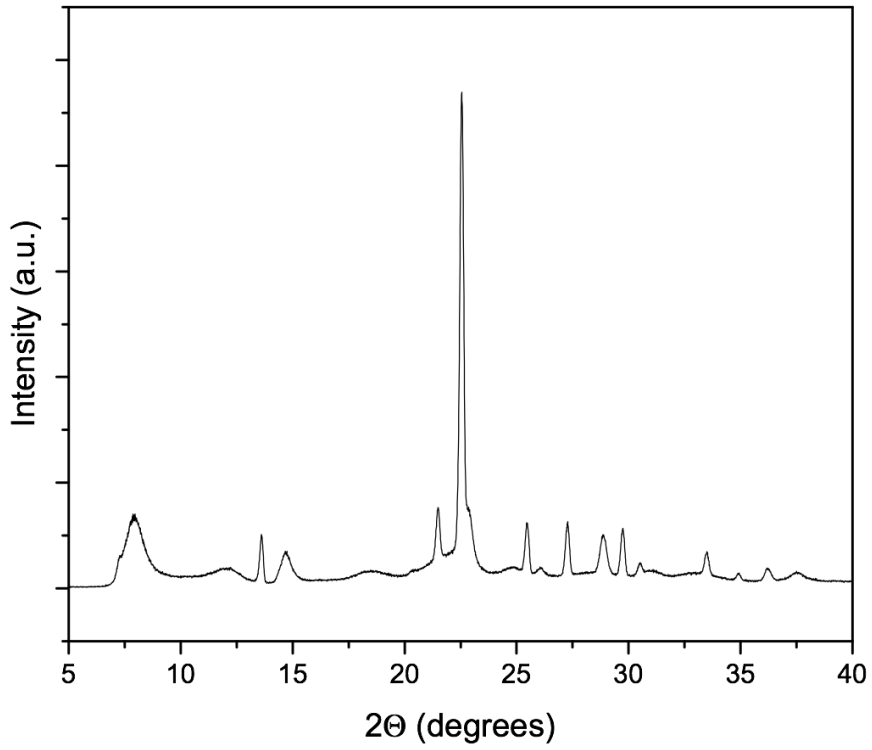

Figure 4.S1. X-ray diffraction pattern of Sn-BEA. The material was calcined at 580 °C before analysis.

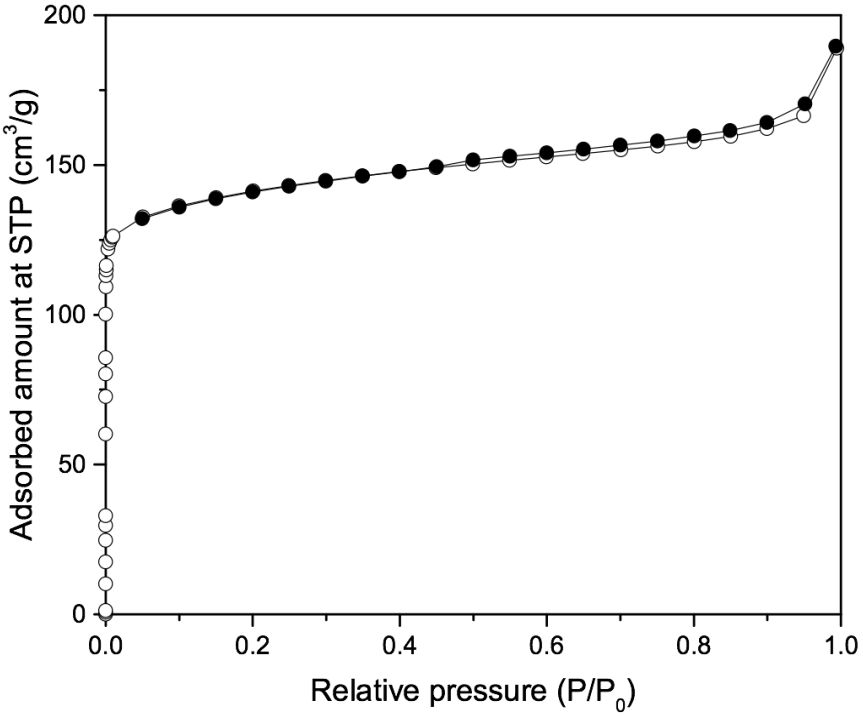

Figure 4.S2. N_2 adsorption (closed symbols) and desorption (open symbols) isotherms of Sn-BEA. The material was calcined at 580 °C before analysis.

dehydrated Si-BEA sample (Figure 4.S3) and exhibits a single band at 203 nm, which is indicative of framework Sn sites.

Fourier transform infrared (FTIR) spectra were acquired using a Bruker Vertex 70 spectrophotometer equipped with a Harrick high temperature transmission cell with KBr windows. Spectra were taken from 4000 to 400 cm^{-1} by averaging 64 scans at 2 cm^{-1} resolution. Zeolite samples (~2 mg) were pressed into 7 mm diameter self-supporting pellets for transmission measurements. Samples were calcined *in situ* under flowing dry air (50 mL/min), with a temperature ramp of 5 °C/min to 300 °C and 1 °C/min to 500 °C, and held at 500 °C for 5 h. After the cell was cooled to 30 °C, dynamic vacuum of roughly 0.1 Pa was established. A reference spectrum of the bare material was then acquired. Under a static vacuum, the cell was dosed with the probe molecule, either pyridine (Figure 4.S4a) or 2,6-ditertbutylpyridine (Figure 4.S4b). The cell was then heated to 150 °C and evacuated for 1 h before the final spectra was collected. The spectra were referenced to the bare material and reported as difference adsorption spectra. For pyridine adsorption, bands at 1611 cm^{-1} and 1452 cm^{-1} were assigned to pyridine adsorbed at Lewis acidic sites of Sn-BEA and the band at 1491 cm^{-1} was assigned to pyridine either adsorbed at Lewis acidic or Brønsted acidic sites of Sn-BEA.[18,40] A band at 1550 cm^{-1}, which is typically associated with protonated pyridine at Brønsted acid sites of zeolites was not present in the spectra (Figure 4.S4a).[18,40] For 2,6-ditertbutylpyridine adsorption (Figure 4.S4b), bands at 3363 cm^{-1}, 1613 cm^{-1}, and 1532 cm^{-1} are assigned to protonated pyridine.[18] The negative band at 3672 cm^{-1} is assigned to Brønsted acid sites strong enough to protonate 2,6-ditertbutylpyridine but not strong enough to protonate pyridine.[18]

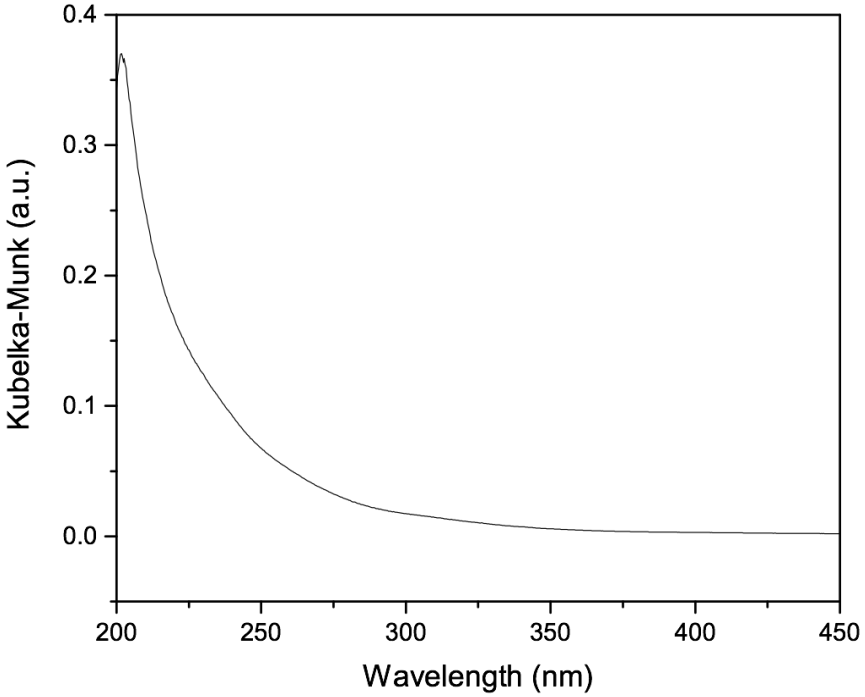

Figure 4.S3. DRUV spectrum of dehydrated Sn-BEA using a dehydrated Si-BEA reference.

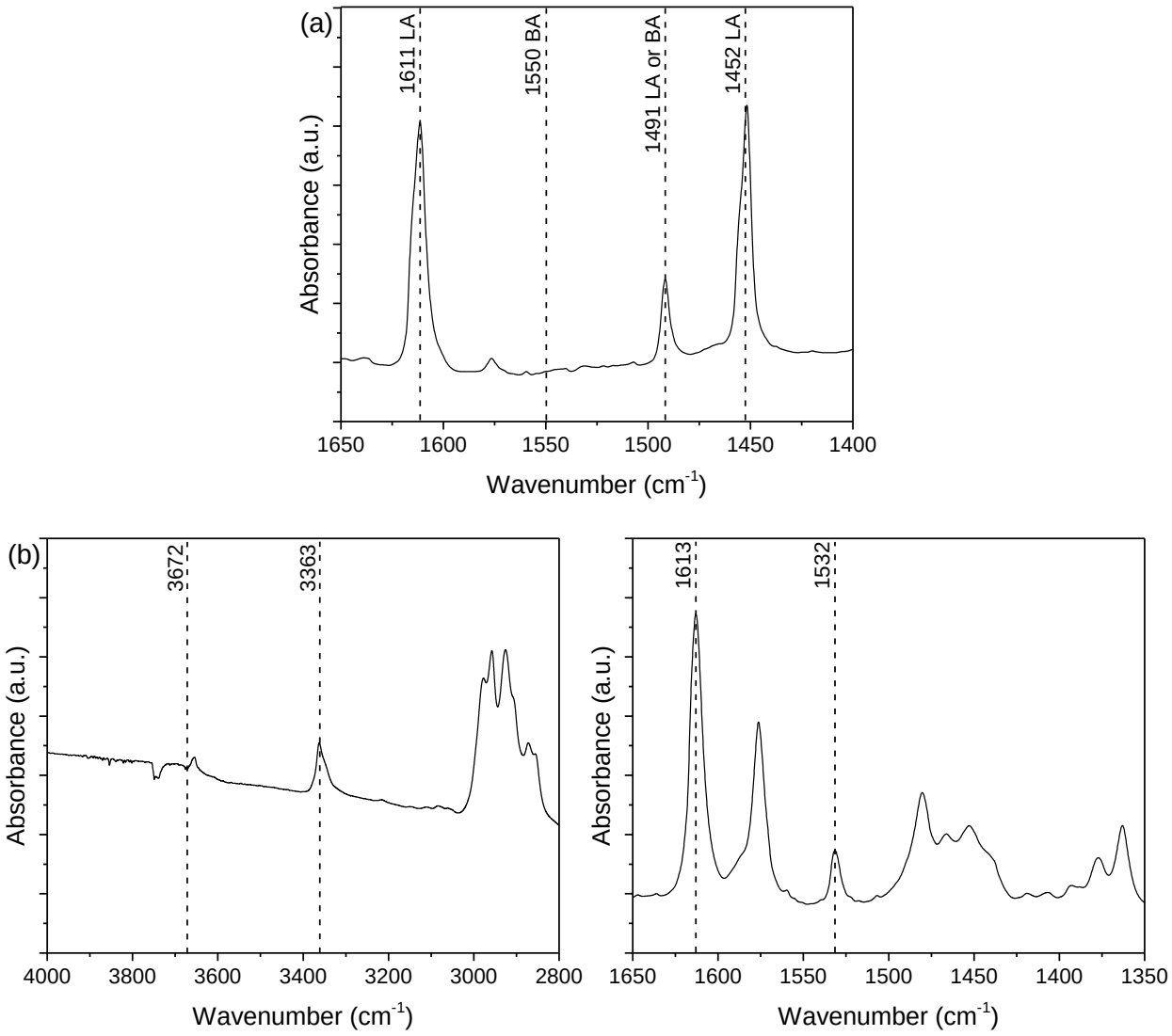

Figure 4.S4. FTIR spectra of (a) pyridine and (b) 2,6-ditertbutylpyridine adsorbed on Sn-BEA after 1 h of evacuation at 150 °C. Adsorption of the probe molecules were performed at room temperature after in-situ calcination in air at 500 °C for 5 h. Absorbance signals are referenced to the bare material.

4.6.2 Product Identification

Figure 4.S5 shows the GC-MS spectra of 2,4,5-trihydroxypentanoic acid, 2,5-dihydroxypent-3-enoic acid, 3-hydroxy-5-(hydroxymethyl)dihydrofuran-2(3*H*)-one, 2,4,5,6-tetrahydroxyhexanoic acid, and 5-(1,2-dihydroxyethyl)-3-hydroxydihydrofuran-2(3*H*)-one after derivatization with excess 1-trimethylsilyl-imidazol. Figures 4.S6-4.S12 show the NMR spectra and Tables 4.S1-4.S2 detail the spectroscopic data.

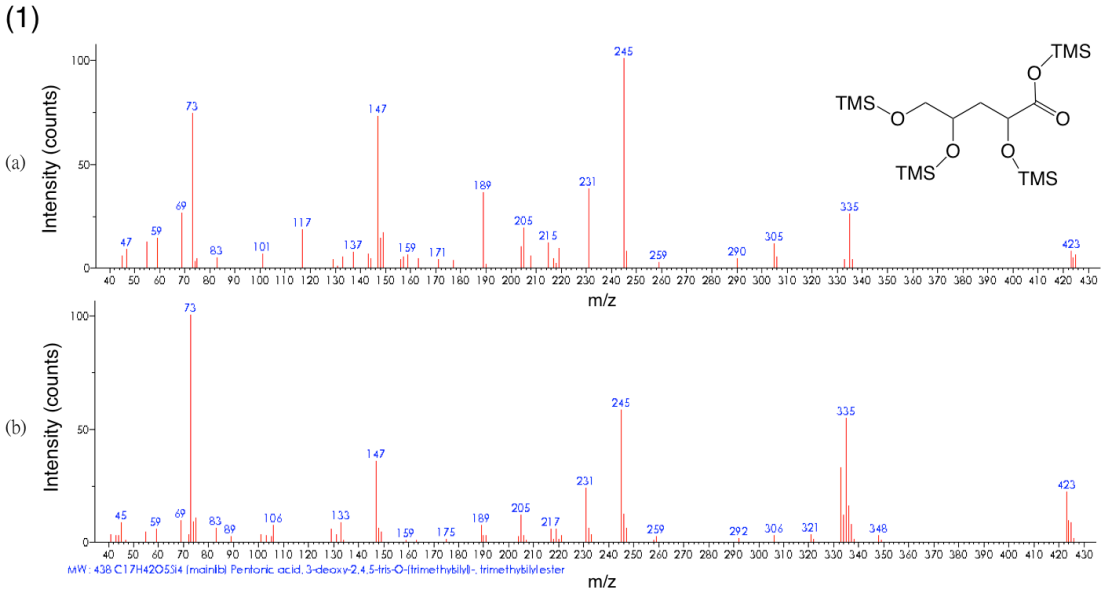
(1)
(a)
Intensity (counts)
m/z
TMS
(b)
Intensity (counts)
m/z
MW: 438 C17H42O5Si4 (main lib) Pentonic acid, 3-deoxy-2,4,5-tris-O-(trimethylsilyl)-, trimethylsilyl ester

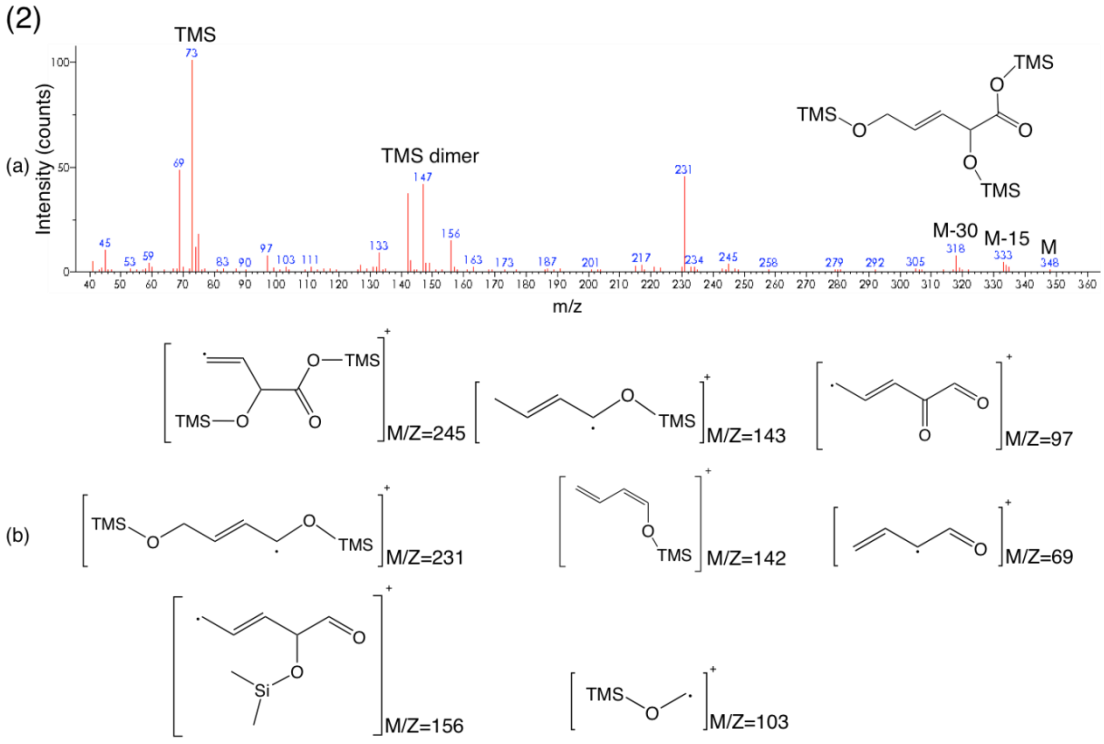
(2)
(a)
Intensity (counts)
m/z
TMS
TMS dimer
M-30
M-15
M
(b)
M/Z=245
M/Z=143
M/Z=97
M/Z=231
M/Z=142
M/Z=69
M/Z=156
M/Z=103

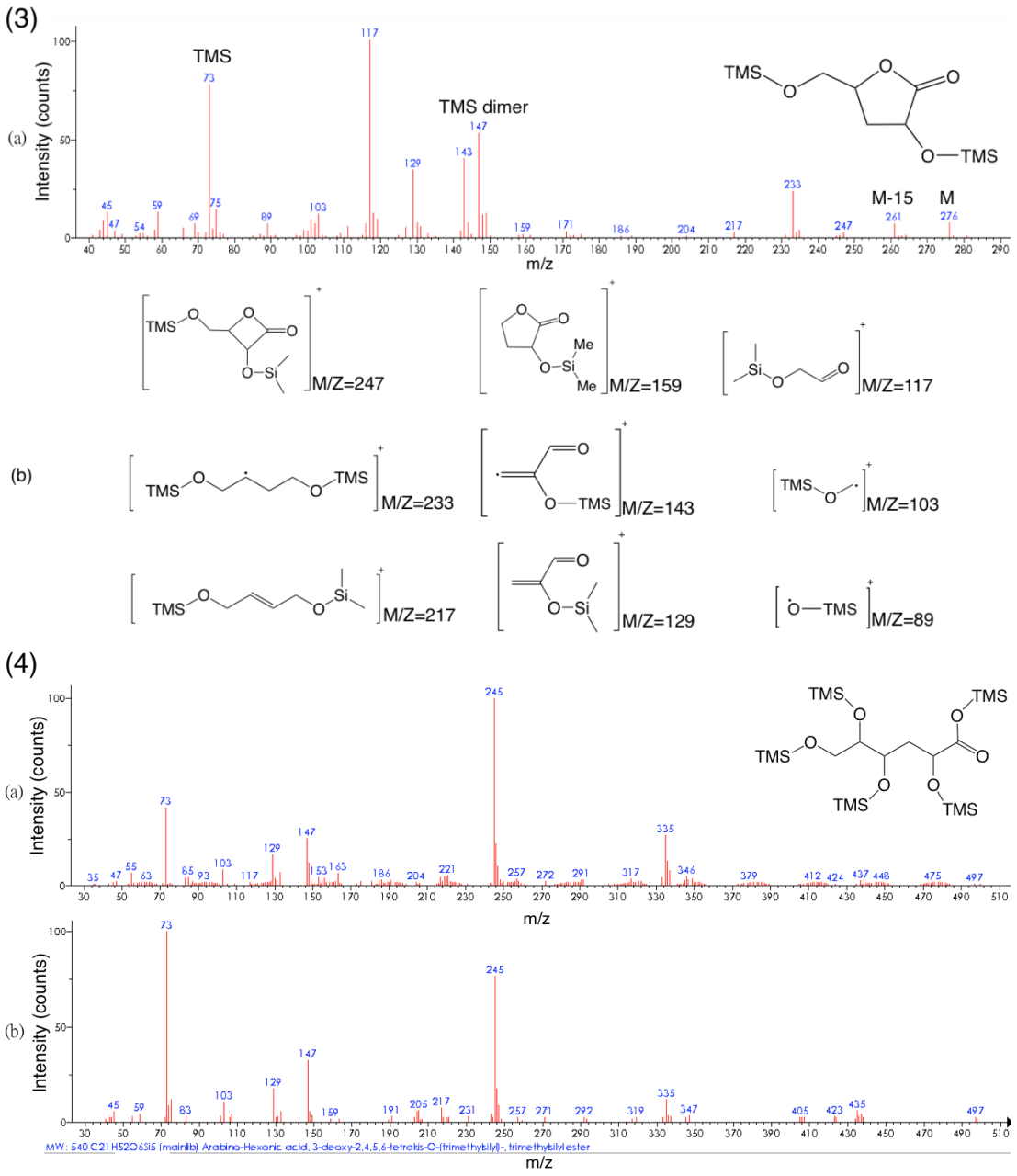
(3)
(a)
Intensity (counts)
m/z
TMS
TMS dimer
M-15
M
M/Z=247
M/Z=159
M/Z=117
(b)
M/Z=233
M/Z=143
M/Z=103
M/Z=217
M/Z=129
M/Z=89
(4)
(a)
Intensity (counts)
m/z
(b)
Intensity (counts)
MW: 540 C21 H52O6Si5 (mainlib) Arabino-Hexonic acid, 3-deoxy-2,4,5,6-tetrakis-O-(trimethylsilyl)-, trimethylsilylester
m/z

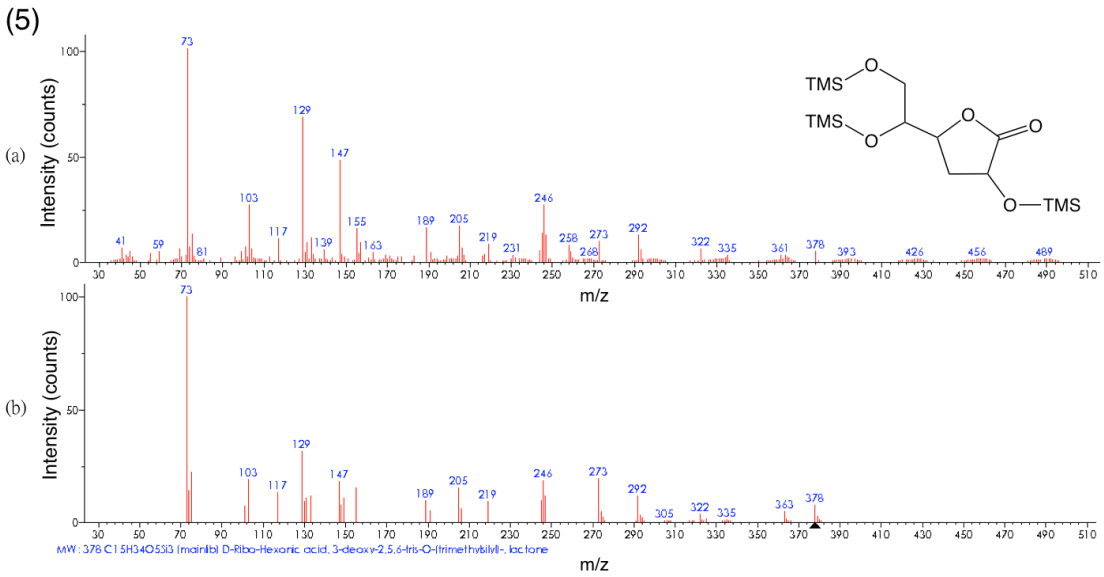

Figure 4.S5. GC-MS spectra of the following after derivatization with excess 1-trimethylsilyl-imidazol: (1a) 2,4,5-trihydroxypentanoic acid from this study (1b) 2,4,5-trihydroxypentanoic acid from NIST database (2a) 2,5-dihydroxypent-3-enoic acid from this study (2b) proposed fragments of 2,5-dihydroxypent-3-enoic acid (3a) 3-hydroxy-5-(hydroxymethyl)dihydrofuran-2(3*H*)-one (3b) proposed fragments of 3-hydroxy-5-(hydroxymethyl)dihydrofuran-2(3*H*)-one (4a) 2,4,5,6-tetrahydroxyhexanoic acid (4b) 2,4,5,6-tetrahydroxyhexanoic acid from NIST database (5a) 5-(1,2-dihydroxyethyl)-3-hydroxydihydrofuran-2(3*H*)-one (5b) 5-(1,2-dihydroxyethyl)-3-hydroxydihydrofuran-2(3*H*)-one from NIST database.

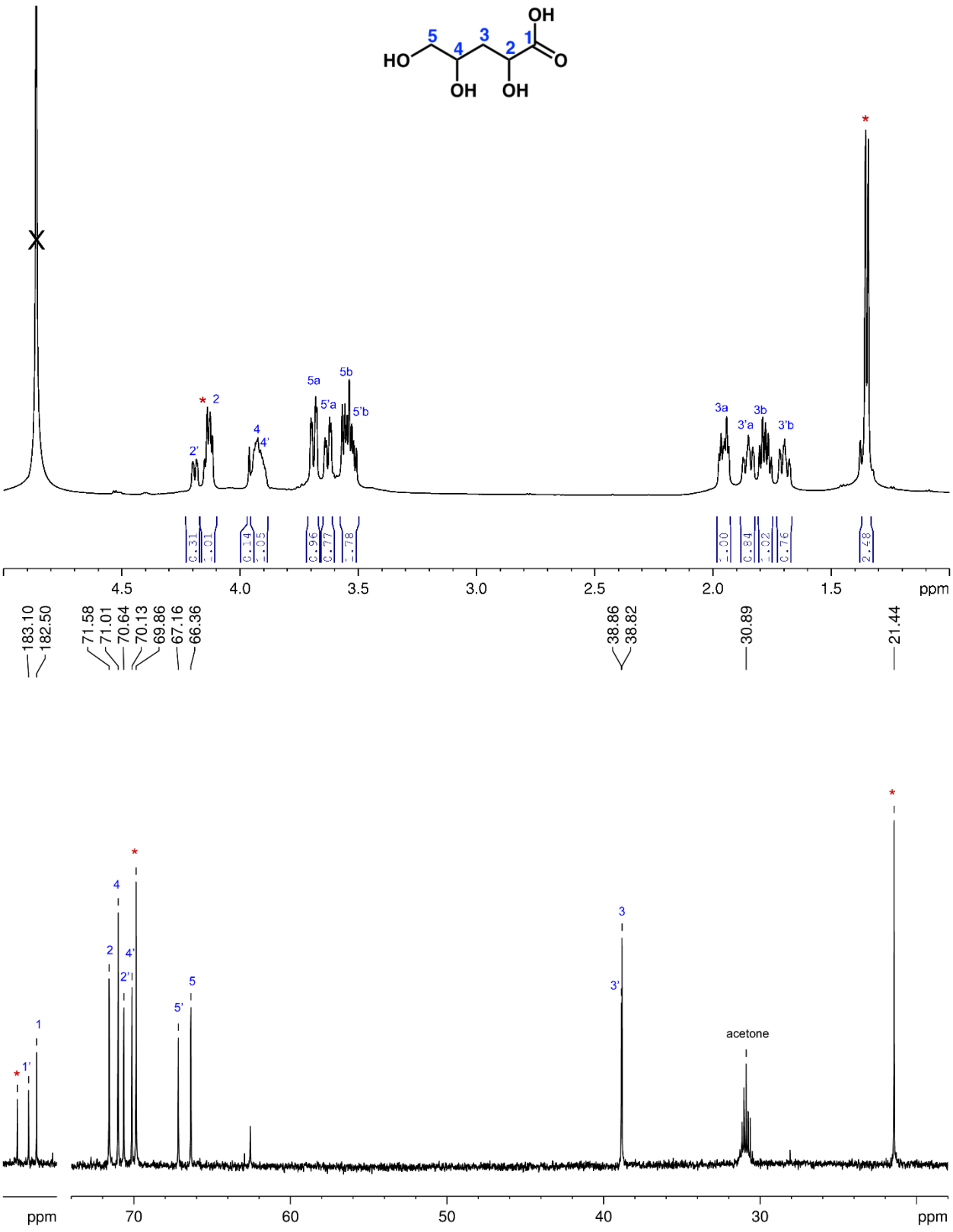

Figure 4.S6. 1D ^{1}H NMR (600 MHz) and ^{13}C NMR (150 MHz) spectra of 2,4,5-trihydroxypentanoic acid in D_2O.

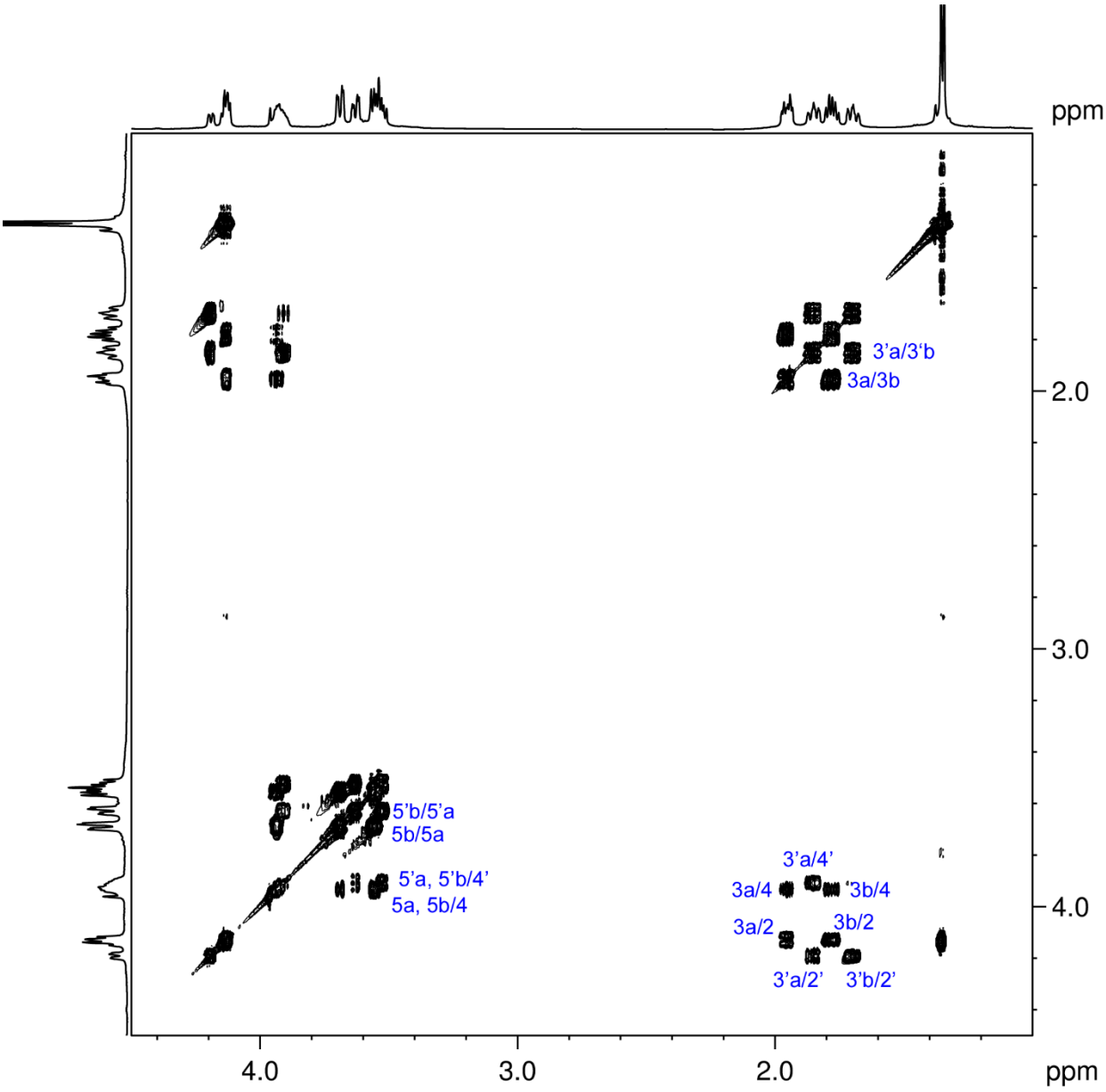

Figure 4.S7. COSY spectrum of 2,4,5-trihydroxypentanoic acid (600 MHz, D_2O).

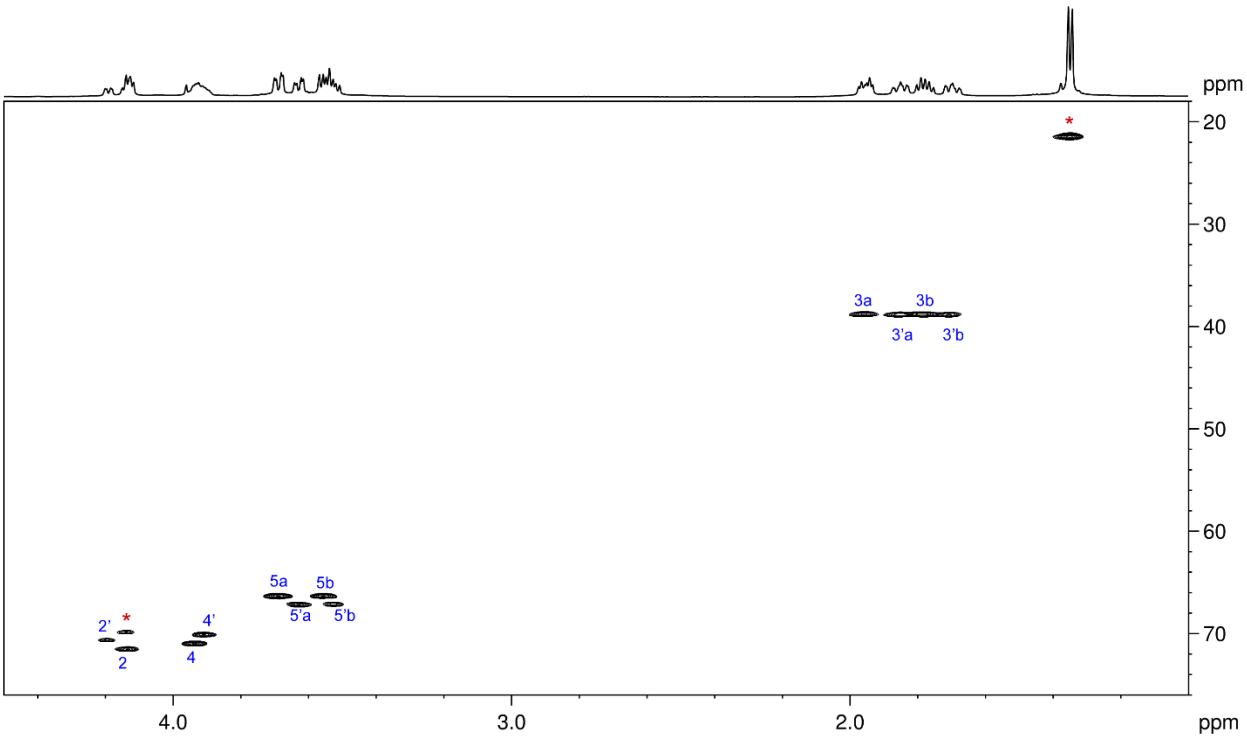

Figure 4.S8. ^{1}H-^{13}C HSQC spectrum of 2,4,5-trihydroxypentanoic acid (600 MHz, D_2O).

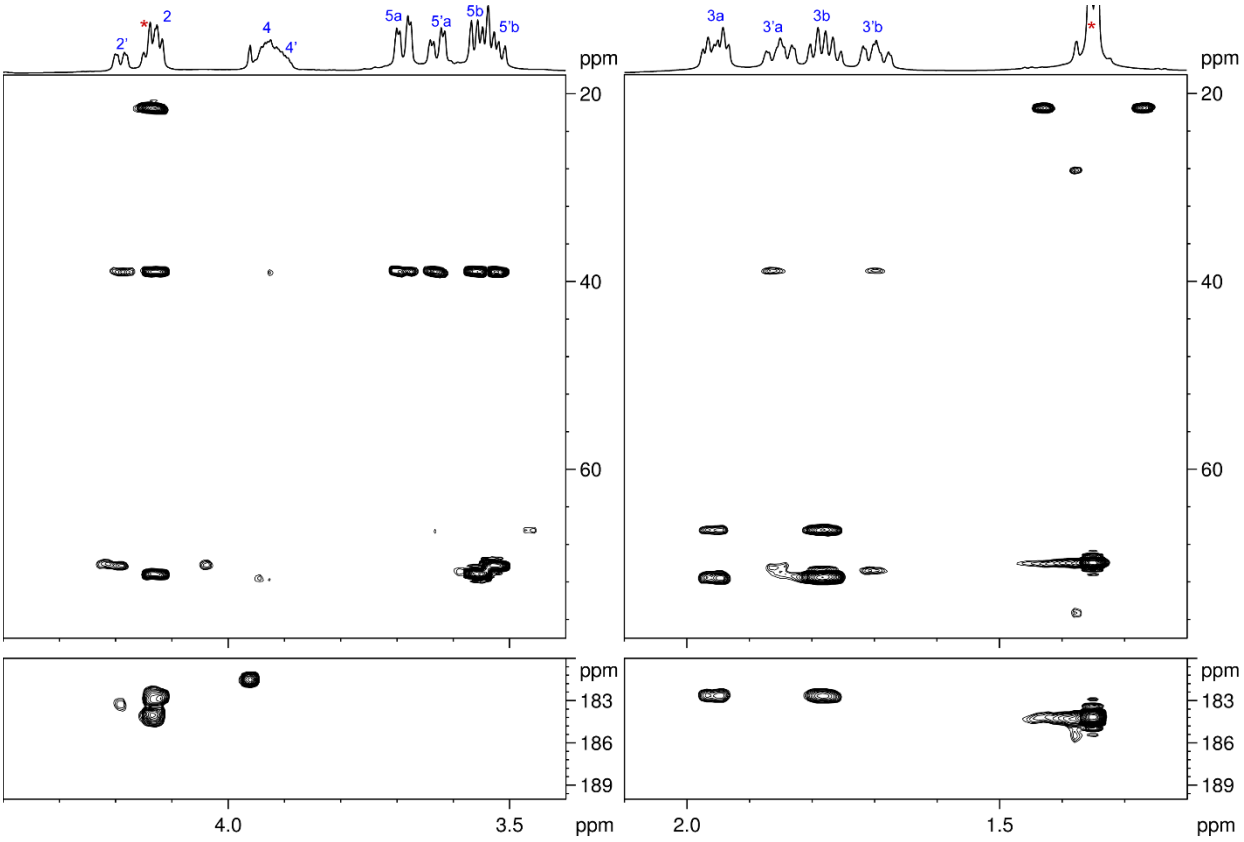

Figure 4.S9. Selected regions from the ^{1}H-^{13}C HMBC spectrum of 2,4,5-trihydroxypentanoic acid (800 MHz, D_2O).

Table 4.S1. NMR spectroscopic data for 2,4,5-trihydroxypentanoic acid (600 MHz, D_2O).

Position	δ^1H	$\delta^{13}C$	COSY	HMBC
1/1'	-	182.5/183.1	-	-
2/2'	4.13 m/4.19 dd (9.5, 2.5)	71.6/70.6	3a, 3b/3'a, 3'b	1, 3, 4/1', 3', 4'
3a	1.95 dt (14.0, 5.5)	38.9	2, 3b, 4	1, 2, 5
3b	1.77 br dt (14.0, 7.4)		2, 3a, 4	
3a'	1.85 ddd (11.5, 7.6, 2.5)	38.8	2', 3'b, 4'	1', 2', 5'
3b'	1.70 ddd (11.5, 7.6, 2.5)		2', 3'a, 4'	
4	3.94 m	71.0	3a, 3b, 5a, 5b	
4'	3.94 m	70.1	3'a, 5'a, 5'b	
5a	3.69 dd (12.0, 3.2)	66.4	4, 5b	3
5b	3.55 dd (11.9, 6.6)		4, 5a	3, 4
5a'	3.62 dd (11.7, 3.7)	67.2	4', 5'b	3'
5b'	3.52 dd (11.7, 5.0)		4', 5'a	3', 4'

Lactic acid (∗ marked in the spectra): δ_H 1.35 (d, 7.0, H-3), 4.14 (m, overlap with H-2), δ_C 21.4 (C-3), 69.9 (C-2), 183.9 (C-1).

2,4,5-trihydroxypentanoic acid. The ^1H NMR spectrum showed a signal pattern and integral values suggesting it is a mixture of two or three compounds. In the ^{13}C NMR spectrum, 13 carbon signals including three carbonyl groups, seven oxygen carrying carbons, two aliphatic methylenes and one methyl were observed. Through analysis of the 2D spectra (COSY, HSQC and HMBC), we confirmed it is indeed a mixture of compounds. The major compound was identified as 2,4,5-trihydroxypentanoic and was isolated as a mixture of stereoisomers (40%:30%) and the other compound was identified as lactic acid (30%).

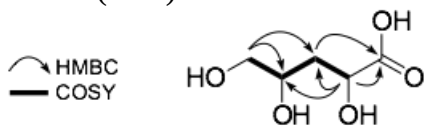

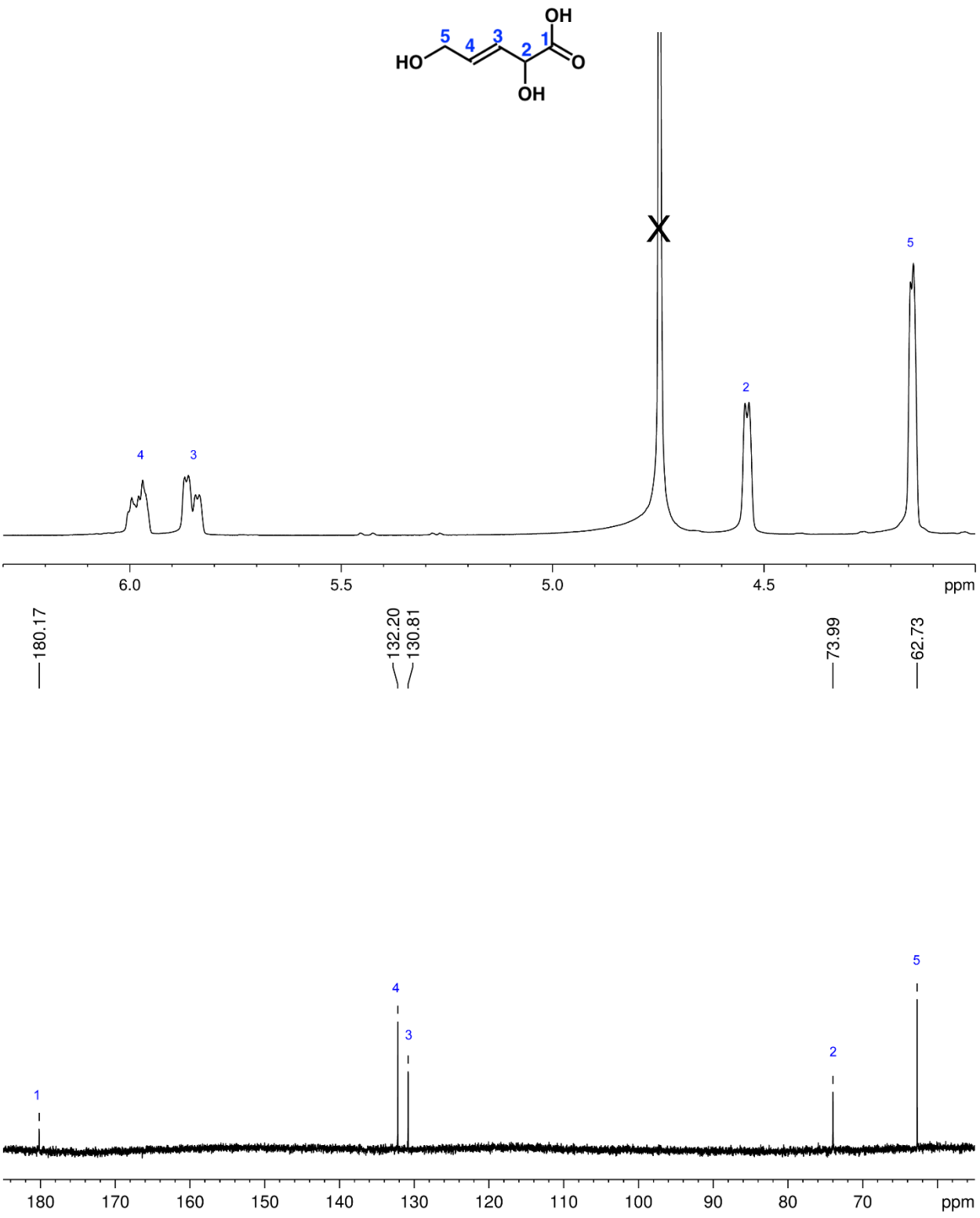

Figure 4.S10. 1D ^{1}H NMR (600 MHz) and ^{13}C NMR (150 MHz) spectra of 2,5-dihydroxypent-3-enoic acid in D_2O.

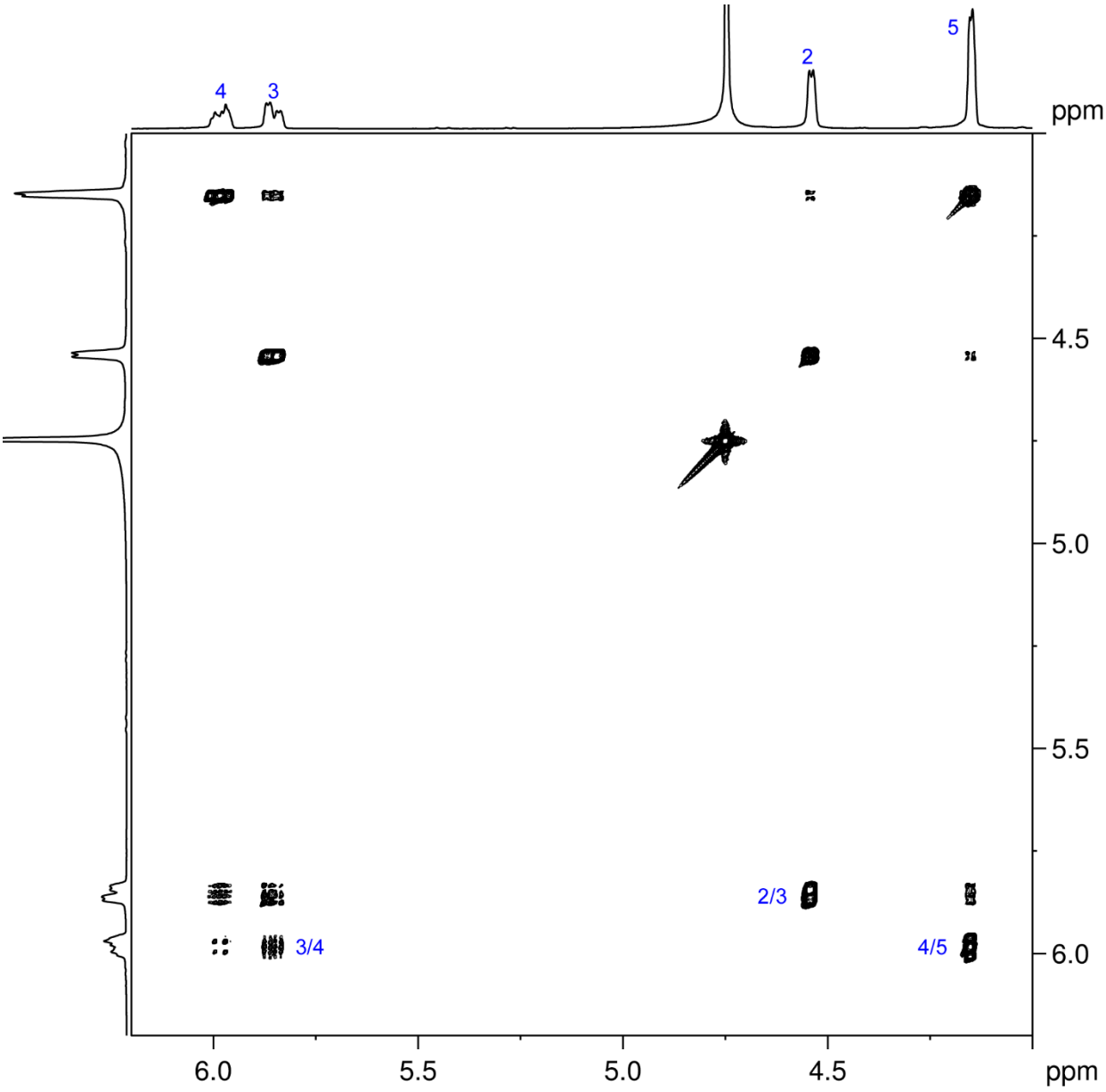

Figure 4.S11. COSY spectrum of 2,5-dihydroxypent-3-enoic acid (600 MHz, D_2O).

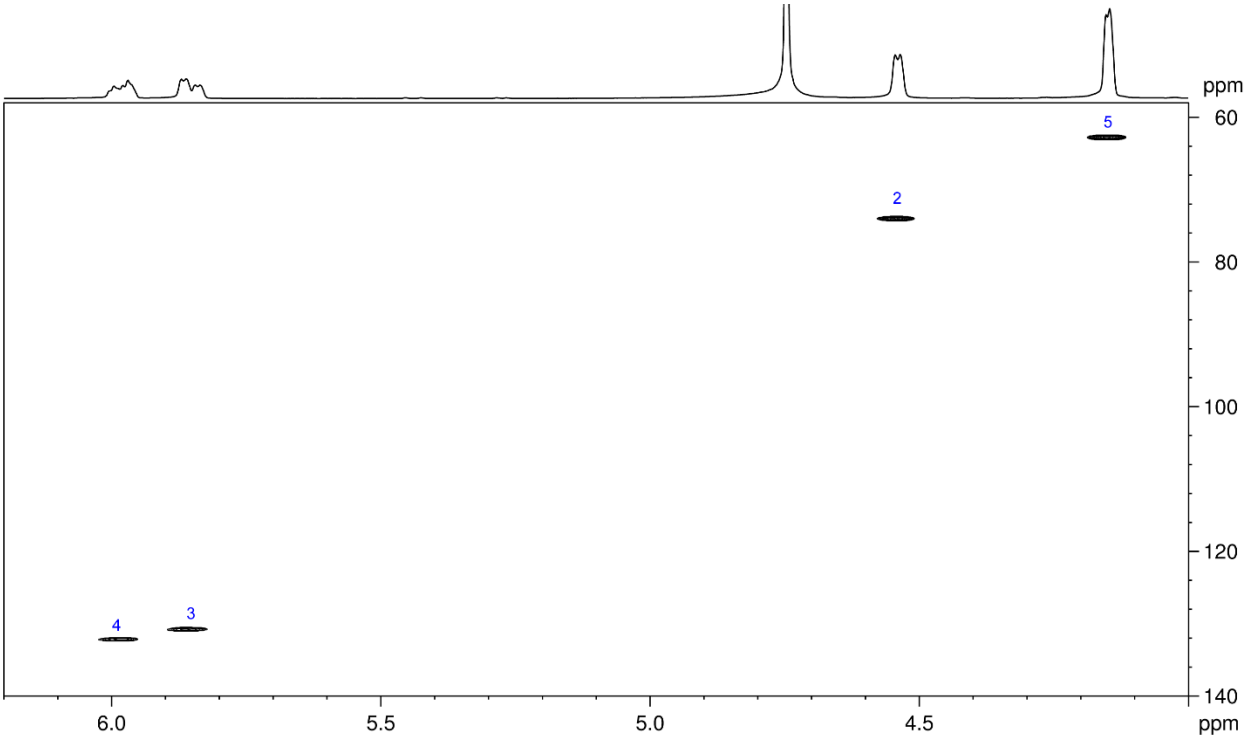

Figure 4.S12. ^{1}H-^{13}C HSQC spectrum of 2,5-dihydroxypent-3-enoic acid (600 MHz, D_2O).

Table 4.S2. NMR spectroscopic data for 2,5-dihydroxypent-3-enoic acid (600 MHz, D_2O).

Position	δ^1H ($J_{H,H}$)	$\delta^{13}C$	COSY	HMBC
1	-	180.2	-	-
2	4.53 d (6.2)	74.1	3	1, 3, 4
3	5.85 dd (15.4, 6.2)	131.0	2, 4	1, 2, 5
4	5.98 dt (15.4, 5.0)	132.2	3, 5	2, 5
5	4.15 (d, 5.0)	62.8	4	3, 4

2,5-dihydroxypent-3-enoic acid. The ^1H NMR spectrum showed four signals including two characteristic double bond protons (5.98 and 5.85 ppm). In the ^{13}C NMR spectrum, we observed five carbon signals including one carbonyl group, with a chemical shift that is characteristic of carboxylic acid, two oxygen carrying carbons and two double bond carbons. The structure elucidation was quite straightforward; by analysis of the 2D spectra (COSY, HSQC and HMBC) we identified the structure as 2,5-dihydroxypent-3-enoic acid. The stereochemistry of the double bond was determined to be *Z* based on the 15.4 Hz coupling.

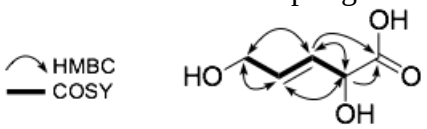

4.6.3 Extended Results of Reactions

Figure 4.S13 shows estimated yields of each of the HPAs: 2,4,5-trihydroxypentanoic acid (abbreviated as THPA) and 2,5-dihydroxypent-3-enoic acid (abbreviated as DHPA), while Figure 4.S14 shows estimated yields of each of the HHAs: 2,4,5,6-tetrahydroxyhexanoic acid (abbreviated as THHA) and 5-(1,2-dihydroxyethyl)-3-hydroxydihydrofuran-2(3*H*)-one (abbreviated as DGL). Additionally, the selectivity of each class of glucose-derived products after 2 h of reaction time at 150-200 °C is shown in Figure 4.S15. These classes of products are HHAs, furanics (*i.e.* formic acid and HMF), retro-aldol products (*i.e.* 2-hydroxybut-3-enoic acid and lactic acid), and humins. Lastly, Figure 4.S16 shows the distribution of pentoses and hexoses for all monophasic reactions in this study.

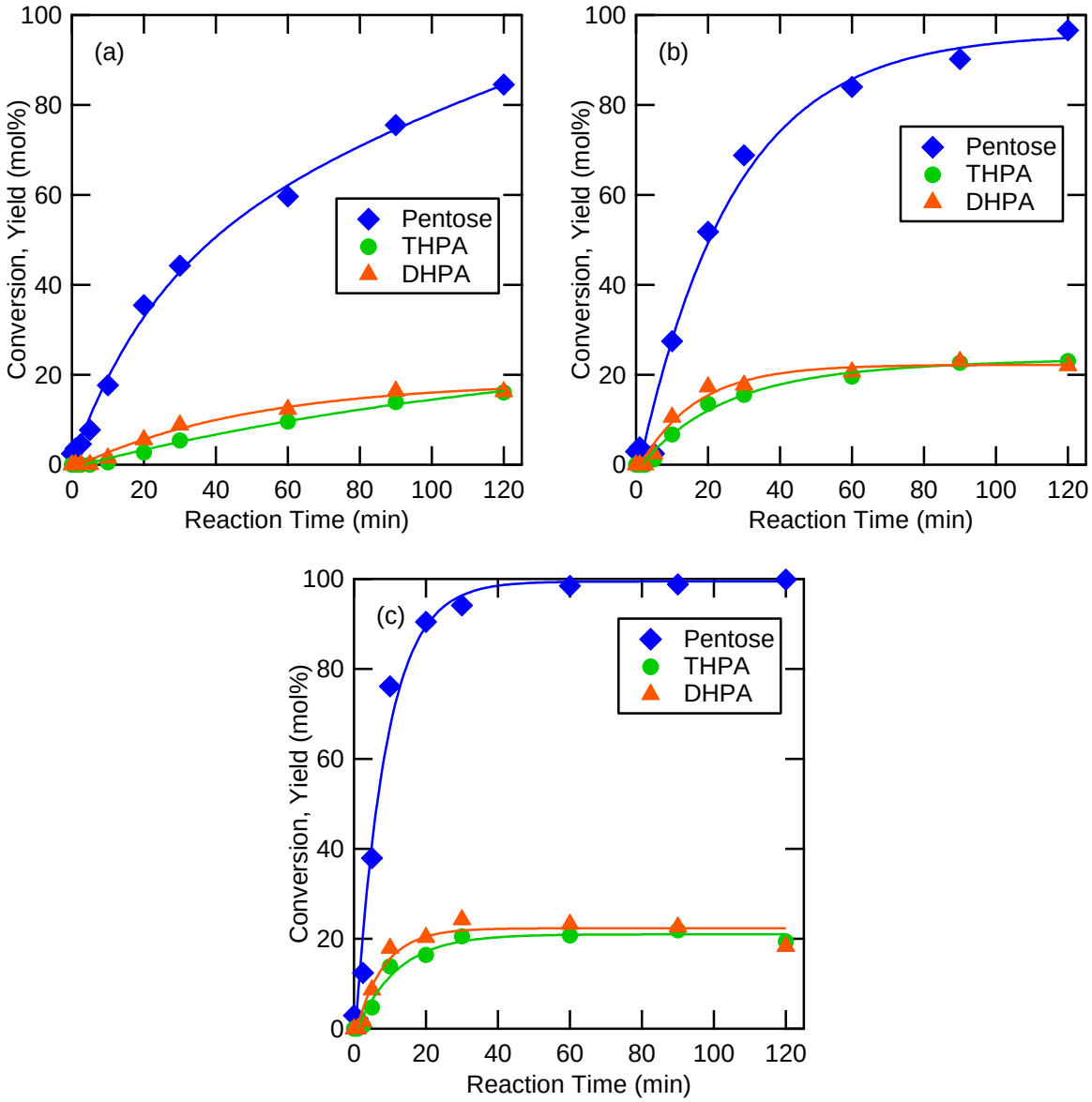

Figure 4.S13. Conversion of pentose and yields of 2,4,5-trihydroxypentanoic acid (abbreviated as THPA) and 2,5-dihydroxypent-3-enoic acid (abbreviated as DHPA) at (a) 100 °C, (b) 120 °C, and (c) 140 °C. 3-hydroxy-5-(hydroxymethyl)dihydrofuran-2(3H)-one was formed in trace amounts.

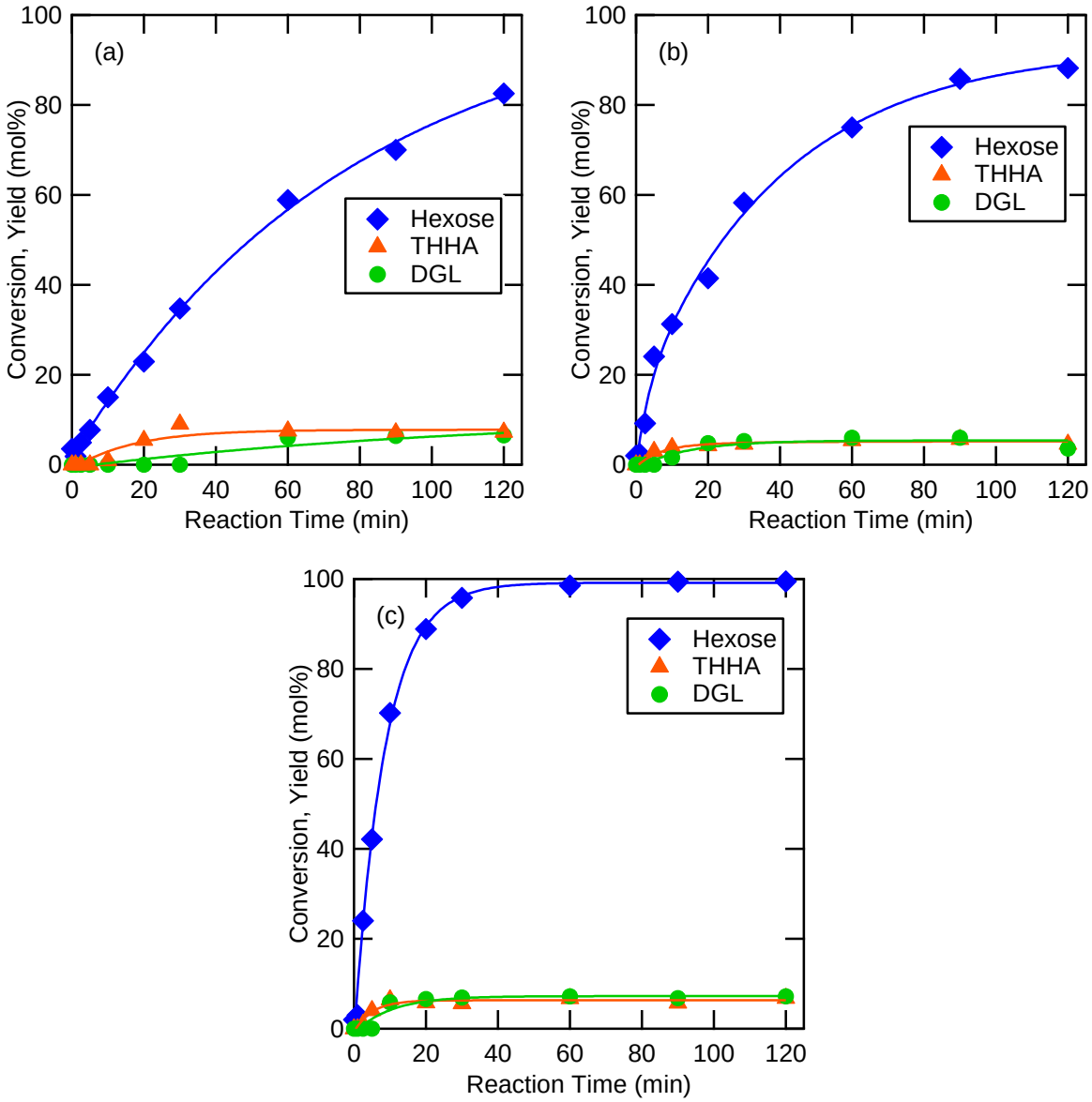

Figure 4.S14. Conversion of hexose and estimated yields of 2,4,5,6-tetrahydroxyhexanoic acid (abbreviated as THHA) and 5-(1,2-dihydroxyethyl)-3-hydroxydihydrofuran-2(3*H*)-one (abbreviated as DGL) at (a) 150 °C, (b) 175 °C, and (c) 200 °C.

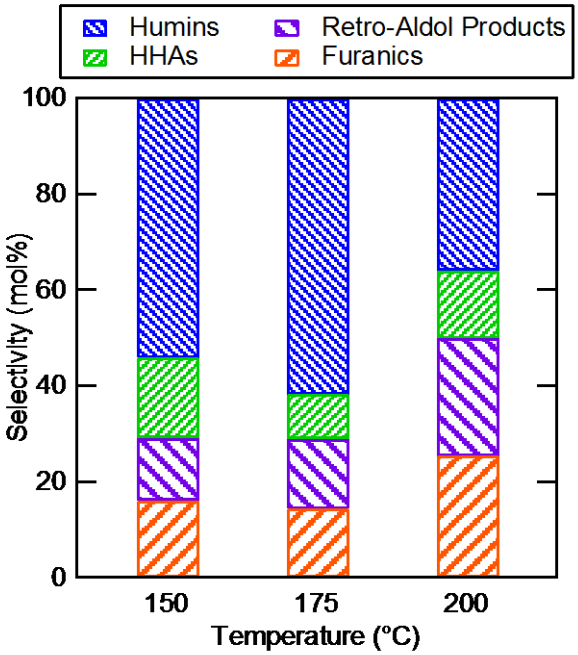

Figure 4.S15. Selectivity of HHAs, furanics (*i.e.* formic acid and HMF), retro-aldol products (*i.e.* 2-hydroxybut-3-enoic acid and lactic acid), and humins after 2 h of glucose conversion at 150-200 °C.

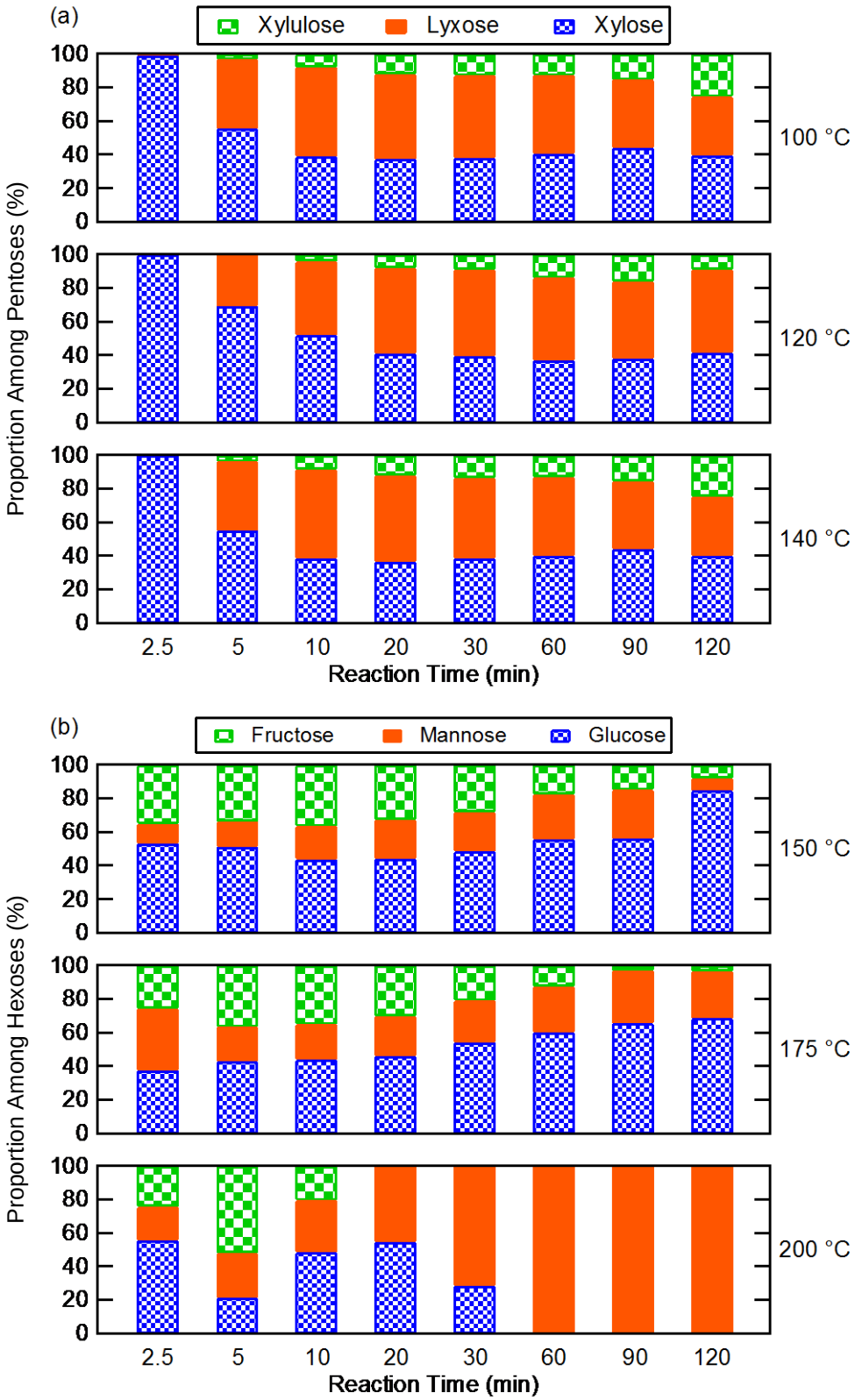

Figure 4.S16. Sugar isomer distributions of (a) pentoses and (b) hexoses throughout the monophasic reactions.

4.7 References

1. D. M. Alonso, S. G. Wettstein and J. A. Dumesic, *Green Chem.*, 2013, **15**, 584.
2. J. C. Serrano-Ruiz, R. Luque and A. Sepulveda-Escribano, *Chem. Soc. Rev.*, 2011, **40**, 5266-5281.
3. G. W. Huber, S. Iborra and A. Corma, *Chem. Rev.*, 2006, **106**, 4044-4098.
4. R. J. van Putten, J. C. van der Waal, E. de Jong, C. B. Rasrendra, H. J. Heeres and J. G. de Vries, *Chem. Rev.*, 2013, **113**, 1499-1597.
5. M. Balakrishnan, E. R. Sacia, S. Sreekumar, G. Gunbas, A. A. Gokhale, C. D. Scown, F. D. Toste and A. T. Bell, *Proc. Natl. Acad. Sci. U. S. A.*, 2015, **112**, 7645-7649.
6. L. Li, J. Ding, J.-G. Jiang, Z. Zhu and P. Wu, *Chin. J. Catal.*, 2015, **36**, 820-828.
7. V. Choudhary, A. B. Pinar, S. I. Sandler, D. G. Vlachos and R. F. Lobo, *ACS Catal.*, 2011, **1**, 1724-1728.
8. M. Moliner, Y. Román-Leshkov and M. E. Davis, *Proc. Natl. Acad. Sci. U. S. A.*, 2010, **107**, 6164-6168.
9. Y. Román-Leshkov and M. E. Davis, *ACS Catal.*, 2011, **1**, 1566-1580.
10. Y.-P. Li, M. Head-Gordon and A. T. Bell, *ACS Catal.*, 2014, **4**, 1537-1545.
11. R. Bermejo-Deval, R. S. Assary, E. Nikolla, M. Moliner, Y. Román-Leshkov, S. J. Hwang, A. Palsdottir, D. Silverman, R. F. Lobo, L. A. Curtiss and M. E. Davis, *Proc. Natl. Acad. Sci. U. S. A.*, 2012, **109**, 9727-9732.
12. V. Choudhary, S. Caratzoulas and D. G. Vlachos, *Carbohydr. Res.*, 2013, **368**, 89-95.
13. S. Roy, K. Bakhmutsky, E. Mahmoud, R. F. Lobo and R. J. Gorte, *ACS Catal.*, 2013, **3**, 573-580.
14. V. Choudhary, S. I. Sandler and D. G. Vlachos, *ACS Catal.*, 2012, **2**, 2022-2028.
15. S. Tolborg, S. Meier, I. Sádaba, S. G. Elliot, S. K. Kristensen, S. Saravanamurugan, A. Riisager, P. Fristrup, T. Skrydstrup and E. Taarning, *Green Chem.*, 2016, **18**, 3360-3369.
16. M. Dusselier, P. Van Wouwe, F. de Clippel, J. Dijkmans, D. W. Gammon and B. F. Sels, *ChemCatChem*, 2013, **5**, 569-575.
17. M. S. Holm, S. Saravanamurugan and E. Taarning, *Science*, 2010, **328**, 602-605.
18. V. L. Sushkevich, A. Vimont, A. Travert and I. I. Ivanova, *J. Phys. Chem. C*, 2015, **119**, 17633-17639.
19. G. Yang, L. Zhou and X. Han, *J. Mol. Catal. A: Chem.*, 2012, **363-364**, 371-379.
20. O. Yemis and G. Mazza, *Bioresour. Technol.*, 2011, **102**, 7371-7378.
21. L. Mao, L. Zhang, N. Gao and A. Li, *Bioresour. Technol.*, 2012, **123**, 324-331.
22. K. R. Enslow and A. T. Bell, *Catal. Sci. Technol.*, 2015, **5**, 2839-2847.
23. J. B. Binder, J. J. Blank, A. V. Cefali and R. T. Raines, *ChemSusChem*, 2010, **3**, 1268-1272.
24. B. Li, S. Varanasi and P. Relue, *Green Chem.*, 2013, **15**, 2149.
25. C. M. Cai, T. Zhang, R. Kumar and C. E. Wyman, *J. Chem. Technol. Biotechnol.*, 2014, **89**, 2-10.
26. R. Weingarten, J. Cho, J. W. C. Conner and G. W. Huber, *Green Chem.*, 2010, **12**, 1423.
27. Y. Román-Leshkov and J. A. Dumesic, *Top. Catal.*, 2009, **52**, 297-303.
28. L. Li, C. Stroobants, K. Lin, P. A. Jacobs, B. F. Sels and P. P. Pescarmona, *Green Chem.*, 2011, **13**, 1175.
29. M. S. Holm, Y. J. Pagán-Torres, S. Saravanamurugan, A. Riisager, J. A. Dumesic and E. Taarning, *Green Chem.*, 2012, **14**, 702.

30. T. M. Aida, Y. Sato, M. Watanabe, K. Tajima, T. Nonaka, H. Hattori and K. Arai, *J. Supercrit. Fluids*, 2007, **40**, 381-388.
31. M. Dusselier, P. Van Wouwe, A. Dewaele, E. Makshina and B. F. Sels, *Energy Environ. Sci.*, 2013, **6**, 1415.
32. K. Marcincinova-Benabdillah, M. Boustta, J. Coudane and M. Vert, *Biomacromolecules*, 2011, **2**, 1279-1284.
33. M. Davis, *Top. Catal.*, 2015, **58**, 405-409.
34. M. Tang, A. F. Haider, C. Minelli, M. M. Stevens and C. K. Williams, *J. Polym. Sci., Part A: Polym. Chem.*, 2008, **46**, 4352-4362.
35. A. F. Haider and C. K. Williams, *J. Polym. Sci., Part A: Polym. Chem.*, 2008, **46**, 2891-2896.
36. B. Witholt and B. Kessler, *Curr. Opin. Biotechnol.*, 1999, **10**, 279-285.
37. R. Sahatjian and K. Amplatz, (Boston Scientific Corporation, Boston, USA), Pub. No. WO/1991/008790 A1, 1991.
38. H. Von Bluecher and E. De Ruiter, Pub. No. DE3132324 A1, 1983.
39. W. Rhee, D. G. Wallace, A. S. Michaels, R. A. J. Burns, L. Fries, F. DeLustro and H. Bentz, (Collagen Corporation, Palo Alto, USA), Pub. No. US 5162430 A, 1992.
40. J. W. Harris, M. J. Cordon, J. R. Di Iorio, J. C. Vega-Vila, F. H. Ribeiro and R. Gounder, *J. Catal.*, 2016, **335**, 141-154.